Evidence for deposition of 10 million tonnes of impact spherules across four continents 12,800 y ago

James H. Wittke[a], James C. Weaver[b], Ted E. Bunch[a,1], James P. Kennett[c], Douglas J. Kennett[d], Andrew M. T. Moore[e], Gordon C. Hillman[f], Kenneth B. Tankersley[g], Albert C. Goodyear[h], Christopher R. Moore[i], I. Randolph Daniel, Jr.[j], Jack H. Ray[k], Neal H. Lopinot[k], David Ferraro[l], Isabel Israde-Alcántara[m], James L. Bischoff[n], Paul S. DeCarli[o], Robert E. Hermes[p,2], Johan B. Kloosterman[q,2], Zsolt Revay[r], George A. Howard[s], David R. Kimbel[t], Gunther Kletetschka[u], Ladislav Nabelek[u,v], Carl P. Lipo[w], Sachiko Sakai[w], Allen West[x], and Richard B. Firestone[y]

[a]Geology Program, School of Earth Science and Environmental Sustainability, Northern Arizona University, Flagstaff, AZ 86011; [b]Wyss Institute for Biologically Inspired Engineering, Harvard University, Cambridge, MA 02138; [c]Department of Earth Science and Marine Science Institute, University of California, Santa Barbara, CA 93106; [d]Department of Anthropology, Pennsylvania State University, University Park, PA 16802; [e]College of Liberal Arts, Rochester Institute of Technology, Rochester, NY 14623; [f]Institute of Archaeology, University College London, London WC1H0PY, United Kingdom; [g]Departments of Anthropology and Geology, University of Cincinnati, Cincinnati, OH 45221; [h]South Carolina Institute of Archaeology and Anthropology, University of South Carolina, Columbia, SC 29208; [i]Savannah River Archaeological Research Program, South Carolina Institute of Archaeology and Anthropology, University of South Carolina, New Ellenton, SC 29809; [j]Department of Anthropology, East Carolina University, Greenville, NC 27858; [k]Center for Archaeological Research, Missouri State University, Springfield, MO 65897; [l]Viejo California Associates, Joshua Tree, CA 92252; [m]Departamento de Geología y Mineralogía, Edificio U4, Instituto de Investigaciones Metalúrgicas, Universidad Michoacana de San Nicólas de Hidalgo, C. P. 58060, Morelia, Michoacán, México; [n]US Geological Survey, Menlo Park, CA 94025; [o]SRI International, Menlo Park, CA 94025; [p]Los Alamos National Laboratory, Los Alamos, NM 87545; [q]Exploration Geologist, 1016 NN, Amsterdam, The Netherlands; [r]Forschungsneutronenquelle Heinz Maier-Leibnitz, Technische Universität München, 85748 Garching, Germany; [s]Restoration Systems, LLC, Raleigh, NC 27604; [t]Kimstar Research, Fayetteville, NC 28312; [u]Faculty of Science, Charles University in Prague, 12843 Prague, Czech Republic; [v]Institute of Geology, Academy of Sciences of the Czech Republic, Public Research Institute, 16500 Prague, Czech Republic; [w]Institute for Integrated Research in Materials, Environments, and Society, California State University, Long Beach, CA 90840; [x]GeoScience Consulting, Dewey, AZ 86327; and [y]Lawrence Berkeley National Laboratory, Berkeley, CA 94720

Edited* by Steven M. Stanley, University of Hawaii, Honolulu, HI, and approved April 9, 2013 (received for review January 28, 2013)

Airbursts/impacts by a fragmented comet or asteroid have been proposed at the Younger Dryas onset (12.80 ± 0.15 ka) based on identification of an assemblage of impact-related proxies, including microspherules, nanodiamonds, and iridium. Distributed across four continents at the Younger Dryas boundary (YDB), spherule peaks have been independently confirmed in eight studies, but unconfirmed in two others, resulting in continued dispute about their occurrence, distribution, and origin. To further address this dispute and better identify YDB spherules, we present results from one of the largest spherule investigations ever undertaken regarding spherule geochemistry, morphologies, origins, and processes of formation. We investigated 18 sites across North America, Europe, and the Middle East, performing nearly 700 analyses on spherules using energy dispersive X-ray spectroscopy for geochemical analyses and scanning electron microscopy for surface microstructural characterization. Twelve locations rank among the world's premier end-Pleistocene archaeological sites, where the YDB marks a hiatus in human occupation or major changes in site use. Our results are consistent with melting of sediments to temperatures >2,200 °C by the thermal radiation and air shocks produced by passage of an extraterrestrial object through the atmosphere; they are inconsistent with volcanic, cosmic, anthropogenic, lightning, or authigenic sources. We also produced spherules from wood in the laboratory at >1,730 °C, indicating that impact-related incineration of biomass may have contributed to spherule production. At 12.8 ka, an estimated 10 million tonnes of spherules were distributed across ∼50 million square kilometers, similar to well-known impact strewnfields and consistent with a major cosmic impact event.

Clovis–Folsom | lechatelierite | tektite | wildfires

An increasing body of evidence suggests that major cosmic airbursts/impacts with Earth occurred at the onset of the Younger Dryas (YD) episode, triggering abrupt cooling and causing major environmental perturbations that contributed to megafaunal extinctions and human cultural changes. (Note that "airburst/impact" is used to refer to a collision by a cosmic body with Earth's atmosphere, producing an extremely high-energy aerial disintegration that may be accompanied by numerous small crater-forming impacts by the fragments.) The impact hypothesis originated from observations of peaks in Fe-rich and Al-Si–rich impact spherules, nanodiamonds, and other unusual impact tracers discovered in the Younger Dryas boundary layer (YDB), a sedimentary stratum typically only a few centimeters thick. The hypothesis was first proposed by Firestone et al. (1) and expanded upon by Kennett et al. (2–4), Kurbatov et al. (5), Anderson et al. (6), Israde et al. (7), Bunch et al. (8), and Jones and Kennett (9). Formerly, the date of the impact event was reported as 10.9 ± 0.145 ka (radiocarbon), calibrated as 12.9 ± 0.10 ka B.P., using the then-standard calibration curve IntCal04. (Unless otherwise noted, all dates are presented as calibrated or calendar

Significance

We present detailed geochemical and morphological analyses of nearly 700 spherules from 18 sites in support of a major cosmic impact at the onset of the Younger Dryas episode (12.8 ka). The impact distributed ∼10 million tonnes of melted spherules over 50 million square kilometers on four continents. Origins of the spherules by volcanism, anthropogenesis, authigenesis, lightning, and meteoritic ablation are rejected on geochemical and morphological grounds. The spherules closely resemble known impact materials derived from surficial sediments melted at temperatures >2,200 °C. The spherules correlate with abundances of associated melt-glass, nanodiamonds, carbon spherules, aciniform carbon, charcoal, and iridium.

Author contributions: J.H.W., J.C.W., T.E.B., J.P.K., D.J.K., A.M.T.M., G.C.H., K.B.T., A.C.G., D.F., I.I.-A., R.E.H., J.B.K., Z.R., D.R.K., G.K., C.P.L., S.S., A.W., and R.B.F. designed research; J.H.W., J.C.W., T.E.B., J.P.K., D.J.K., A.M.T.M., G.C.H., K.B.T., A.C.G., C.R.M., I.R.D., J.H.R., N.H.L., D.F., I.I.-A., J.L.B., P.S.D., R.E.H., J.B.K., Z.R., G.A.H., D.R.K., G.K., L.N., C.P.L., S.S., A.W., and R.B.F. performed research; J.H.W., J.C.W., T.E.B., J.P.K., D.J.K., A.M.T.M., K.B.T., A.C.G., D.F., I.I.-A., P.S.D., R.E.H., J.B.K., Z.R., G.K., L.N., C.P.L., S.S., A.W., and R.B.F. analyzed data; and J.H.W., J.C.W., T.E.B., J.P.K., D.J.K., A.M.T.M., K.B.T., A.C.G., C.R.M., I.R.D., J.H.R., N.H.L., D.F., I.I.-A., J.L.B., P.S.D., R.E.H., J.B.K., G.A.H., D.R.K., G.K., A.W., and R.B.F. wrote the paper.

The authors declare no conflict of interest.

*This Direct Submission article had a prearranged editor.

[1]To whom correspondence should be addressed. E-mail: tbear1@cableone.net.

[2]Retired.

This article contains supporting information online at www.pnas.org/lookup/suppl/doi:10.1073/pnas.1301760110/-/DCSupplemental.

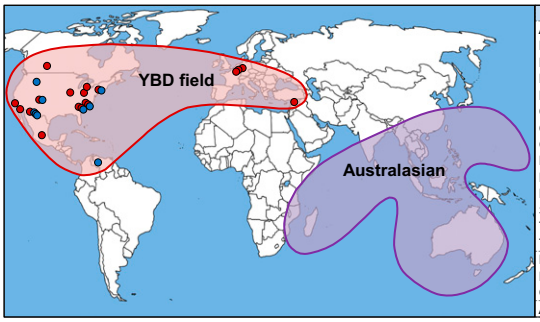

Site/Location	Details	Strat	Env	Setting
Arlington Cyn, CA	B,C,A,M	A	A	Coastal cyn
Barber Crk, NC	A	A,E	A	Relict dune
Big Eddy, MO	A	A	A	Flood-plain
Blackville, SC	--	A,E	I	Carolina bay
Blackwater, NM	B,C,A,M	A,L	A	Streambed
Chobot, ALB	B,C,A,M	A,L	A	Lakeshore
Cuitzeo, MEX	B,C,M	L	A	Lake bed
Gainey, MI	B,C,A,M	A,G	I	End-glacial
Kimbel Bay, NC	--	C,E	A	Carolina bay
Melrose, PA	--	C,G	I	End-glacial
Murray Spgs AZ	B,C,A,M	C,L	A	Streambed
Sheriden Cv, OH	B,C,A,M	C	A	Karst-cave
Talega, CA	B,A	A,C	I	Streambed
Topper, SC	A	A,C	I	River bank
Lingen, GER	B,C	E	A	Paleo-dunes
Lommel, BEL	B,CA	E	A	Paleo-dunes
Ommen, NED	B,C	E	A	Paleo-dunes
Abu Hureyra, SYR	B,C,A	A,E	I	Mound (tell)

Fig. 1. YDB impact field, based on data from 27 locations. In the YDB strewnfield (red), there are 18 YDB sites in this study (red dots; see table on *Right*). Eight independent studies have found spherules and/or scoria-like objects at nine additional sites (blue dots) located in Arizona, Montana, New Mexico, Maryland, South Carolina, Pennsylvania, Mexico, and Venezuela. The largest accepted impact strewnfield, the Australasian (purple), is shown for comparison with each strewnfield covering ~50 million square kilometers or ~10% of the planet. Table shows location of sites and lists site details (A, archeological material; B, black mat; C, charcoal; M, megafaunal remains, present either at the sampling location or in the vicinity). Also given are stratigraphic settings (Strat: A, alluvial; C, colluvial; E, eolian; G, glacial; and L, lacustrine) and relative physical stability of depositional paleoenvironments (Env: A, active, e.g., riverine, lacustrine, or eolian; I, inactive).

kiloannum.) Using the most recent curve, IntCal09, the same radiocarbon date calibrates as 12.8 ± 0.15 ka.

Impact-related spherules have long been considered one of the most distinctive proxies in support of this hypothesis. However, despite increasing evidence for YDB peaks in impact spherules, their presence and origin remain disputed (10, 11). In the latest example of this dispute, Boslough et al. (ref. 12, p. 21) stated that "magnetic microspherule abundance results published by the impact proponents have not been reproducible by other workers." However, the authors neglected to cite nine independent spherule studies on two continents (shown in Fig. 1) that reported finding significant YDB spherule abundances, as summarized in high-profile previously published papers by Israde et al. (7), Bunch et al. (8), and LeCompte et al. (13). The nine additional sites are located in Arizona (14–16), Montana[†], New Mexico, Maryland, South Carolina (13), Pennsylvania (17); Mexico[‡], and Venezuela (18–21). In response to such claims, we here present the results of one of the most comprehensive investigations of spherules ever undertaken to address questions of geochemical and morphological characteristics, distribution, origin, and processes involved in the formation of YDB spherules.

We refer here to all melted, rounded-to-subrounded YDB objects as spherules. At a few locations, spherules are found in association with particles of melted glass called scoria-like objects (SLOs), which are irregular in shape and composed of highly vesicular, siliceous melt-glass, as described in Bunch et al. (8). Collectively, YDB spherules and SLOs are here referred to as YDB objects. Peaks in spherules were observed at the onset of the YD at 27 sites—18 sites in this study and nine sites independently studied in North and South America (Fig. 1). Whereas most independent studies concluded that the YDB spherules formed during a high-temperature cosmic impact event, one study by Surovell et al. (10) was unable to find any YDB spherule peaks at seven sites. However, LeCompte et al. (13) repeated the analyses at three of those sites and verified the previous observations (1), concluding that the inability of Surovell et al. (10) to find YDB spherule peaks resulted from not adhering to the prescribed extraction protocol (1, 7). For example, Surovell et al. did not conduct any analyses using scanning electron microscopy (SEM) and energy dispersive X-ray spectroscopy (EDS), a necessary procedure clearly specified by Firestone et al. (1). In another study, Pigati et al. (14) confirmed the previously reported YDB peak in spherules at Murray Springs, Arizona, and also claimed to find several non-YDB spherule peaks in Chile. However, the Chilean sites are known to contain abundant volcanic spherules (22), and yet Pigati et al. (14) did not perform any analyses of candidate spherules with SEM and EDS, which are crucial for differentiating impact-related YDB spherules from volcanic spherules, detrital magnetic grains, framboids, and other spherule-like particles.

In another study, Pinter et al. (11) claimed to have sampled the YDB layer at a location "identical or nearly identical" with the location reported by Kennett (2–4), as part of three studies that reported finding no YDB spherules or nanodiamonds (11, 23, 24). However, the published Universal Transverse Mercator coordinates reveal that their purported continuous sequence is actually four discontinuous sections. These locations range in distance from the site investigated by Kennett et al. (2) by 7,000 m, 1,600 m, 165 m, and 30 m (*SI Appendix*, Fig. S1*B*), clearly showing that they did not sample the YDB site of Kennett et al. (2). Furthermore, this sampling strategy raises questions about whether Pinter et al. (11) sampled the YDB at all, and may explain why they were unable to find peaks in YDB magnetic spherules, carbon spherules, or nanodiamonds.

It is widely accepted that spherules form during cosmic impacts (25–29), and spherules also form as ablation products from the influx of meteorites and cosmic dust. However, not all terrestrial spherules are cosmic in origin; abundant spherules commonly occur throughout the geological record due to non-impact processes. For example, spherules and glass can be produced by continental volcanism (30), hydrovolcanism (31), metamorphism (29), lightning strikes (18, 32), and coal seam fires (32). In addition, detrital magnetite and quartz grains are frequently rounded from wind and water action and may appear spherulitic, as can authigenic framboids, all of which are common in sediments (33). Spherules and melt-glasses can also be produced anthropogenically, especially by coal-fired power plants and smelters (34), although these are normally restricted to surface deposits of industrial age (<300 y old). Al-Si–rich spherules have been produced under laboratory conditions from the combustion of charcoal at ~1,600–2,000 °C (35). Also, numerous spherules and melt-glass have been produced in atomic explosions (36, 37), including the Trinity detonation in New Mexico in 1945, where the airburst produced spherules similar to those from the Tunguska cosmic airburst in 1908 (8, 38). More specifically, the Trinity explosion was a surface burst because the aerial fireball intersected the ground.

In summary, although there are many processes by which spherules can be produced, each type of spherule exhibits a unique set of geochemical, morphological, and/or microstructural characteristics that allow it to be differentiated from impact-related spherules. All types appear similar to YDB spherules under a light microscope, and so, the use of SEM/EDS is crucial for the differentiation of YDB impact spherules from other types.

[†]Baker DW, Miranda PJ, Gibbs KE, Montana evidence for extra-terrestrial impact event that caused Ice-Age mammal die-off, American Geophysical Union Spring Meeting, May 27–30, 2008, Ft. Lauderdale, FL, abstr P41A-05.

[‡]Scruggs MA, Raab LM, Murowchick JS, Stone MW, Niemi TM, Investigation of sediment containing evidence of the Younger Dryas Boundary (YPB) Impact Event, El Carrizal, Baja California Sur, Mexico, Geological Society of America Abstracts with Programs, vol 42, no. 2, p 101 (abstr).

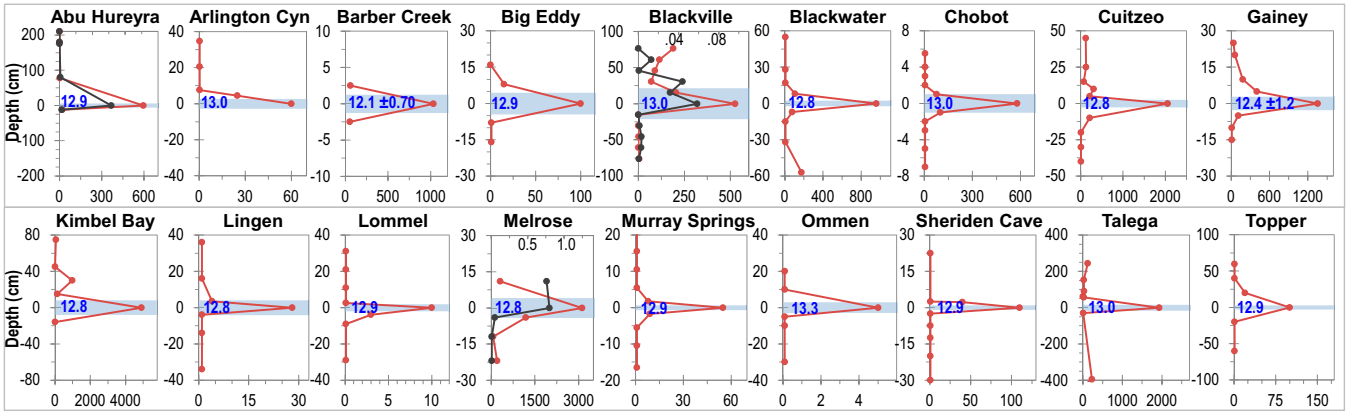

Fig. 2. Stratigraphic distribution. Abundances of spherules by site (red lines), plotted on lower *x* axis in number per kilogram relative to the YDB depth at 0 cm. SLO concentrations (black lines) are plotted on upper *x* axis in grams per kilogram (*SI Appendix*, Table S3). Thickness of sample containing YDB is indicated by blue bar. Dates for YDB layer are in blue, as determined by age-depth models (*SI Appendix*, Table S1).

Results and Discussion

Site Details. To quantitatively investigate YDB spherules, we examined 18 sites across three continents (Fig. 1), selecting most because they contained independently dated chronostratigraphic profiles that spanned the onset of the YD at ~12.8 ka, thus providing identifiable candidate strata for the YDB layer. Investigations of spherules were previously conducted at seven of those sites (1, 10, 11, 13). The stratigraphy, chronology, and archaeological significances of each site are summarized in Fig. 1. Also, each of 15 sites is described in detail in *SI Appendix*, Figs. S1–S15; the other three sites were previously described in Bunch et al. (8).

The YDB sequences were dated by accelerator-mass spectrometry radiocarbon dating at 11 of 18 sites, and optically stimulated luminescence (OSL) or thermal luminescence at six others. Eleven new radiometric and OSL dates for four sites are presented here, along with 67 previously published dates for the other sites (*SI Appendix*, Table S1); most sites are well dated, but several have large uncertainties. The stratigraphic position of the YDB for each site is determined from its interpolated age-depth model, and overall, the interpolated ages of the YDB layers are consistent with the revised age of ~12.8 ka.

Other criteria helped confirm the identification of the YDB layer, including the stratigraphic distribution of archaeological artifacts, found either at the sampling location or in the vicinity for 12 sites, including 10 in North America that contain projectile points and other artifacts from Paleoamerican cultures (Clovis, Folsom, Gainey, and Archaic projectile points are shown in *SI Appendix*, Figs. S2–S5, S11, S13, and S15); some are well-documented Clovis sites, displaying projectile points that establish a date range of 12.80–13.25 ka (39). Clovis points have never been found in situ in strata younger than ~12.8 ka. One site was radiometrically undated, but abundant, temporally diagnostic Clovis Paleoamerican artifacts indicated the likely stratigraphic position of the YDB at the top of the artifact layer, as later confirmed by a peak in impact spherules. Furthermore, identification of the YDB layer was aided by visual changes in lithology, including the presence at 12 sites of darker lithologic units, e.g., the "black mat" layer (40), along with charcoal abundance peaks at 11 sites.

Across North America, the YDB layer coincides with the extinction of late-Pleistocene megafauna, including mammoth (*Mammuthus*), American horse (*Equus*), American camel (*Camelops*), and dire wolf (*Canis dirus*), which have never been found in known chronostratigraphic context that is <12.8 ky old (40).

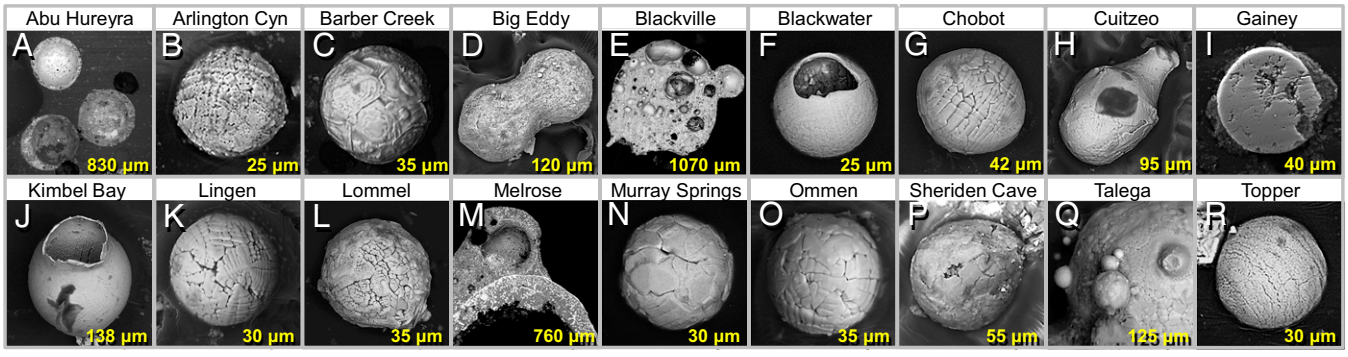

Fig. 3. YDB spherules from 18 sites. SEM images illustrate the wide variety of sizes, shapes, and microstructures of YDB spherules. Diameters are in yellow. EDS compositional percentages corresponding to the letter designations of these 36 YDB spherules are in *SI Appendix*, Table S5. Most spherules are rounded, but there are also dumbbells (*D*), bottle shapes (*H*), gourd shapes (*J*), and ovoids (*P*). Most small spherules are solid, although a few are hollow (*F* and *J*), whereas most large spherules are vesicular and/or hollow (*A*, *E*, and *M*). A large number of spherules were cross-sectioned (n = 137 EDS; *A*, *E*, *I*, and *M*); all others were analyzed whole (n = 335 EDS). Lechatelierite and flow marks (schlieren) that formed at >2,200 °C were observed in spherules from three sites (*A*, *E*, and *M*). Many large spherules display accretion with other spherules (*E*, *M*, and *Q*) and microcratering by smaller spherules (*Q*). Interior and exterior compositions of both spherules are similar, but occasionally, Fe-rich material (thin, light-colored bands) migrated or accreted to the outside of the spherule while molten (*M*). Some spherules have high percentages of TiO_2 (*B*, *L*, and *R*; averaging 42 wt%), inconsistent with anthropogenic and most cosmic origins, but consistent with impact melting of titanomagnetite or ilmenite.

Megafaunal bones, found either at the sampling location or in the vicinity at five sites, were dated approximately to the YD onset (40) and are associated with temporally diagnostic projectile points. Abu Hureyra, the archaeological site in Syria, is unique in representing the origin of domesticated plant cultivation that began at ~12.8 ka, when inhabitants transitioned from hunting-gathering to hunting-cultivating. The western European locations in Germany, Belgium, and the Netherlands were coeval with the decline near 12.8 ka of the Magdalenian and related cultures, known for their elaborate cave paintings and intricate carvings (6).

Bulk sediment was processed in aliquots averaging 228 g (range: 10–1,600 g). On occasion, material was limited, e.g., due to use of small-diameter coring tools. For the 15 noncored sites, the YDB layer was contained in samples that averaged 3.9 cm in thickness (median: 5 cm; range: 1–8 cm). At one hand-cored site, the YDB layer was contained in a sample that was 15-cm thick, and the machine-cored sample was 30-cm thick. The burial depth of the YDB layer averaged 2.52 m (median 1.50 m; range: 0.13–15.00 m). Sampling details are in *SI Appendix*, Table S2.

Abundances and Compositions of Magnetic Grains. After analyzing the magnetic grains and the YD spherules they contain, Firestone et al. (1) and LeCompte et al. (13) reported strong to moderate correlation, respectively, between abundances of the two proxies. To test that correlation, we created slurries of bulk sediment and magnetically extracted the magnetic grain fraction. The maximum YDB magnetic grain concentration in bulk sediments ranged from 0.4 to 73.6 g/kg (average: 7.2 g/kg), and in most samples, concentrations decreased outside the YDB to 0.02–8.9 g/kg (average: 2.0 g; *SI Appendix*, Table S3). Some magnetic grains (but not spherules) were analyzed using neutron activation analysis and prompt gamma activation analysis (*SI Appendix*, Table S4), indicating they are dominantly comprised of magnetite and titanomagnetite. For seven sites, a peak in magnetic grains coincided with a peak in magnetic spherules, whereas for seven other sites, they were found in immediately adjacent layers. For four sites, they were not adjacent. These results support a moderate correlation between peaks in spherules and magnetic grains, indicating that the YDB layer is enriched in both.

Abundances and Stratigraphic Distribution of Spherules. We investigated abundances of YDB spherules at 18 sites, seven of which were common to Firestone et al. (1) and two to LeCompte et al. (13). We identified and measured 771 YDB objects, of which 684 were spherules and 87 were SLOs. Spherule diameters ranged from 5 μm to 5.5 mm (average: 135 μm) with ~50% ≤30 μm (see distribution in *SI Appendix*, Fig. S16). YDB SLOs ranged from 300 μm to 11.75 mm, averaging 2.6 mm (8). Concentrations of spherules in the YDB layer varied widely from 5 to 4,900 spherules per kilogram (average: 955/kg; median: 388). At stratigraphic levels more distant above or below the YDB, spherules were absent or rare, indicating that the influx of normal cosmic spherules was negligible. Layers adjacent to the YDB typically contained lower concentrations of spherules, whose presence is most likely due to redeposition and/or bioturbation from the YDB layer. See Fig. 2 for graphs of spherule and SLO concentrations. At every site investigated, the abundance peak in spherules coincided with the YDB depths previously reported, although estimated concentrations varied from those reported by Firestone et al. (1) by an average of 56% (range: 10–160%), and from LeCompte et al. (13) by 94% (range 19–168%), presumably due to variable deposition, preservation, and preparation. All sites investigated exhibited abundance peaks in spherules at or close to ~12.8 ka, as interpolated in the age-depth models.

Morphologies of Magnetic Spherules. To investigate potential formation mechanisms of YDB spherules, we examined their morphologies using light microscopy followed by SEM. Three types of spherulitic objects were typically encountered in the sedimentary profiles: (*i*) nonimpact, quasi-spherical, detrital magnetite grains that are typically black or dark gray and are common throughout sedimentary profiles; (*ii*) nonimpact, authigenic framboidal spherules that are typically black, gray, or rusty red in color and are common throughout sediments; and (*iii*) YDB spherules that are black, brown, red, blue, green, gray, tan, or white, ranging in clarity from opaque to transparent; these were confined to the YDB layer and closely adjacent strata. Light photomicrographs revealed that all three types are rounded and reflective (*SI Appendix*, Fig. S17). SEM imagery of the rounded detrital magnetite grains indicated that formerly euhedral monocrystals are now rounded but still display remnant faceting, thus eliminating them as impact products. Authigenic framboids appear round when viewed optically, but SEM imaging reveals distinctive blocky surface texturing that results from slow crystalline growth, thus eliminating them as impact spherules. Accurate differentiation of YDB spherules from magnetite grains and framboids is impossible by light microscopy alone and requires the use of SEM/EDS.

There are several accepted groups of melt-products ascribed to known impacts that are relevant to this study; the first is a condensation group, in which glassy impact spherules can condense from rocks that were vaporized during an impact. Such spherules can appear as multiples (i.e., are accretionary), are typically nonvesicular, and do not contain lechatelierite (27, 41). The second is a melt-and-quench group, in which compressive and frictional heating by the impactor subjected the target rocks and impactor to high temperatures that boiled both of them (41). The liquefied rock was then ejected and aerodynamically shaped into spherules, teardrops, ovoids, and dumbbells that are often vesicular and often contain lechatelierite. Collectively, these are called splash-form tektites or microtektites (8, 27, 41). Most YDB spherules are highly reflective spheroids similar to those in each group, but ~10–20% of them exhibit complex aerodynamic shapes, consistent only with splash-formed microtektites. The shapes and surface textures of all YDB spherules are similar to those formed in the Cretaceous–Paleogene extinction (KPg) impact ~65 Ma (28), Chesapeake Bay impact at ~35 Ma (27), Meteor Crater at ~50 ka (8), Tunguska airburst in 1908 (8), and Trinity atomic airburst (8). The similarity of YDB spherules to those from known airbursts (e.g., Tunguska and Trinity) suggests they were caused by an impact/airburst. See SEM images in Fig. 3 and *SI Appendix*, Figs. S17, S18, S24, and S25.

Nearly all of the largest YDB spherules (maximum: 5.5 mm) are vesicular, consistent with outgassing at high temperatures, followed by rapid cooling that preserved the gas bubbles, and in some samples formed quench crystals within the bubbles. The prevalence of vesicles decreases with spherule diameter, and most small spherules <50 μm in diameter are solid. All Fe-rich spherules and some Al-rich ones display dendritic crystals on their surfaces, consistent with high-temperature melting and quenching (8). Most Al-Si–rich spherules are smooth, but sometimes display flow marks, or schlieren, along with melted SiO_2 (lechatelierite) inclusions, both indicative of high-temperature melting at >2,200 °C (8). Approximately 10% of YDB spherules display evidence of accretion (nondestructive fusion of two or more spherules) and/or collisions (destructive interactions between two or more spherules) (8). Destructive collisions require high differential velocities between spherules, and therefore, they frequently result from impacts and meteoritic ablation, but not from other processes, such as volcanism and anthropogenesis (8). SEM images of spherules from four sites illustrate the results of both processes (8). Together, the collective shapes, surface textures, and inferred formation temperatures of YDB spherules are inconsistent with known volcanic or anthropogenic spherules but are consistent with impact spherules.

Geochemical and Petrological Evidence for Spherule Origin. We conducted 750 SEM/EDS analyses (472 on YDB spherules, 153 on SLOs, and 125 on reference materials, including fly ash). Spherules that were ≥50 μm in diameter were typically analyzed both whole and in cross-section (n = 269 EDS). Due to technical difficulties in making cross-sections of very small objects, spherules <50 μm in diameter were only analyzed whole (n = 203 EDS). This analysis is consistent with the methodology of Brownlee et al. (42), who did not obtain cross-sections for the subset of 500 cosmic spherules <50 μm in diameter that were recovered from deep-sea sediments, polar ice, and the stratosphere.

SEM/EDS analyses of candidate spherules provided oxide weight percentages (wt%) for 13 elements. Spherule compositions ranged from homogeneous to heterogeneous, with the three most abundant oxides being iron oxide (expressed as total FeO) with an average of 44.9 wt% (range: 0–100%); silica (SiO_2) averaged 30.9 wt% (range: 0–95%); and aluminum oxide (Al_2O_3) averaged 12.2 wt% (range: 0–65%). The other 10 oxides ranged from 0.1 to 3.5 average wt% (*SI Appendix*, Table S6). The oxide concentrations were inferred from normal oxidation states and not measured directly, making it likely that other compounds are also present. EDS compositional percentages for 36 selected spherules, including those in Fig. 3, are in *SI Appendix*, Table S5. Variation diagrams comparing SiO_2 to FeO, CaO, and Al_2O_3 are shown in *SI Appendix*, Fig. S19. Many of the higher oxide concentrations were found in melted mineral inclusions, e.g., Al_2O_3 at 65 wt% appeared as mullite and sillimanite crystals; CaO at 55 wt% and P_2O_5 at 37 wt% as calcium phosphate; MgO at 41 wt% as olivine; and TiO_2 at 70 wt% as ilmenite–rutile. We also compared oxide abundances of YDB spherules with those of SLOs, but found no significant compositional differences, consistent with formation from similar source minerals (*SI Appendix*, Fig. S20*A*). Similarly, we investigated whether SEM/EDS surface analyses were different from those of cross-sections, but found no significant differences (*SI Appendix*, Fig. S20*B*), indicating that most individual YDB objects are relatively homogeneous.

Our SEM/EDS analyses allow YDB spherules and SLOs to be grouped into two general compositional categories: those enriched in Fe and those enriched in Al-Si, with significant mixing between categories (*SI Appendix*, Figs. S19*A* and S21*A*), e.g., occasionally, Al-Si–rich cores were surrounded by thin high-Fe rims. A flowchart illustrating identification parameters for the two types is shown in *SI Appendix*, Fig. S22. The Fe-rich group is dominated by crystalline minerals requiring high temperatures, including magnetite (Fe_3O_4, melting point >1,550 °C), hematite (Fe_2O_3, >1,550 °C), titanomagnetite (Fe_2TiO_4, >1,400 °C), schreibersite [$(Fe,Ni)_3P$, >1,400 °C], hercynite ($FeAl_2O_4$, >1,700 °C), rutile (TiO_2, >1,840 °C), native Fe (>2,000 °C), and suessite (Fe_3Si, >2,300 °C) (8, 35, 43). The Al-Si–rich group is typically represented by minerals such as high-temperature wollastonite ($CaSiO_3$, melting point >1,500 °C), corundum (crystalline Al_2O_3, >1,800 °C), mullite ($3Al_2O_3$-$2SiO_2$ and $2Al_2O_3$-SiO_2, >1,800 °C), sillimanite (Al_2SiO_5, >1,800 °C), and lechatelierite (SiO_2 glass, >2,200 °C for low-viscosity flow) (8, 35, 43). Because YDB objects contain multiple oxides that are not in equilibrium, the liquidus temperatures may be lower than indicated. Even so, the complete assemblage of minerals in YDB objects is inconsistent with non-impact terrestrial origins, where maximum temperatures are too low (8). The results are consistent with formation by high-temperature, hypervelocity airbursts/impacts.

Potential Biases Favoring Fe-Rich Spherules. In previous spherule work, it was observed that the abundance ratio of Fe-rich spherules to Si-rich ones may suffer from various biases (42). The first bias is magnetic separation bias, which is known to decrease the observed number of nonmagnetic, Si-rich ocean spherules, but is estimated to decrease the totals by only ∼10% (42), a negligible bias. YDB spherules ≥200 μm were usually collected by sieving, and therefore unaffected by magnetic bias. However, spherules <200 μm were typically collected using magnets, and therefore the number of Fe-rich spherules was almost certainly enhanced. The second bias is selection bias. When searching for YDB spherules, it is easier to detect small, dark Fe-rich spherules than lighter Si-rich ones (7, 13), creating a potential cognitive bias. However, experiments designed to detect Si-rich spherules suggest that this bias is negligible, estimated at <10%. The third bias is fractionation bias, due to the melting and cooling of impact material. When boiling impact rock is transported rapidly through the atmosphere, FeO tends to migrate to the rim (41) and may ablate as small spherules, potentially increasing the relative percentage of Fe-rich spherules. Finally, there is preservation bias. Fe-rich spherules are less susceptible to chemical or mechanical alteration than Si-rich spherules; this is observed for Si-rich stony meteorites that decompose with a half-life of 10–15 ky in dry areas of continents (44), and in as little as 2 ky in wetter environments, whereas Ni-Fe meteorites decompose far more slowly. After 13 ky on land, the majority of Si-rich YDB objects may have suffered such decomposition, artificially increasing the ratio of Fe to Si spherules.

To investigate potential preservation biases, we plotted FeO concentrations against spherule diameters. For sites with active depositional paleoenvironments (e.g., rivers, streams, and dunes), all YDB objects averaged 86 wt% FeO, whereas sites with less active paleoenvironments had an average of 25 wt% FeO, ∼3.4× less (*SI Appendix*, Fig. S21 *B* and *C* and Table S6). For YDB objects <50 μm, FeO was 77 wt%, whereas for YDB objects ≥200 μm in all paleoenvironments, the average FeO abundance was 15 wt%, ∼5× less (*SI Appendix*, Table S6). This disparity reveals that Al-Si–rich spherules are significantly underrepresented both in the <50-μm group and at sites with active paleoenvironments, most likely due to the preferential destruction over time of smaller Al-Si–rich spherules, producing a bias in favor of Fe-rich spherules. We conclude that compositions of spherules and SLOs of ≥200 μm are more representative of parent YDB impact materials, and we use those for comparison below with most reference materials.

Potential Origin of YDB Objects by Cosmic Flux. To explore the hypothetical origin of YDB spherules by meteoritic ablation or cosmic influx (10, 11, 34), we compiled data for known cosmic material. First, we compared elemental abundances of 605 previously reported Al-Si–rich cosmic spherules (all <67 wt% FeO)

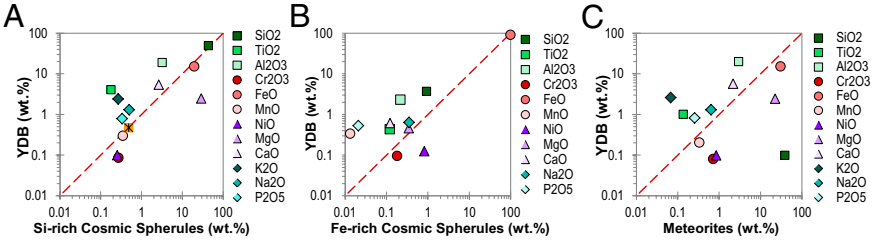

Fig. 4. Comparison of oxide weight percentages; red line marks equivalent values. YDB spherule subsets are in same range for comparability. (*A*) Comparison with Si-rich cosmic spherules (<67 wt% FeO). (*B*) Comparison with Fe-rich cosmic spherules (>63 wt%). (*C*) YDB objects ≥200 μm compared with meteorites and micrometeorites. Some values differ by >10×. Data in *SI Appendix*, Tables S6 and S7.

with Al-Si–rich YDB objects (a subset at <67 wt% FeO, for comparability; Fig. 4*A*; *SI Appendix*, Table S6). Most cosmic Si-rich spherules derive from the most common type of cosmic object, stony meteorites, which are enriched in MgO, so that ~98% of those spherules have >10 wt% MgO (average: 29%; range: 1–55%; *SI Appendix*, Fig. S23*A*) (45, 46). Similarly, ~90% of grains captured from the near-Earth stony asteroid Itokawa had >10 wt% MgO (47), and cometary material captured from Comet 81P/Wild 2 included extraterrestrial grains that averaged 35 wt% MgO (range: 21–55%) (48). By comparison, only ~0.2% of 626 measurements on YDB spherules had >10% MgO, indicating almost none originated from stony meteorites.

We also compared elemental abundances of 90 Fe-rich cosmic spherules having >63 wt% FeO with YDB objects (subset >63 wt % FeO), but found them to be dissimilar (Fig. 4*B*; *SI Appendix*, Table S6). For example, Ni is common in Ni-Fe meteorites with an average concentration of 10 wt% (range: 5–25 wt%) (49), whereas Ni is depleted 100× in YDB spherules with an average concentration of 0.1 wt% (range: 0–2 wt%). None of the YDB objects (184 EDS cross-sectioned; 441 EDS whole) have concentrations of Ni of >1 wt%, demonstrating a poor match for Ni-Fe meteorites. We also compared elemental abundances of YDB objects ≥200 μm with 262 different meteorites and micrometeorites, finding a poor match (Fig. 4*C*; *SI Appendix*, Table S6). Furthermore, most meteorites except, for example, those from the Moon and Mars, have low percentages of TiO_2, averaging >0.14 wt%. YDB spherules with diameter <50 μm averaged 5.0 wt% TiO_2, or 35× higher, and 26 of those had average TiO_2 of 41 wt% (range: 12–70 wt%), including those exhibited in Fig. 3 *B*, *R*, and *L*. Together, the geochemical comparisons indicate that the vast majority of YDB objects are unlikely to have formed from material found in known stony asteroids, Ni-Fe meteorites, or comets, but that does not preclude formation of spherules from target rocks during impacts by such objects.

We compared abundances of YDB spherules with the influx rate of cosmic spherules observed in the Antarctic ice sheet. The 1991 European Meteorite Collection Program Antarctic Expedition discovered an average of only one cosmic spherule in 67 kg (0.015 spherules per liter) (50) of continuously deposited preindustrial ice. In contrast, the average value for the YDB layer is 955 spherules per kilogram, or 67,000× higher. Similarly, Badyukov et al. (51) calculated the terrestrial flux rate of cosmic spherules at one spherule per square centimeter of Earth's surface per 1–2 million years. For the YDB layer with an average density of 6.3 spherules per square centimeter, this flux rate would require >6 million years to produce the observed accumulation of YDB spherules. As one proposed explanation, some researchers (10, 11, 34) have countered that the apparent concentrations of YDB spherules may result from formation of lag deposits that accumulated over thousands to millions of years on a geologically stable surface. However, based on age-depth models for YDB sites that show no significant hiatuses, and based on the paucity of spherules outside of the YDB, that hypothesis is not supported by the age-depth models in *SI Appendix*, Figs. 2–15. Cosmic spherules appear to comprise an extremely small percentage of YDB spherules.

Potential Anthropogenic Origin of YDB Spherules. To evaluate the proposed anthropogenic origin of YDB materials (34), we studied one of the most common industrial contaminants, fly ash grains (n = 143 EDS) and anthropogenic spherules (n = 42 EDS) from 13 countries in North America and Europe. If YDB spherules are anthropogenic, then they are young and would not have experienced degradation of Si-rich spherules in sediment; consequently, we compared the anthropogenic material to all YDB spherules and SLOs. YDB objects contain more Fe (5×), Cr (9×), and Mn (×5) than fly ash and related spherules, and thus are unlikely to be anthropogenic (Fig. 5*A*). Additionally, most YDB layers were located at depths of 2–15 m, and great care was taken during sample collection to reduce the possibility of anthropogenic contamination. Furthermore, millimeter-sized airborne objects tend to fall out of the atmosphere close to their source (8), and there are no major anthropogenic sources sufficiently close to most of the 18 study sites. Therefore, YDB spherules with diameters of up to 5.5 mm are inconsistent with long-range atmospheric transport of anthropogenic materials. In addition, when temporally diagnostic cultural artifacts and/or megafaunal remains were present at sampling locations, there was no indication of displacement of the YDB layers, indicating that contamination by modern materials is unlikely. We conclude that the majority of YDB spherules were found in situ, and that anthropogenic glass or spherules represent a small percentage of the assemblage, if any.

Potential Volcanic Origin of YDB Spherules. We compiled >10,000 compositional analyses of volcanic glass and spherules from sites in four oceans. Compositions of YDB objects ≥200 μm are higher in oxides of Cr (8×) and K (11×) and lower in Mg (3×) and Na (2×) than volcanic material, and thus are geochemically dissimilar (Fig. 5*B*). YDB compositions are also enriched in K (89×) and P (37×) over mantle material (52). This poor correspondence indicates that YDB objects are not comprised of volcanic or mantle material (Fig. 5*C*). The YDB layers and contiguous strata at 18 sites also do not contain visible tephra or volcanogenic silica (tridymite) that typically occurs as bipyramidal euhedral crystals. In summary, it is unlikely that a volcanic eruption could have deposited millions of tonnes of volcanic spherules across a 12,000-km-wide region without leaving any other mineralogical, geochemical, or geological evidence.

Potential Origin of YDB Spherules by Lightning. Another hypothesis for spherule formation is that the YDB spherules formed through atmospheric lightning discharges (53). Besides cosmic impact, lightning is the only documented process that can account for lechatelierite inside YDB spherules (54). Such discharges generate intense magnetic fields, and after rapid cooling of lightning-melted spherules, strong magnetic characteristics should remain (53, 55, 56). Even though formation by lightning is unlikely given the wide geographical distribution of YDB spherules and the paucity of lightning melt products (e.g., fulgurites) above, below, or inside the YDB, we measured the magnetic characteristics of YDB spherules from two sites: Gainey, Michigan, and Blackwater Draw, New Mexico. To pre-

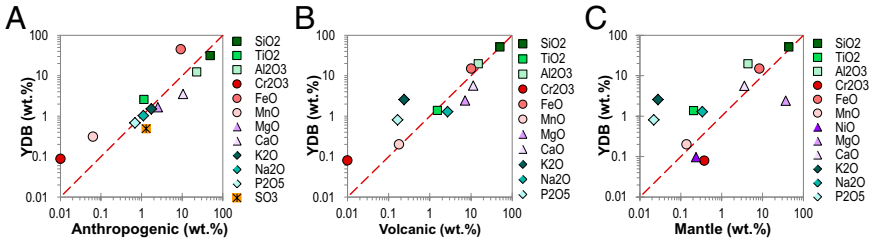

Fig. 5. Comparison of compositions of YDB spherules and SLOs with (*A*) anthropogenic spherules and fly ash. (*B*) YDB objects ≥200 μm compared with volcanic glass and spherules, and (*C*) material from Earth's mantle. Red dashed line marks equivalent values. Note that some values differ by more than an order of magnitude. Data shown are in *SI Appendix*, Tables S6 and S7.

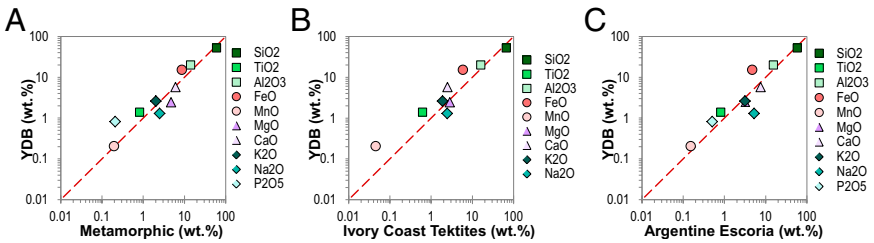

Fig. 6. Comparison of composition of YDB spherules and SLOs at ≥200 μm with (*A*) metamorphic rocks; (*B*) Ivory Coast tektites; and (*C*) Argentine Escoria. Red dashed line represents equivalent values. Data shown are in *SI Appendix*, Tables S6 and S7.

serve the spherules original magnetic state, nonmagnetic separation techniques were used (heavy liquids), followed by nonmagnetic, mechanical separation that was performed using sieves of various sizes (~37, 44, 74, and 149 μm). The separates were cleaned of excess clay using ultrasonication and then analyzed under an optical microscope. When candidate spherules were identified, they were manually placed on glass plates and examined using SEM. Remanent magnetization in the spherules was measured using a magnetic scanner and a superconducting magnetometer. There was no excess magnetization of the spherules while in Earth's ambient geomagnetic field (50 μT). However, after being subjected to a powerful laboratory-generated magnetic field (1 T), the YDB spherules displayed substantial remanent magnetization, indicating their ability to become magnetized toward saturation (*SI Appendix*, Fig. S24). These results are consistent with the hypothesis that when the spherules formed during an extraterrestrial impact, they were subjected only to the ambient geomagnetic field, and exclude the possibility that these spherules formed during lightning discharges.

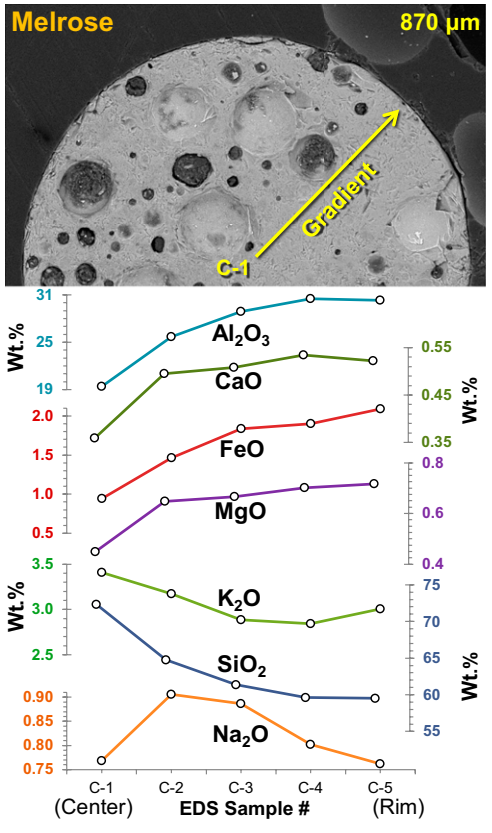

Fig. 7. Melrose spherule with diameter in yellow, showing approximate radial traverse for seven EDS analyses. Refractory oxides (Al, Ca, Fe, and Mg) increase toward rim; less-refractory oxides (Si and K) decrease toward rim. Na weight percentages are mixed, but generally decrease. These variations are consistent with boiling rock at temperatures of ~2,200 °C to 3,600 °C. Data are in *SI Appendix*, Table S8.

Evidence for an Impact Origin of YDB Spherules. If an impact occurred at the YD onset, then YDB spherules should be geochemically similar to terrestrial rocks and sediment, and to investigate that, we compared spherule compositions with those of >100,000 samples of terrestrial sediments and minerals from across North America, including sedimentary, igneous, and metamorphic rocks from the US Geological Survey National Geochemical Database (59, 60). YDB spherules are compositionally similar to surficial sediments and metamorphic rocks, e.g., mudstone, shale, gneiss, schist, and amphibolite (Fig. 6*A*; *SI Appendix*, Table S6), which suggests that YDB objects formed by the melting of heterogeneous surficial sediments comprised of weathered metamorphic and other similar rocks. This is consistent with a cosmic impact, in which the impactor contributed an unknown percentage of material.

We also reviewed >1,000 analyses of impact-related material, including spherules and tektites—melt-glasses that typically contain lechatelierite—to compare the YDB event with 12 known craters and strewnfields on six continents. Some melt-glasses (Argentine Escoria and Dakhleh glass) are morphologically similar to YDB SLOs (8), whereas other types are not (Australasian tektites and moldavites from Ries Crater). Most tektites are derived from melted surficial sediments and/or metamorphic rocks, typically comprised of silicates, limestone, shale, and/or clay (61, 62). The compositions of YDB objects are different from the KPg and Chesapeake Bay impactites, but similar to Ivory Coast tektites (Fig. 6*B*), Argentine Escoria (Fig. 6*C*), Tasman Sea tektites (*SI Appendix*, Fig. S23*B*), and Tunguska spherules (*SI Appendix*, Fig. S23*C* and Table S6).

YDB spherules and SLOs also are morphologically and compositionally similar to spherule-rich materials, called trinitite, produced by the melting of surficial sediments by two nuclear aerial detonations (8). One detonation was at the Trinity site near Socorro, New Mexico (36, 37), and the other at Yucca Flat, Nevada (63); both were near-surface airbursts rather than below-ground detonations. Trinity produced highly abundant spherules from a crater that was 80 m wide and 1.4 m deep, providing an analog for a cosmic airburst/impact (8). The thermal pulse and air shock were produced by different mechanisms (a rapidly moving cosmic object vs. a pulse of atomic radiation), but even so, the resulting melted material is indistinguishable.

To investigate the thermochemical history of the spherules, we reviewed the work of Elkins-Tanton et al. (41, §), who analyzed cross-sectioned spherules from five known impact events (Australasian, Ries, Bosumtwi, Chesapeake Bay, and Popigai) and

[§]Elkins-Tanton LT, Kelly DC, Bico J, Bush JWM, Microtektites as vapor condensates, and a possible new strewn field at 5 Ma. Thirty-Third Annual Lunar and Planetary Science Conference, March 11–15, 2002, Houston, TX, abstr 1622.

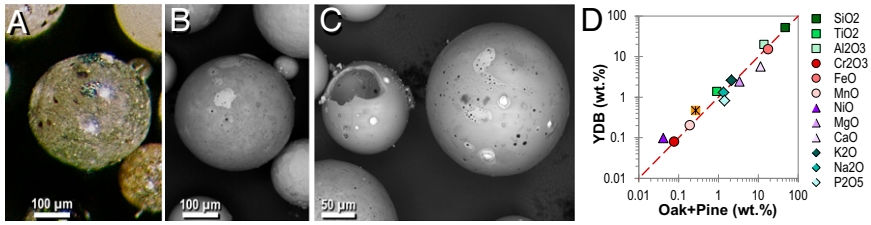

Fig. 8. Al-Si–rich laboratory spherules made at >1,730 °C. (*A*) Micrograph of oak spherules; largest = 350 μm. (*B*) SEM image of same oak spherule group. (*C*) SEM image of pine spherules; largest = 220 μm. (*D*) YDB objects ≥200 μm compared with Al-Si–rich oak and pine. Red dashed line represents equivalent values. Data shown are in *SI Appendix*, Tables S6 and S7.

found that each spherule displayed compositional gradients between the rim and center. The authors argued that the gradients resulted from two processes, the first of which, vaporization, occurred when surface tension shaped boiling impact rock into spherules, after which constituent oxides vaporized at varying rates. Refractory oxides, such as MgO (boiling point: 3,600 °C), FeO (3,414 °C), Al_2O_3 (2,980 °C), and CaO (2,850 °C) (43) reached their boiling points later and became enriched toward the rim. Conversely, SiO_2 (2,230 °C) and Na_2O (1,950 °C) usually were depleted toward the rim because of their lower boiling points. The second process, condensation, occurred as various oxides or elements condensed from their vapor state to form spherules. According to Elkins-Tanton et al. (41), condensation had the opposite effect on composition, because higher-temperature oxides condensed from vapor to liquid earliest as plume temperatures fell, producing enrichment at the center of the spherule, and lower-temperature oxides or elements condensed from vapor last, becoming enriched toward the rim. For condensation, the presence of a reverse gradient implies that temperatures of the melted rock possibly were >3,600 °C, the boiling point of MgO.

To investigate whether compositional gradients are present in YDB spherules, we acquired data on 4–5 points along a radius from center to rim of cross-sectioned spherules from three sites (Abu Hureyra, Blackville, and Melrose). For 11 of the 13 spherules analyzed (85%), there were discernible gradients of oxide values (Fig. 7; *SI Appendix*, Fig. S25 and Table S8): 7 of 13 displayed generally decreasing trends for SiO_2, indicating boiling; 4 of 13 displayed increasing trends for SiO_2, suggesting condensation; and 2 of 13 displayed no clear gradients. Oxides with abundances of less than a few percent were more variable, presumably due to high analytical uncertainties. Nearly all oxides behaved predictably, but occasionally, one or more oxides displayed an opposite trend to that predicted, for reasons that are unclear. Several spherules displayed a distinct high-Fe shell a few microns thick surrounding an Al-Si interior, presumably due to condensation, ablation, or accretion. The presence of both increasing and decreasing gradients in YDB spherules suggests that there were sufficiently high temperatures and flight times for vaporization and condensation to occur. No plausible process besides a cosmic airburst/impact is capable of boiling or vaporizing airborne rock at >2,200 °C long enough to produce millimeter-sized spherules that display compositional gradients.

Possible Spherule Formation by Impact-Related Wildfires. Burleigh and Meeks (35) reported the formation of glassy spherules by combustion of wood charcoal, and speculated that temperatures >2,000 °C were required for optimum spherule production. We explored this possible origin for YDB spherules by conducting wood-burning laboratory experiments using an oxygen/propylene burner with a maximum temperature of ~2,900 °C; temperatures were confirmed using pyrometry. For the wood source, we used dried twigs of oak (*Quercus turbinella*) and pine (*Pinus ponderosa*) with a diameter of 0.5–1.0 cm.

At temperatures of ~1,600 °C, the flame transformed the wood into charcoal and then rapidly to whitish-gray ash. At ~1,730 °C, the melting point of SiO_2, the ash began to melt and transform by surface tension into spherules that were ejected from the twig by flame pressure (Fig. 8 *A* and *B*). Spherule production increased up to 2,600 °C, the maximum temperature measured. Within a few minutes, a small twig (6 × 0.5 cm) produced >600 spherules, ranging in diameter from 30 to 700 μm, with the majority at the lower end of that range (50–80 μm). Of the original weight of oak and pine, ~97% was transformed into water vapor and other gases, ~1% remained as ash, and ~2% by weight of spherules were formed from biogenic silica and other trace mineral oxides (e.g., Al, Si, and Ca). Most of the melted objects formed as spherules, although a small percentage (<5%) formed as aerodynamically shaped teardrops and ovoids; often, multiple spherules fused together. Colors included black, brown, red, blue, green, gray, tan, and white, with clarity ranging from opaque to transparent. Nearly all spherules are highly vesicular, and some are hollow with a thin glass shell (Fig. 8*C*); some display flow marks or schlieren consistent with high temperatures and low viscosity, as seen in YDB spherules. Average compositions of oak and pine closely match compositions of Al-Si–rich YDB objects (Fig. 8*D*). Although we observed inclusions of up to 75 wt% FeO, we found no complete high-Fe spherules with Fe quench crystals. These results show that the incineration of biomass at ~1,730–2,600 °C can produce glassy spherules, and we conclude that a significant percentage of YDB Al-Si–rich spherules could have formed by the impact-related incineration of biomass, but not the high-Fe spherules. The requisite temperature of 1,730 °C is above the maximum temperature ever recorded in a wildfire (8).

Geographical Distribution of Spherules. There are three major impact strewnfields, the largest of which is the 780,000-y-old Australasian tektite field, spanning 50 million square kilometers (Fig. 1; Table 1) (25, 26). Another is the 35-million-y-old North American tektite field, covering 42 million square kilometers and associated with the 85-km-wide Chesapeake Bay crater (25, 26). The last strewnfield is the 970,000-y-old Ivory Coast field, covering 4 million square kilometers and associated with the 10.5-km-wide Bosumtwi crater in Ghana, Africa (Table 1) (25, 26). Although the maximum extent of the YDB field has not yet been established, its known extent is ~50 million square kilometers, making it 10× larger than the smallest field in Table 1 and equal

Table 1. Comparison of tonnage in the YDB strewnfield with known impact strewnfields

Field name	Age	~% of Earth	Size, km^2	Metric tons	Source
Eocene	~35 Ma	8	4.2×10^7	100×10^7	19
Australasian	~780 ka	10	5.0×10^7	10×10^7	18
Ivory Coast	~970 ka	1	0.4×10^7	2×10^7	18
YDB field	~12.9 ka	10	5.0×10^7	1×10^7	This work

in size to the largest one, the Australasian field (Fig. 1). Using standard calculations for determining the mass of spherules deposited in an impact strewnfield (25, 26), and assuming that currently observed average values are representative of the entire field, we estimate the mass of the YDB field to equal ~10 million tonnes; this is approximately half the tonnage of the Ivory Coast field associated with the Bosumtwi Crater (10.5 km wide), thus implying a major impact event (Table 1; computational variables in *SI Appendix*, Table S9).

Preliminary Impact Model. At present, there are insufficient data to characterize the YDB impactor and impact event, and more research is required to determine the type and size of impactor, maximum extent of the strewnfield, and abundances of minor elements. However, existing data suggest the following scenario, as also discussed by Israde et al. (7). The impactor was most likely an asteroid or comet greater than several hundred meters in diameter with maximum size unknown, but probably less than several kilometers in diameter. The impactor most likely broke apart in solar orbit before encountering Earth, as do most comets (64), including Comet Shoemaker–Levy 9, which impacted Jupiter as multiple fragments, the largest of which was ~1 km in diameter. When fragments of the YDB impactor entered Earth's atmosphere, they fragmented even further, yielding multiple atmospheric airbursts that each produced shock fronts. This multi-impact scenario is supported by two lines of evidence: first, the concentrations of multimillimeter-sized YDB melt-glass and spherules in Syria, Pennsylvania, South Carolina (8, 17), Arizona (15), and Venezuela (18–21) are separated by up to 12,000 km. Such multimillimeter-sized, aerodynamically shaped objects are probably too large to have traveled 12,000 km during a single airburst/impact (8). Second, the compositions of YDB objects differ substantially between regions, as indicated in *SI Appendix*, Fig. S26, showing that YDB objects from the relatively close Blackville and Melrose sites are compositionally similar to each other, but dissimilar to those of Abu Hureyra, arguing that multiple airbursts/impacts interacted with different types of regional target rocks.

Beneath the flight path of the impactor fragments, thermal radiation from the air shocks was intense enough to melt Fe-rich and Si-rich surficial sediments, transforming them into lechatelierite-rich melt-glass and spherules at >2,200 °C. Multiple airbursts/impacts over a wide area can account for the heterogeneity of the melt materials. In addition, high temperatures may have produced spherules and melt-glass by incinerating vegetation within the fireballs and shock fronts. High-velocity winds and attenuated air shocks lofted the melted material into the upper atmosphere, where high-altitude winds transported them over a wide area. As previously suggested (7), nanodiamonds potentially formed from vaporized carbon within localized, transiently anoxic regions of the shock front. This impact model is speculative because the exact nature of airbursts is poorly constrained. For example, the complexity of airburst phenomena is only hinted at by the recent hydrocode modeling of Boslough and Crawford (65), who concluded that more realistic airburst simulations are needed to understand the phenomenon.

Methods

To determine replicability of the protocol for magnetic grain and spherule extractions, various samples were processed by nine coauthors (J.P.K., D.J.K., D.F., I.-I.A., J.B.K., Z.R., D.R.K., G.K., and A.W.), using previously published protocol (1, 7, 13). After size-sorting with multiple American Society for Testing and Materials screens, we used a 150–300× reflected light microscope to manually count, photograph, and extract selected spherules. Next, cross-sectioned and whole spherules were examined by 10 coauthors (J.H.W., J.C.W., T.E.B., J.P.K., D.J.K., I.-I.A., J.L.B., R.E.H., G.K., and A.W.), using SEM and EDS to distinguish between impact-related spherules and other types. To ensure acquisition of correct bulk compositions of spherules, EDS analyses were acquired multiple times and/or at large beam spot sizes of ~30 μm. A flowchart illustrating identification parameters is in *SI Appendix*, Fig. S22. Standard techniques were followed for all analytical methods (*SI Appendix*, *SI Methods*).

Conclusions

The analyses of 771 YDB objects presented in this paper strongly support a major cosmic impact at 12.8 ka. This conclusion is substantiated by the following:

Spherules and SLOs are (*i*) widespread at 18 sites on four continents; (*ii*) display large abundance peaks only at the YD onset at ~12.8 ka; (*iii*) are rarely found above or below the YDB, indicating a single rare event; and (*iv*) amount to an estimated 10 million tonnes of materials distributed across ~50 million square kilometers of several continents, thus precluding a small localized impact event.

Spherule formation by volcanism, anthropogenesis, authigenesis, and meteoritic ablation can be rejected on geochemical, morphological, and/or thermochemical grounds, including the presence of lechatelierite (>2,200 °C).

Spherule formation by lightning can be eliminated due to magnetic properties of spherules and the paucity of lightning melt-products (e.g., fulgurites) above or below the YDB.

Morphologies and compositions of YDB spherules are consistent with an impact event because they (*i*) are compositionally and morphologically similar to previously studied impact materials; (*ii*) closely resemble terrestrial rock compositions (e.g., clay, mud, and metamorphic rocks); (*iii*) often display high-temperature surface texturing; (*iv*) exhibit schlieren and SiO_2 inclusions (lechatelierite at >2,200 °C); (*v*) are often fused to other spherules by collisions at high-temperatures; and (*vi*) occasionally display high-velocity impact cratering.

High-temperature incineration of biomass (>1,730 °C) produced laboratory spherules that are similar to YDB spherules, providing a complementary explanation that some unknown percentage of YDB spherules may have formed that way.

Abundances of spherules covary with other YDB impact proxies, including nanodiamonds, high-temperature melt-glass, carbon spherules, aciniform carbon, fullerenes, charcoal, glass-like carbon, and iridium.

The geographical extent of the YD impact is limited by the range of sites available for study to date and is presumably much larger, because we have found consistent, supporting evidence over an increasingly wide area. The nature of the impactor remains unclear, although we suggest that the most likely hypothesis is that of multiple airbursts/impacts by a large comet or asteroid that fragmented in solar orbit, as is common for nearly all comets. The YD impact at 12.8 ka is coincidental with major environmental events, including abrupt cooling at the YD onset, major extinction of some end-Pleistocene megafauna, disappearance of Clovis cultural traditions, widespread biomass burning, and often, the deposition of dark, carbon-rich sediments (black mat). It is reasonable to hypothesize a relationship between these events and the YDB impact, although much work remains to understand the causal mechanisms.

ACKNOWLEDGMENTS. We are grateful for receiving crucial samples, data, and/or assistance from William Topping, Vance Haynes, Joanne Dickinson, Don Simons, Scott Harris, Malcolm LeCompte, Mark Demitroff, Yvonne Malinowski, Paula Zitzelberger, and Lawrence Edge. Bulk sample collection and/or preparation for various sites were conducted by Brendan Culleton, Carley Smith, and Karen Thompson. Dustin Thompson produced an age-depth plot for the Big Eddy site. Ferdi Geerts, Ab Goutbeek, and Henri Jutten provided field assistance in the Netherlands and Belgium. The assistance and support of Keith Hendricks of Indian Trail Caverns (Sheriden Cave), Brian Redmond, and the Cleveland Museum of Natural History are greatly appreciated, as are the suggestions of four anonymous reviewers. Support for this study was provided by the Court Family Foundation, Charles Phelps Taft Foundation, and University of Cincinnati Research Council (K.B.T.); US Department of Energy Contract DE-AC02-05CH11231 and US National Science Foundation Grant 9986999 (to R.B.F.); US National Science Foundation Grants ATM-0713769 and OCE-0825322, Marine Geology and Geophysics (to J.P.K.); and Ministry of Education Youth and Sports Grant LK21303 (to G.K.).

1. Firestone RB, et al. (2007) Evidence for an extraterrestrial impact 12,900 years ago that contributed to the megafaunal extinctions and the Younger Dryas cooling. *Proc Natl Acad Sci USA* 104(41):16016–16021.
2. Kennett DJ, et al. (2008) Wildfire and abrupt ecosystem disruption on California's Northern Channel Islands at the Ållerød–Younger Dryas boundary (13.0–12.9 ka). *Quat Sci Rev* 27:2530–2545.
3. Kennett DJ, et al. (2009) Shock-synthesized hexagonal diamonds in Younger Dryas boundary sediments. *Proc Natl Acad Sci USA* 106(31):12623–12628.
4. Kennett DJ, et al. (2009) Nanodiamonds in the Younger Dryas boundary sediment layer. *Science* 323(5910):94.
5. Kurbatov AV, et al. (2011) Discovery of a nanodiamond-rich layer in the Greenland ice sheet. *J Glaciol* 56:749–759.
6. Anderson DG, et al. (2011) Multiple lines of evidence for possible Human population decline/settlement reorganization during the early Younger Dryas. *Quat Int* 242: 570–593.
7. Israde-Alcántara I, et al. (2012) Evidence from central Mexico supporting the Younger Dryas extraterrestrial impact hypothesis. *Proc Natl Acad Sci USA* 109(13):E738–E747.
8. Bunch TE, et al. (2012) Very high-temperature impact melt products as evidence for cosmic airbursts and impacts 12,900 years ago. *Proc Natl Acad Sci USA* 109(28): E1903–E1912.
9. Jones TL, Kennett DK (2012) . A land impacted? The Younger Dryas boundary event in California. *Contemporary Issues in California Archaeology*, eds Jones TL, Perry JE (Left Coast, Walnut Creek, CA), pp 37–48.
10. Surovell TA, et al. (2009) An independent evaluation of the Younger Dryas extraterrestrial impact hypothesis. *Proc Natl Acad Sci USA* 106(43):18155–18158.
11. Pinter N, et al. (2011) The Younger Dryas impact hypothesis: A requiem. *Earth Sci Rev* 106:247–264.
12. Boslough MBE, et al. (2012) Arguments and evidence against a Younger Dryas Impact Event. *Geophys Monogr Ser* 198:13–26.
13. LeCompte MA, et al. (2012) Independent evaluation of conflicting microspherule results from different investigations of the Younger Dryas impact hypothesis. *Proc Natl Acad Sci USA* 109(44):E2960–E2969, 10.1073/pnas.1208603109.
14. Pigati JS, et al. (2012) Accumulation of impact markers in desert wetlands and implications for the Younger Dryas impact hypothesis. *Proc Natl Acad Sci USA* 109(19): 7208–7212.
15. Fayek M, Anovitz LM, Allard LF, Hull S (2012) Framboidal iron oxide: chondrite-like material from the black mat, Murray Springs, Arizona. *Earth Planet Sci Lett* 319-320: 251–258.
16. Haynes CV, Jr., et al. (2010) The Murray Springs Clovis site, Pleistocene extinction, and the question of extraterrestrial impact. *Proc Natl Acad Sci USA* 107(9):4010–4015.
17. Wu Y (2011) Origin and provenance of magnetic spherules at the Younger Dryas boundary. PhD thesis (Dartmouth College, Hanover, NH).
18. Mahaney WC, Krinsley D (2012) Extreme heating events and effects in the natural environment: Implications for environmental geomorphology. *Geomorphology* 139-140:348–359.
19. Mahaney WC, et al. (2010) Evidence from the northwestern Venezuelan Andes for extraterrestrial impact: The black mat enigma. *Geomorphology* 116(1-2):48–57.
20. Mahaney WC, et al. (2011) Fired glaciofluvial sediment in the northwestern Andes: Biotic aspects of the Black Mat. *Sediment Geol* 237(1-2):73–83.
21. Mahaney WC, et al. (2011) Notes on the black mat sediment, Mucunuque Catchment, northern Mérida Andes, Venezuela. *J Adv Microscop Res* 6(3):177–185.
22. Wright FW, Hodge PW (1965) Studies of particles for extraterrestrial origin, Part 4. Microscopic spherules from recent volcanic eruptions. *J Geophys Res* 70(16): 3889–3898.
23. Scott AC, et al. (2010) Fungus, not comet or catastrophe, accounts for carbonaceous spherules in the Younger Dryas "impact layer". *Geophys Res Lett* 37(14):L14302.
24. Daulton TL, Pinter N, Scott AC (2010) No evidence of nanodiamonds in Younger-Dryas sediments to support an impact event. *Proc Natl Acad Sci USA* 107(37):16043–16047.
25. Glass BP, Swincki MB, Zwart PA (1979) Australasian, Ivory Coast and North American tektite strewnfields: Size, mass and correlation with geomagnetic reversals and other earth events. *Proceedings of the 10th Annual Lunar Planet Science Conference* (Pergamon, New York), pp 2535–2545.
26. Glass BP, Burns CA, Crosbie JR, DuBois DL (1985) Late Eocene North American microtektites and clinopyroxene-bearing spherules. *J Geophys Res* 90(S01):D17S–D196.
27. Glass BP, Huber H, Koeberl C (2004) Geochemistry of Cenozoic microtektites and clinopyroxene-bearing spherules. *Geochim Cosmochim Acta* 69:3971–4006.
28. Mathur SC, Gaur SD, Loyal RS, Tripathi A, Sisodia MS (2005) Spherules from the Late Cretaceous phosphorite of the Fatehgarh Formation, Barmer Basin, India. *Gondwana Res* 8:579–584.
29. Korchagin OA (2010) Metallic microspheres and microparticles in lower Cenomanian sediments of the Crimea: Evidence for the cosmic dust event. *Dokl Earth Sci* 431(Pt 2): 441–444.
30. Smit J (1990) Meteorite impact, extinctions and the Cretaceous-Tertiary boundary. *Geol Mijnb* 69:187–204.
31. Mukhopadhyay R, Iyer SD, Ghosh AK (2002) The Indian Ocean nodule field: Petrotectonic evolution and ferromanganese deposits. *Earth Sci Rev* 60:67–130.
32. Thy P (1995) Implications of prehistoric glassy biomass slag from east-central Botswana. *J Archaeol Sci* 22:629–637.
33. Hein JR, Griggs GB (1972) Distribution and scanning electron microscope (SEM) observations of authigenic pyrite from a Pacific deep-sea core. *Deep Sea Res* 19(2): 133–138.
34. Del Monte M, Sabbioni C (1984) Morphology and mineralogy of fly ash from a coal-fueled power plant. *Arch Met Geoph Biocl B* 35(1-2):93–104.
35. Burleigh R, Meeks N (1986) Glassy microspherules from bomb combustion of charcoal. *Radiocarbon* 28(1):165–166.
36. Eby N, Hermes R, Charnley N, Smoliga JA (2010) Trinitite—the atomic rock. *Geol Today* 26:181–186.
37. Hermes RE, Strickfaden WB (2005) A new look at trinitite. *Nucl Weap J* 2:2–7.
38. Wasson JT (2003) Large aerial bursts: An important class of terrestrial accretionary events. *Astrobiology* 3(1):163–179.
39. Waters MR, Stafford TW, Jr. (2007) Redefining the age of Clovis: Implications for the peopling of the Americas. *Science* 315(5815):1122–1126.
40. Haynes CV, Jr. (2008) Younger Dryas "black mats" and the Rancholabrean termination in North America. *Proc Natl Acad Sci USA* 105(18):6520–6525.
41. Elkins-Tanton LT, Aussillous P, Bico J, Quere D, Bush JWM (2003) A laboratory model of splash-form tektites. *Meteorit Planet Sci* 38(9):1331–1340.
42. Brownlee DE, Bates B, Schramm L (1997) The elemental composition of stony cosmic spherules. *Meteorit Planet Sci* 32:157–175.
43. Kracek FC (1963) Melting and transformation temperatures of mineral and allied substances. *Geological Survey Bulletin 1144-D* (US Government Printing Office, Washington, DC).
44. Jull AJT, Donahue DJ, Cielaszyk E, Wlotzka F (1993) Carbon-14 terrestrial ages and weathering of 27 meteorites from the southern high plains and adjacent areas (USA). *Meteoritics* 28(2):188–195.
45. Taylor S, Brownlee DE (1991) Cosmic spherules in the geologic record. *Meteoritics* 26: 203–211.
46. Taylor S, Lever JH, Harvey RP (2000) Numbers, types, and compositions of an unbiased collection of cosmic spherules. *Meteorit Planet Sci* 35:651–666.
47. Nakamura E, et al. (2012) Space environment of an asteroid preserved on micrograins returned by the Hayabusa spacecraft. *Proc Natl Acad Sci USA* 109(11):E624–E629.
48. Flynn GJ, et al. (2006) Elemental compositions of comet 81P/Wild 2 samples collected by Stardust. *Science* 314(5806):1731–1735.
49. Daode W, Yongheng C (1996) The chemical compositions of Antarctic iron meteorites and their classification. *Advances in Polar Science* 7:41–49.
50. Maurette M, Pourchete M, Perreau M (1992) The 1991 EUROMET micrometeorite collection at Cap-Prudhomme, Antarctica. *Meteoritics* 27:473–475.
51. Badyukov DD, Ivanov AV, Raitala J, Khisina NR (2011) Spherules from the Tunguska event site: Could they originate from the Tunguska Cosmic Body? *Geochem Int* 49: 641–653.
52. McDonough WF (1991) Chemical and isotopic systematics of continental lithospheric mantle. *Kimberlites, Related Rocks and Mantle Xenoliths*, eds Meyer HOA, Leonardos OH (Companhia de Pesquisa de Recursos Minerais, Rio de Janeiro), Vol 1, pp 478–485.
53. Kletetschka G (2001) Electric discharge in carbonaceous meteorites? *First Steps in the Origin of Life in the Universe*, eds Chela-Flores J, et al. (Springer, Dordrecht), pp 157–159.
54. French BM (1998) *Traces of Catastrophe: A Handbook of Shock-Metamorphic Effects in Terrestrial Meteorite Impact Structures*. LPI Contribution No. 954 (Lunar and Planetary Inst, Houston), pp 102–103.
55. Kletetschka G, Kohout T, Wasilewski PJ (2003) Magnetic remanence in the Murchison meteorite. *Meteorit Planet Sci* 38(3):399–405.
56. Wasilewski P, Kletetschka G (1999) Lodestone: Natures only permanent magnet—what it is and how it gets charged. *Geophys Res Lett* 26(15):2275–2278.
57. Kletetschka G et al. (2006) TRM in low magnetic fields: a minimum field that can be recorded by large multidomain grains. *Phys Earth Planet In* 154(3-4):290–298.
58. Wasilewski P, Acuna MH, Kletetschka G (2002) 433 Eros: Problems with the meteorite magnetism record in attempting an asteroid match. *Meteorit Planet Sci* 37(7):937–950.
59. US Geological Survey (2001) *Geochemistry of Soils in the US from the PLUTO Database* (USGS, Reston, VA).
60. US Geological Survey (2008) *Geochemistry of Rock Samples from the National Geochemical Database* (US Geological Survey, Reston, VA), http://mrdata.usgs.gov/ngdb/rock/.
61. Koeberl C (1986) Geochemistry of tektites and impact glasses. *Annu Rev Earth Planet Sci* 14:323–350.
62. Claeys P, Casier J-G (1994) Microtektite-like impact glass associated with the Frasnian-Famennian boundary mass extinction. *Earth Planet Sci Lett* 122:303–315.
63. Glass BP, Senftle FE, Muenow DW, Aggrey KE, Thorpe AN (1987) Atomic bomb glass beads: Tektite and microtektite analogs. *Proceedings of the Second International Conference on Natural Glasses*, ed Konta J (Charles Univ, Prague), pp 361–369.
64. Napier WM (2010) Palaeolithic extinctions and the Taurid Complex. *Mon Not R Astron Soc* 405:1901–1906.
65. Boslough MBE, Crawford DA (2008) Low altitude airbursts and the impact threat. *Int J Impact Eng* 35(12):1441–1448.

Evidence for Deposition of 10 Million Tonnes of Cosmic Impact Spherules across Four Continents 12,800 years ago

SUPPORTING MATERIAL:

HYPERLINKS:

METHODS

We extracted magnetic grains and spherules according to the protocol of Firestone et al. (2007), as updated by Israde et al. (2012) and LeCompte et al. (2012). We used neodymium magnets (NdFeB): 5.15 × 2.5 × 1.3 cm; grade N52; magnetization vector along 2.5-cm face; surface field density = 0.4 T; pull force = 428 N. The magnets were tightly wrapped in 4-mil plastic bags. The magnetic grain fraction (dominantly magnetite and titanomagnetite) was extracted from slurries of bulk sediment and then dried. In one protocol refinement, the magnetic fraction was sorted into multiple size fractions using a stack of ASTM sieves of 850, 425, 250, 106, 53, and 38 µm, which were cleaned thoroughly between samples. Most spherules were in the smallest three fractions. Aliquots of each grain fraction were examined using a 150-300× reflected light zoom microscope to manually count and photograph candidate spherules. For statistical validity, multiple aliquots were examined until they yielded a minimum count of approximately five spherules, sometimes requiring inspection of the entire magnetic fraction. Light microscopy provides only preliminary identification, because spherules are superficially similar to detrital grains and/or framboids. Selected spherules and SLOs were cross-sectioned or mounted on SEM stubs and analyzed whole, using standard procedures.

Next, candidate spherules were analyzed by scanning electron microscopy (SEM) with energy dispersive x-ray spectroscopy (EDS) at four universities to distinguish YDB spherules from rounded detrital grains, framboids, volcanic spherules, and cosmic spherules. Standard analytical techniques were used for the SEM, which were calibrated with the appropriate reference standards. EDS is precise to within approximated ±5 wt% (Goldstein et al., 2003), suitable for the purposes of this paper. Correct identification of YDB impact spherules requires SEM for high-resolution imaging of the spherule surface microstructure, and EDS to provide data on the chemical composition of candidate spherules. Both are essential for determining the mode of formation of candidate spherules. Firestone et al. (2007) used SEM-EDS to investigate a few YDB spherules, but not all, whereas in the current work, we analyzed nearly all candidate spherules using SEM-EDS, a practice that we now consider standard. A flow chart describing identification parameters is in **SI Fig. 22.**

SITES DESCRIPTIONS

Stratigraphy, chronology, and archaeology for each of three sites below are in Supporting Information in Bunch et al. (2012):

ABU HUREYRA, SYRIA. This site is located on an archaeological mound, or "tell," about 14 km west of Al Thawra, Syria (lat/long: 35.866700°N, 38.400000°E)**.** The site was excavated before being flooded by Lake Assad in 1974. We adopted the chronology of Moore et al. (2000), who radiocarbon dated charcoal, bones, seeds, and grains.

BLACKVILLE, SC. Core #1. This sampling site is about 3.2 km WNW of the town of Blackville (lat/long: 33.361545°N, 81.304348°W). We utilized the stratigraphic details and chronology of Bunch et al. (2012), who acquired optically stimulated luminescence (OSL) dates on sediment from the site.

MELROSE SITE. ***A)*** This site is located about one km SW of the town of Melrose in northeastern PA (lat/long: 41.925410°N, 75.510436°W). We utilized the stratigraphic details and chronology of Bunch et al. (2012), who acquired an optically stimulated luminescence (OSL) date on sediment from the site.

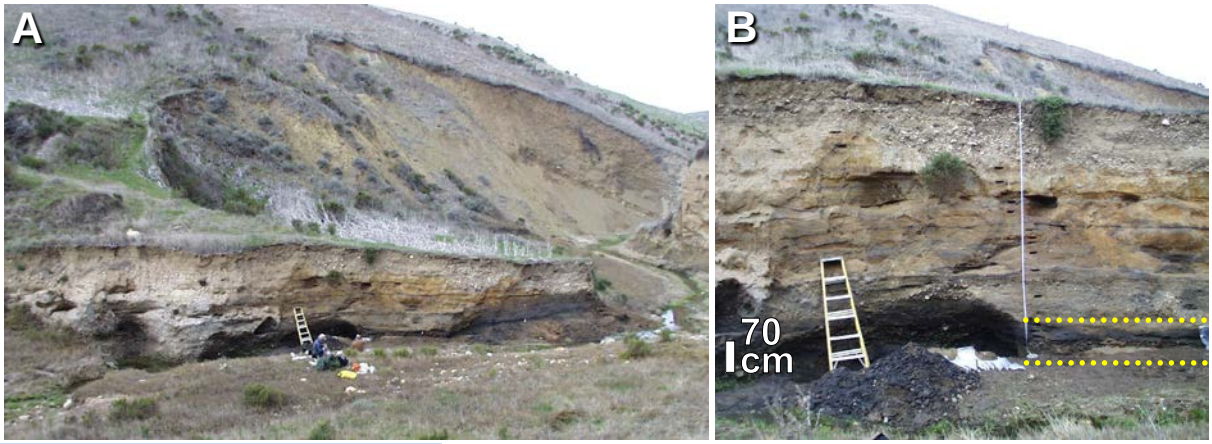

SI FIG. 1a. ARLINGTON CANYON SITE (lat/long: 33.990333°N, 120.1580555°W, using WGS84 projection, or as Universal Transverse Mercator (UTM) coordinates 10S 0762524, 3764532, using NAD27 CONUS projection). ***A)*** Site AC-003 is located in Arlington Canyon, Santa Rosa Island, one of the Channel Islands about 52 km southwest of Santa Barbara in Southern California. The AC-003 profile is exposed on a 5-m-high cliff section of a low terrace, cut by the stream on the western side of the canyon at the base of a moderately steep incline (marked aluminum stake on terrace at site location). Located about two kilometers upstream in Arlington Canyon from the NW coast of Santa Rosa Island, this canyon is relatively broad at this location. Abundance peaks in YDB proxies occur in black layers of silty mud, conspicuous at the base of cliff section at, and close to, stream level (Kennett, 2009a; 2009b). Stratigraphy and chronology of this site were described in detail in Kennett et al. (2008). ***B)*** The 44-cm-thick YDB layer is between yellow lines (images courtesy J. West).

Arlington Canyon Site. Stratigraphy and the YDB layer. Detailed stratigraphy of the Arlington Canyon section is in Kennett et al. (2008). At the base of the section, a 44-cm-thick, organic-rich, dark blue-gray, silty mud layer rests directly on a gravel deposit at 5m. This layer is capped with a coarse cobble lag deposit (≈60 cm thick) and in turn by a second less dark layer (20 cm thick) of gray to black laminated sandy silt. The remainder of the overlying sequence is represented by alluvial sands and gravels. Ten nearly continuous samples, varying from 2 to 6 cm thick, were collected from the 44-cm lower dark layer between 464 and 503 cm below surface (cmbs). Four more samples were collected from the upper dark layer (Kennett et al., 2008). Magnetic grains were extracted from nine samples and five of them were examined for spherules. The sample at the base of the lower black layer from 498 to 503cmbs contained 60 spherules/kg (**SI Tables 2 & 3**). It was deepest in the 44-cm-thick YDB layer section.

Chronology and the YDB layer. We adopted the chronology of Kennett et al. (2008), who obtained accelerator mass spectrometry (AMS) ^{14}C dates on charcoal, wood, carbon spherules, and glassy carbon. Those authors selected samples across 111 cm of sediment from the canyon wall between 503 and 392 cmbs. For those samples, 12 accelerator mass spectrometry (AMS) ^{14}C dates were acquired, ranging from 11.01 ± 0.03 ^{14}C ka BP (12.96 ± 0.05 cal ka BP) to 11.44 ± 0.09 ^{14}C ka BP (13.31 ± 0.08 cal ka BP) (**Table S1).** The YDB, encompassing both dark layers, dates close to 12.8 ka by linear interpolation. The upper and lower sequences of ^{14}C dates are statistically similar,

suggesting rapid accumulation of fluvial deposits after ≈12.95 ± 0.05 ka (Kennett et al., 2008; 2009a).

Archaeological/Paleontological Importance. Arlington Canyon contains the oldest well-dated North American human bones (13.0 to 12.9 ka) collected in clear stratigraphic context (Johnson et al., 2002; Waters and Stafford, 2007). These data provide evidence that these humans were present on the Northern Channel Islands coeval with Clovis Paleoindian peoples found throughout North America. This also demonstrates that these people were capable of ocean travel (Erlandson et al., 2007). The bones of pygmy mammoths found nearby appear to have become extinct on the island at ≈12.8 ka (Agenbroad et al., 2005; Kennett et al., 2008).

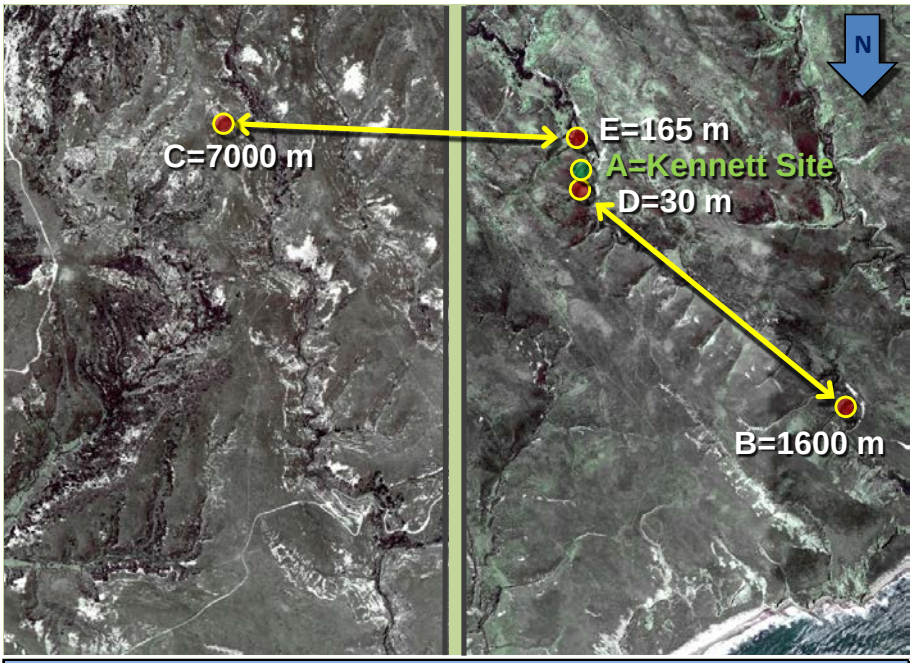

ARLINGTON CANYON RADIOCARBON AGES

#	Sample #		UTM	East (m)	North (m)	Projection	Date	Distance (m)	Proxies
Kennett et al. (2009)									
A	AC	003A	10S	762524	3764532	NAD27-CONUS	12980	0	S, CS, ND
Scott et al. (2010); Pinter et al. (2011)									
B	SRI09	16a	10S	761228	3765781	NAD83 or WGS84	11467	1600	CS
C	SRI09	28	10S	769429	3764606	NAD83 or WGS84	12890	7000	S, CS, ND
D	SRI09	29c	10S	762434	3764754	NAD83 or WGS84	13456	30	CS, ND
E	SRI09	80	10S	762436	3764546	NAD83 or WGS84	15289	165	CS
E	SRI09	82	10S	762436	3764546	NAD83 or WGS84	13739	165	CS
E	SRI09	86	10S	762436	3764546	NAD83 or WGS84	13615	165	CS
E	SRI09	88	10S	762436	3764546	NAD83 or WGS84	13730	165	CS

SI FIG. 1b. Independent Research at Arlington Canyon. Landsat image of Santa Rosa Island. Green dot is the YDB sampling location from Kennett et al. (2009a, 2009b). Red dots are sampling sites of Scott et al. (2010). Numbers are approximate distance in meters from red sites to the original site of Kennett et al. (2008) (table above). Scott *et al.* claimed their site *"is identical or nearly identical with the location reported by Kennett (2008, 2009a, 2009b)"* and that their radiocarbon dates were acquired from a *"continuous"* stratigraphic sequence. In three papers, they published (Scott et al., 2010; Daulton et al., 2010; and Pinter et al., 2011), they concluded: a) YDB carbon spherules are not impact-related; b) there are no YDB nanodiamonds; and c) YDB spherules are simply framboids and detrital magnetite. These conclusions were refuted by Israde et al. (2012), Tian et al. (2011), and LeCompte et al. (2012), respectively. In addition, coordinates, photographs, stratigraphic descriptions, and radiocarbon ages presented in their papers conclusively demonstrate that none of their samples collected were taken from the same stratigraphic section studied by Kennett et al. (2008). Their purported *"continuous"* sequence is actually four discontinuous sections that are distant from the Kennett et al. (2008) site by 7000 m, 1600 m, 165 m, and 30 m (table above). One of those sites (C=7000 m) was not in Arlington Canyon at all, but rather in distant Verde Canyon. Three of their four sites have no dates close to 12.9 ka; this lack of fully dated sequences spanning the YDB boundary most reasonably explains their inability to detect YDB proxies.

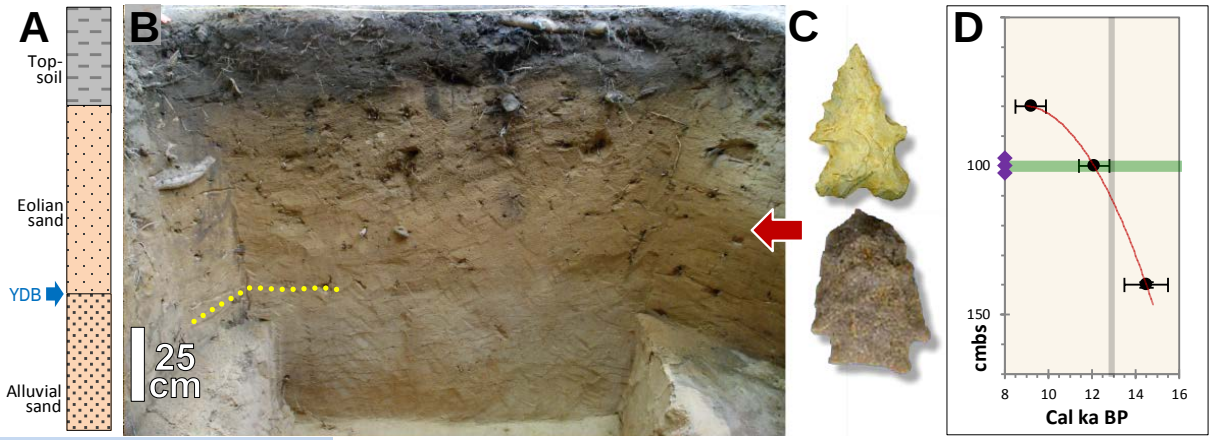

SI FIG. 2. BARBER CREEK SITE (lat/long: 35.6000592°N, 77.303636°W) is approximately 5.7 km east of Greenville, North Carolina. ***A)*** Lithostratigraphic column with YDB indicated in blue. ***B)*** Wall of excavation trench in which the 2.5-cm-thick YDB layer is buried about 1 m deep (yellow dotted line). ***C)*** Lower inset is an Archaic Palmer Corner-Notched point from a depth of ≈80 cm dating to ≈10.8 kyrs, and the upper inset shows a 3-cm-long, St. Albans projectile point dating to ≈9 kyrs. These artifacts from the Early Holocene were found above the YDB layer and provide confirmation of the robustness of the age-depth model. ***D)*** Interpolation by second-order polynomial regression was used to develop an age-depth model (red line) based on three optically stimulated luminescence (OSL) dates (**Table S1**). The vertical gray bar represents 12.8 ± 0.15 ka, and the purple diamonds represent sample depths. The green bar shows depth of the YDB peak in spherules in the 2.5-cm layer centered at 100 cmbs. Based on the error bars of the middle OSL date (12.1 ± 0.7 ka), the age of the YDB layer is determined to be close to 12.8 ka.

Barber Creek Site. Stratigraphy and the YDB layer. This site is located at ≈6 meters above sea level (masl) along a paleo-braidplain near the confluence of the Tar River and Barber Creek, North Carolina. It is oriented roughly parallel to the Tar River channel, extending about 300 meters along the scarp separating the lower paleo-braidplain from the modern Tar River floodplain and channel. Sediments from 1 to 3 meters below surface (mbs) consist variably of coarse to fine sand with some small gravel that is predominantly alluvial in origin, originally deposited as braided river deposits by a rejuvenated Tar River during the lower sea level at the end-Pleistocene. The upper one meter of the site is composed of medium to fine quartz sand mainly of eolian origin, representing sediments deposited as sand-sheets or source-bordering dunes over remnant braidplain topography (Choate, 2011; Daniel, 2002; Daniel and Moore, 2011; Daniel et al. 2008; McFadden, 2009; Moore, 2009; Moore and Daniel, 2011). There is no black mat/layer associated with the YDB, although at a depth of ≈100 cmbs, the sediments abruptly change from alluvial to eolian deposition, producing a clear lithologic break and color change. The age-depth model indicates that this shift corresponds to the onset of Younger Dryas cooling. Guided by the age-depth model and by the change in sedimentation, three 2.5-cm-thick sediment samples were taken across the 7.5-cm interval from 97.5 to 105 cmbs, and the YDB layer at a depth of 100 cmbs contained 1035 spherules/kg (**SI Tables 2 & 3**). No spherules were detected above or below that layer.

Chronology and the YDB layer. We adopted the chronology of Moore and Daniel (2011), using three OSL dates acquired on quartz grains. Those authors selected samples across ≈60 cm of sediment from the trench wall beginning at 1.4 mbs and obtained three OSL dates of 9.2 ± 0.7, 12.1 ± 0.7, and 14.5 ± 1.0 ka (**Table S1**). Interpolation by second-order polynomial regression dates the YDB layer to 12.1 ± 0.7 ka (range of 11.4 to 12.8 ka), so that the age of the sample at 100 cmbs falls is within the expected age of the YDB layer at ≈12.8 ka.

Archaeological Importance of Site. Extensive shovel testing and unit excavations (≈250 m^2) revealed stratified Woodland and Archaic period remains concentrated in the upper 80 cm of the site, indicating that the site began to be used near the end of the Younger Dryas and the beginning of the Holocene. The presence of cultural features, artifact clusters, and isolated artifacts in chronological order suggest that former occupation surfaces were buried by wind-blown sand with minor alluvial contributions that are the result of infrequent overbank flooding events.

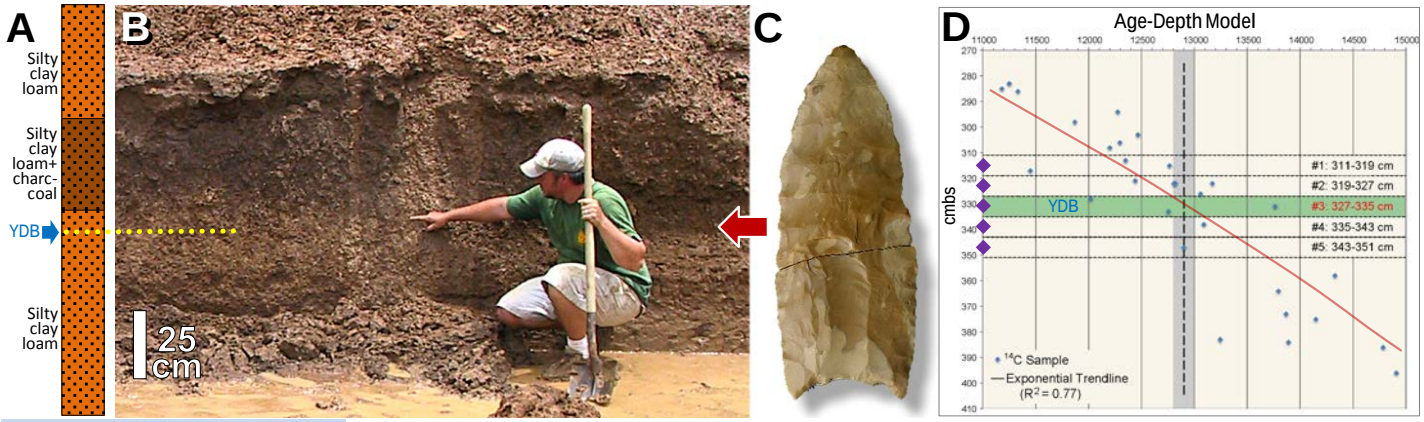

SI FIG. 3. BIG EDDY SITE (lat/long: 37.736470°N, 93.786128°W) is ≈4.5 km north of Stockton, southwest Missouri in the lower Sac River valley. The photo shows ***A)*** lithostratigraphic column with the YDB layer marked in blue and ***B)*** the sampling location on the wall of a deep block excavation. YDB spherules peak within an 8-cm-thick sample buried about 3.31 m deep (yellow dotted line). ***C)*** The site yielded a Clovis-aged hearth feature, along with a 10-cm-long, post-Clovis, late-stage Gainey preform (unfinished failed point) (Ray, et al., 1998). ***D)*** Logarithmic interpolation was used to develop an age-depth model (red line) based on 30 ^{14}C dates (seven key dates are in **Table S1**). Error bars are smaller than the dot size. The vertical gray bar represents 12.8 ± 0.15 ka, and the purple diamonds represent sample depths. The green bar shows the depth of a peak in impact spherules in the 8-cm-thick layer at 327 -335 cmbs identified as the YDB. Based on the age-depth model, the YDB layer dates to ≈12.8 ka.

Big Eddy Site. Stratigraphy and the YDB layer. The site lies in the Sac River drainage, where frequent slackwater, overbank flooding produced a thick stratigraphic profile dominated by alluvial, fine-grained, silty clay loam, occasionally intercalated with weakly developed soils. There is little difference between the YDB layer and surrounding alluvial sediment, although the deposits from 10-40 cm above the YDB appear slightly darker, a likely result of a greater intensity of post-Gainey human activities. Five 8-cm-thick continuous samples were taken across a 40-cm interval from 311 to 351 cmbs. The 8-cm-thick YDB sample (#3) displays a peak of 100 spherules/kg at a depth of 327 to 335 cmbs (**SI Tables 2 & 3**).

Chronology and the YDB layer. We adopted the chronology of Lopinot et al. (1998, 2000, 2005), who acquired 30 AMS radiocarbon dates based on charcoal from this sequence. Those authors collected discontinuous charcoal samples in the sequence over about 1.2 m from about 283 to 397 cmbs, and this interval includes the five sediment samples obtained for the YDB study. Key AMS ^{14}C dates ranged from 10.47 ± 0.08 ^{14}C ka BP (12.40 ± 0.18 cal ka BP) to 11.38 ± 0.08 ^{14}C ka BP (13.26 ± 0.10 cal ka BP) (**Table S1**). An age-depth model was generated using logarithmic interpolation, and the proxy-rich YDB layer from 327 to 335 cmbs dates close to 12.8 ka, consistent with the age of the YDB at other sites. Accurately dating individual layers was difficult because some charcoal fragments have clearly moved up and down within the sequence, and some older charcoal may have been introduced by flood-induced redeposition from sources upstream. However, based upon the presence of hearth features, much of the charcoal from Paleoindian deposits (i.e., above 355 cmbs) can be attributed to human agency.

Archaeological Importance of Site. This site contains well-stratified, culturally rich deposits that span most of prehistory, and some of the richest and least disturbed deposits are the oldest (Dorale et al., 2010; Lopinot et al., 1998, 2000, 2005). Although no Clovis points were recovered from Big Eddy, Clovis usage of the site is inferred based on three Clovis-aged dates for a hearth feature that displayed a dense concentration of wood charcoal, bone fragments, and a sparse scatter of chipped-stone artifacts. The Late Paleoindian horizon (280–320 cmbs), e.g., Dalton and San Patrice projectile points, contained a dense deposit of mixed habitation and lithic workshop debris, whereas the underlying Middle and Early Paleoindian deposits (321–355 cmbs) contained only a light scatter of artifacts.

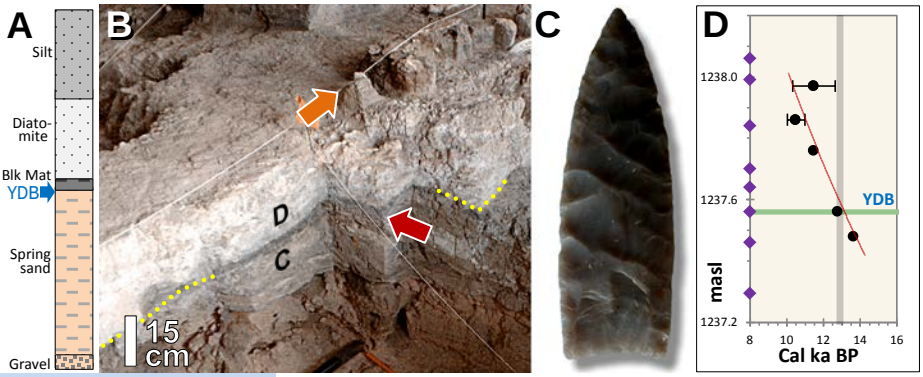

SI FIG. 4. BLACKWATER DRAW SITE (lat/long: 34.275687°N, 103.326101°W) is about 18 km SE of Clovis, New Mexico. ***A)*** Lithostratigraphic column illustrating location of YDB and black mat layer. ***B)*** Sampling site is located inside the South Bank Interpretive Center. Impact spherules were found in a 1-cm-thick dark gray YDB layer at a depth of ≈2.5 m (yellow dotted line). The YDB layer is capped by a layer of whitish-gray diatomite considered by Haynes (2008) to be the stratigraphic equivalent of the black mat. Numerous bones representing a post-Clovis Folsom-aged bison kill are shown >20 cm above the mat layer at orange arrow. ***C)*** An 11-cm-long Clovis point was found in the YDB layer nearby at the equivalent depth of the red arrow. ***D)*** Based on five conventional and AMS radiocarbon dates, we show an age-depth model (red line) using logarithmic interpolation. Errors of the older three dates are smaller than the dots. The vertical gray bar represents 12.8 ± 0.15 ka, and the purple diamonds represent sample depths. The green bar indicates the depth to the peak in impact spherules and other impact proxies in the 1-cm thick YDB layer (Firestone et al. 2007). Based on interpolation, the YDB proxy layer at 1237.55 masl dates to ≈12.8 ka.

Blackwater Draw Site. Stratigraphy and the YDB layer. At this site, the latest Pleistocene sediment is sandy alluvium largely sourced by a near-by spring and capped by lacustrine diatomite and silty muds. Based on the presence of Clovis artifacts and mammoth bones, Haynes et al. (1999, 2008) concluded that stratigraphic Unit C is of Clovis age and that diatom-rich Unit D was deposited atop Unit C immediately at the onset of YD cooling (12.8 ± 0.15 ka). Haynes (2008) also referred to Unit D as a black mat. The thin contact between Units D and C represents the YDB layer. Using exploratory coring within a 500×750 m area, Haynes (1995) demonstrated that the Clovis-aged C stratum and YD-aged D stratum occurs across ≈50% of the area (Figs. 3 and 4 in Haynes, 1995). Concerning the possibility of a hiatus in deposition between Units C and D, Haynes et al. (1999) wrote that it *"is probably no more than a decade and possibly much less, that is, geologically instantaneous."* This is inconsistent with speculations by Surovell et al. (2009) and Pinter et al. (2011) that YDB spherules are cosmic and simply accreted gradually during a long hiatus in deposition. Furthermore, morphological and geochemical analysis of the YDB spherules at this location indicates that they are not accreted cosmic forms (see Blackwater spherule images in **Figs. 3** and **S18**).

For this study, Blackwater Draw curator Joanne Dickenson sampled an exposure inside the South Bank Interpretive Center, collecting fifteen discontinuous bulk sediment samples, ranging from 1 to 10 cm thick across a 1.67-m interval between 1237.8 and 1238.87 masl. She identified Units C and D, as well as the adjacent units (A, B, E, F, and G). Of the fifteen samples, nine were investigated for spherules, and a peak of 960 YDB spherules/kg was observed in a 1-cm–thick sample from an elevation of 1238.32 to 1238.33 masl (**SI Tables 2 & 3**), identified by the site curator as the contact between Units C and D. In an aliquot of the same sediment sample, Firestone et al. (2007) reported finding 770 spherules/kg, whereas in a sample from the identical location, Surovell et al. (2009) reported finding none, causing those authors to question the results of Firestone et al. (2007). Subsequently, LeCompte et al. (2012) reported concentrations of 1318/kg in an identical sample from the same layer. The finding of 960 spherules per kg in this contribution is consistent with Firestone et al. (2007) and LeCompte et al. (2012) and contradicts the results of Surovell et al. (2009)

Chronology and the YDB layer. For this site, we adopted the chronology of Haynes et al. (1995), who conducted excavations in 1983 along an 800-m east-west transect that passes near our sampling site on the south bank. Those authors published detailed stratigraphic profiles and acquired 34 radiocarbon dates mostly on humates in samples from selected spots along the transect. They found that the ages of Units B, C, D, and E are consistent across the profile with Unit C dating prior to ≈12.8 ka and Unit D dating to just afterward. The nearest sampling interval investigated by Haynes et al. (1995) is ≈60 m east of our

sampling location in the Interpretive Center and is ≈0.75 m lower stratigraphically. They sampled a 0.49-m interval from 1237.48 to 1237.97 masl, acquiring four dates, of which two were conventional ^{14}C dates on Unit E of 10.00 ± 0.91 ^{14}C ka BP (11.48 ± 1.16 cal ka BP) at 1237.97 masl and 9.26 ± 0.32 ^{14}C ka BP (10.50 ± 0.47 cal ka BP) at 1237.86 masl. In addition, Unit D was AMS dated to 9.95 ± 0.10 ^{14}C ka BP (11.48 ± 0.18 cal ka BP) at 1237.76 masl, and Unit B was AMS dated to 11.81 ± 0.09 ^{14}C ka BP (13.65 ± 0.11 cal ka BP) at 1237.48. Haynes et al. (1995) did not date Unit C at that location, but Johnson and Holliday (1997) examined a previously excavated block of mammoth and bison bones taken from ≈175 m northeast of our site. There, they found that some bones showed apparent evidence of Clovis modification, including cut and percussion marks. The bones were embedded in Unit C, from which humates were AMS dated to 10.78 ± 0.11 ^{14}C ka BP (12.77 ± 0.08 cal ka BP), consistent with the YD onset. We integrated the three locations to produce a generalized composite age-depth model that is consistent with the geochronology of the Units B through D published by Haynes et al. (1995) for the site. Logarithmic interpolation dates the YDB layer in Unit C to ≈12.8 ka, consistent with the age of the YDB at other sites.

Archaeological/Paleontological Importance. The world's first discovery of Clovis projectile points occurred on this 157-acre site located near Clovis, NM, which gave its name to those points (Haynes et al., 1995). The points were found associated with bones of butchered mammoths within Unit C, the spherule-rich YDB layer and beneath Unit D, the black mat layer. American camels and American horses also became extinct at the top of Unit C prior to deposition of Unit D (Haynes et al. 1999). According to Haynes (2008), no *in situ* Clovis artifacts or bones of extinct megafauna have ever been found above the YDB layer at Blackwater Draw or any other site, indicating that they went extinct at that time.

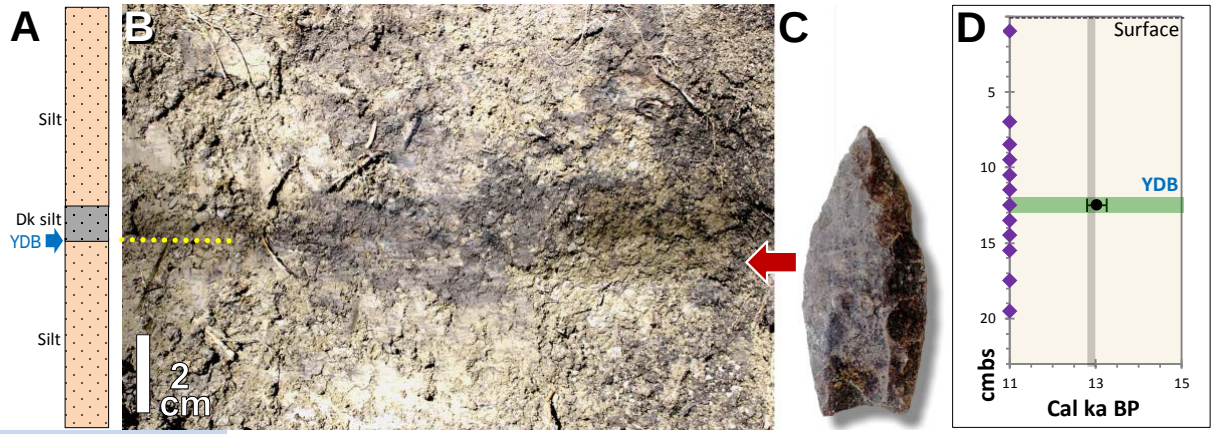

SI FIG. 5. CHOBOT SITE (lat/long: 52.956004°N, 114.734872°W) is about 105 km SE of Edmonton, Alberta, Canada. ***A)*** Lithostratigraphic column shows silty sediment sequence with a black layer. ***B)*** Trench wall with 1-cm-thick YDB layer (yellow dotted line) at a depth of 0.12 m beneath a carbon-rich black mat/layer. ***C)*** The 6-cm Clovis point shown was collected nearby immediately below the black layer at the level of red arrow. ***D)*** No radiometric dates exist for this site, and so, the age at the black dot is based on archaeological stratigraphy, with observed Clovis artifacts located at the base of the black layer. This is comparable to numerous North American Clovis sites elsewhere with dates that range from 12.80 to 13.25 ka (**Table S1**; Waters and Stafford, 2007). The vertical gray bar represents 12.8 ± 0.15 ka, and the purple diamonds represent sample depths. Ground surface is denoted by black dashed line. The green bar shows the depth of a peak in impact spherules in a 1-cm layer centered at 12-13 cmbs. The age of this spherule-rich layer is consistent with archaeological stratigraphy indicating an age of no less than12.8 ka.

Chobot Site. Stratigraphy and the YDB layer. The entire sedimentary sequence is comprised of fine alluvial and lacustrine mud, silt, and fine gravel deposited during a highstand of the lake. Eleven 1-cm-thick continuous samples were taken across an interval extending from the surface to 20 cmbs. Firestone et al. (2007) reported finding 578 spherules/kg at a depth of 12 to 13 cm in the 1-cm-thick YDB layer. We observed concentrations of 250 spherules per kg in the same layer (**SI Tables 2 & 3)**.

Chronology and the YDB layer. We were unable to date the site radiometrically because of bioturbation by plant roots. However, the stratigraphic position of the spherule layer is immediately above the uppermost level containing abundant Clovis points and artifacts, and thus is

consistent with an age of ≈12.8 ka for the end of Clovis occupation at other sites (Waters and Stafford, 2007).

Archaeological Importance of Site. Currently located on the shore of Buck Lake, this site at 12.8 ka was located on the margin of a much larger meltwater lake, where a chert quarry with high-quality lithic material attracted hunter-gatherers. Tens of thousands of Clovis-age flakes and tools were found at this site.

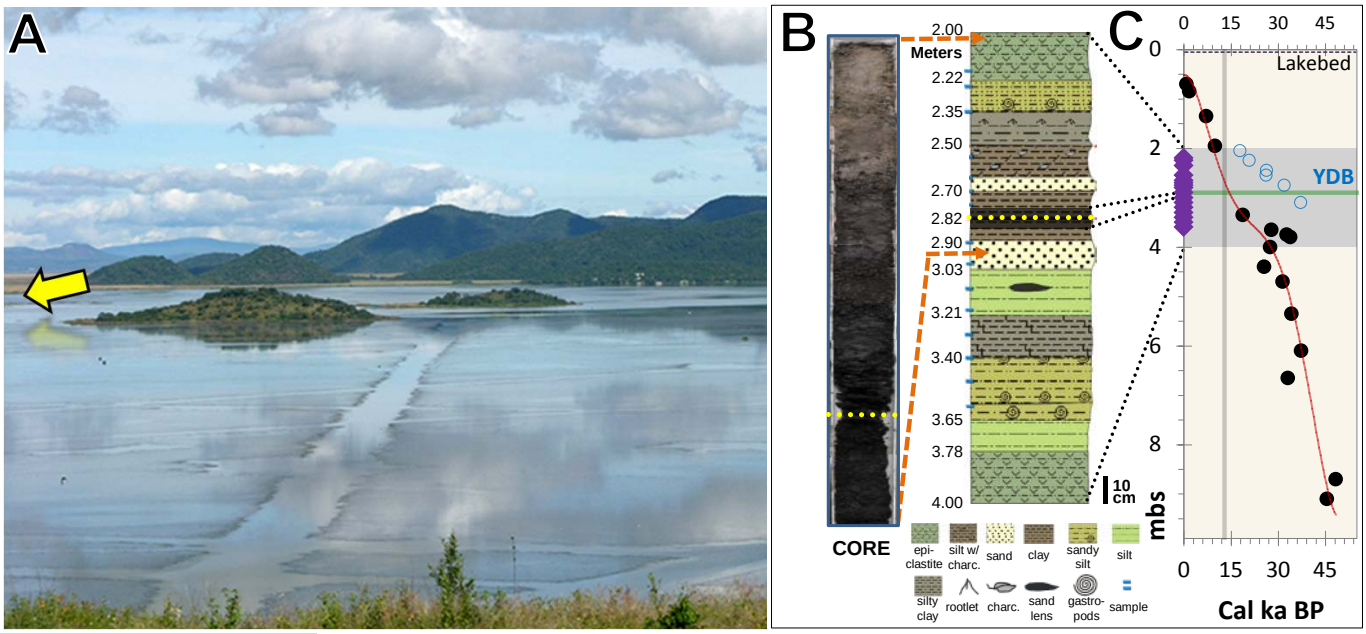

SI FIG. 6. CUITZEO SITE (lat/long: 19.936516°N, 101.155676°W) is 26 km north of Morelia, Michoacán, Mexico. ***A)*** Core location is in shallow lake waters (near yellow arrow). ***B)*** Photo of 2-to-4-m interval of core (left), shows black mat. Lithostratigraphic column (right) shows the position of the YDB layer as a yellow dotted line at 2.8 mbs (Israde et al., 2012). ***C)***. Interpolation by fifth-order polynomial regression was used to develop an age-depth model (red line) based on 16 ^{14}C dates in black (Israde et al., 2012). Blue circles are dates that were rejected due to chronostratigraphic reversals. The vertical gray bar represents 12.8 ± 0.15 ka, and the purple diamonds represent sample depths. Lake floor is represented as black dashed line. The green bar shows the depth of peak in spherules in a 5-cm layer centered at 2.8 mbs. Based on interpolation, the age of the YDB layer is ≈12.8 ka, as supported by biostratigraphic correlations with regional lake sequences.

Cuitzeo Site. Stratigraphy and the YDB layer. These samples are from the second largest lake in Mexico, covering 300-400 km² in the state of Michoacán (Israde et al., 2010, 2012). The 27-m-long lake core consists of interbedded lacustrine sands, silts, clays, epiclastites, and tephra layers. A conspicuous, dark, carbon-rich layer, dominated by clay and silt, occurs between 2.50 and 2.82 mbs and resembles the black mat at other YDB sites across North America. Ten 5- to 10-cm-thick discontinuous samples were taken across a 1.4-m interval from 2.20 to 3.60 mbs. A peak of 2055 spherules/kg occurs in a 5 cm layer between 2.75 to 2.80 mbs (**SI Tables 2 & 3**) and is associated with nanodiamonds (Israde et al., 2012).

Chronology and the YDB layer. We adopted the chronology of Israde et al. (2012), who acquired AMS radiocarbon dates on bulk sedimentary carbon. Twenty-two AMS ^{14}C dates were obtained across an 8.4-m interval from 0.7 to 9.1 mbs with dates ranging from 0.93 ± 0.06 ^{14}C ka BP (0.86 ± 0.06 cal ka BP) to 42.40 ± 1.00 ^{14}C ka BP (45.54 ± 1.10 cal ka BP. The three dates closest to 12.8 ± 0.15 ka are listed in **Table S1**, with the others shown in Israde, et al. (2012), who generated the age-depth model shown above, using a fifth-order polynomial regression. The age-depth model provides an interpolated date of ≈12.8 ka for the YDB layer at 2.8 mbs.

Archaeological/Paleontological Importance. No cultural artifacts or megafaunal remains were found in this core, but numerous extinct horse and mammoth bones occur in exposed lake deposits southwest and north of the modern lake (Corona-Nuñez, 1988). Radiocarbon dates on bones of extinct megafaunal species along the shore of Lake Cuitzeo are consistent with megafaunal extinctions at ≈12.8 ka.

SI FIG. 7. GAINEY SITE (lat/long: 42.885973°N, 83.614324°W) is about 5.5 km south of Grand Blanc, Michigan. ***A)*** Lithostratigraphic column shows alluvium overlying glacial till. ***B)*** A peak in YDB spherules was found in a 5-cm-thick sample 32.5 cmbs at the base of the darker layer (yellow dotted line) just above glacial till (light tan stratum). ***C)*** The age of the YDB layer is supported only by a single OSL date of 12.36 ± 1.23 ka (range, 11.13 to 13.58 ka) (**Table S1**), and the age of the YDB layer is ≈12.8 ka. The vertical gray bar represents 12.8 ± 0.15 ka. Sample depths indicated by purple diamonds. Ground surface is denoted by black dashed line. The green bar shows the peak in spherules centered at 30 cmbs.

Gainey Site. Stratigraphy and the YDB layer. At this site, local sediments began to be deposited after a lobe of the Laurentide Ice Sheet retreated from its maximum extent at ≈17 ka (Colgan et al., 2003). The sedimentary sequence is composed of glacial till, or diamicton, overlain by fine-grained, dark silty alluvium. Ten 5-cm-thick continuous samples of bulk sediment were collected between the ground surface and 55 cmbs. Eight samples were examined for spherules, revealing a peak of 1350 spherules/kg in a 5-cm-thick YDB layer centered at 32.5 cmbs between 30 to 35 cmbs (**SI Tables 2 & 3**). A peak in nanodiamonds (Kennett et al., 2009b) that occurs at the lithologic break between these units also marks the YDB layer at this depth. Firestone et al. (2007) reported finding 2144 magnetic spherules/kg in the YDB at this site, which was the first YDB site discovered (by W. Topping). We report similar values at 1350 spherules/kg (**TABLE S2)**.

Chronology and the YDB layer. It was not possible to obtain accurate ^{14}C dates from this site due to extensive bioturbation caused by plant roots. We used the dating of Simons et al. (1984), who acquired one OSL date of 12.36 ± 1.23 ka at a depth of approximately 30 cm. The error bars of that date (± 1.23 ka at 1σ probability) intersect the 12.8 ka layer at 30 cm, consistent with the age of the YDB at other sites.

Archaeological Importance of Site. This site was a Paleoindian campsite located a few hundred kilometers south of the Laurentide Ice Sheet at 12.8 ka. In and just above the YDB layer, there were numerous artifacts attributed to the Gainey culture (Simons et al., 1984: Goodyear, 2006, 2010) that is considered to be immediately post-Clovis at up to 100 years (Anderson et al., 2011), a short time after apparent deposition of the spherules and nanodiamonds.

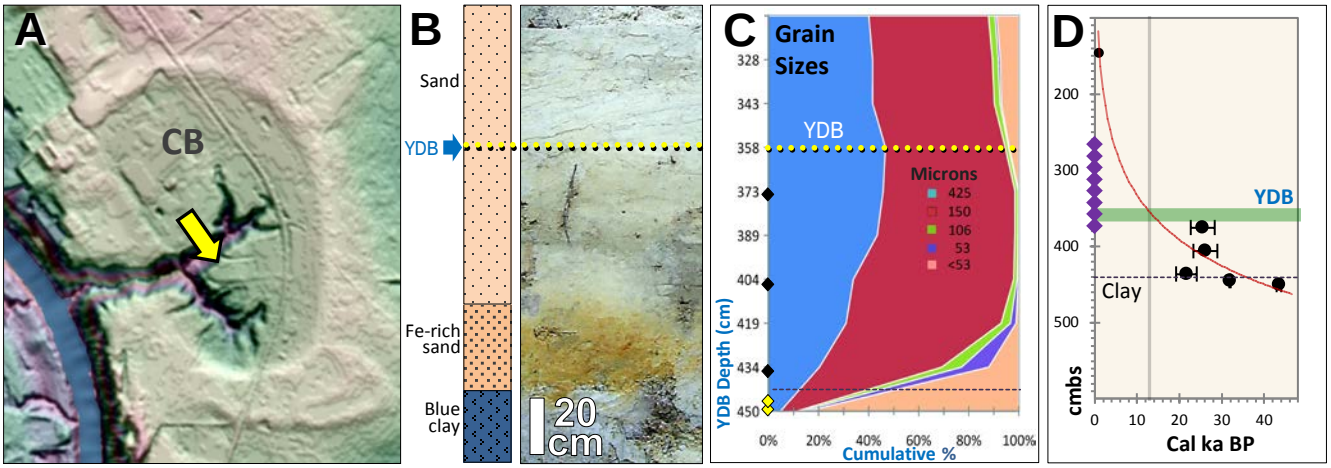

SI FIG. 8. KIMBEL BAY SITE (lat/long: 34.981811°N, 78.776820°W) is 12 km southeast of Fayetteville, North Carolina. ***A)*** Site map shows the sample location (yellow arrow) in the center of Kimbel Bay, a Carolina Bay that is incised by a drainage that breached the rim. ***B)*** Stratigraphic column shows unconsolidated sand overlying clay. The excavation trench penetrated a dense clay unit (blue-gray clay at bottom in photo) overlain by iron-stained sands. ***C)*** Grain size plot is from a 5-m sediment core extracted near the trench. The percentages of smaller grains increase with depth. Black diamonds are OSL sample depths; yellow diamonds are ^{14}C sample depths. Top of blue clay is denoted by black dashed line. ***D)*** Logarithmic interpolation is used to develop an age-depth model (red line) based on three AMS ^{14}C dates and three OSL dates (**Table S1**). The error bars for three samples are smaller than the dot size. The vertical gray bar represents 12.8 ± 0.15 ka, and the purple diamonds represent sample depths. The approximate top of blue clay is denoted by black dashed line. The green bar shows depth of peak in spherules in the 15-cm layer centered at 385 cm. The YDB layer dates to ≈12.8 ka.

Kimbel Bay Site. Stratigraphy and the YDB layer. At this site, an exploratory trench was dug by hand, and a hand auger was used to extract a 490-cm-deep core. The upper 440 cm of sediments consists of unconsolidated, fine-to-coarse-grained eolian and colluvial sands, occasionally intercalated with thin, discontinuous silty clay cross-beds, unconformably underlain by a layer of massive blue clay beneath a transition zone of mixed clay and upper sands. A USGS geologic map of the area (Horton and Dicken, 2001) identifies the unconformity as the top of Cretaceous-age Black Creek Formation represented by fine-grained marine clay, consistent with the sharp increase in the percentage of fine grains (<53 µm) with depth, beginning at 434 cmbs. Eight 15-cm-thick continuous samples of bulk sediment were collected from a 76-cm-thick interval of sediment between 297 and 373 cmbs. The six deepest samples were examined for spherules. A 15-cm-thick layer centered at 358 cmbs (350-365 cmbs), contains a peak of 4900 spherules/kg, the highest value for all sites measured (**SI Tables 2 & 3**). The use of a hand core to a depth of 358 cm to acquire the YDB sample most likely precludes anthropogenic contamination.

Chronology and the YDB layer. For dating, we selected discontinuous samples from different locations in the trench over a 303-cm-thick sediment sequence from 147 to 450 cmbs. We acquired three AMS ^{14}C dates, ranging from 1.20 ± 0.02 ^{14}C ka BP (1.13 ± 0.04 cal ka BP) to 3.97 ± 0.71 ^{14}C ka BP (43.46 ± 0.61 cal ka BP) and three OSL dates, ranging from to 21.64 ± 2.63 to 26.08 ± 2.94 ka BP (**Table S1**). At the clay interface at 440 cm, there is an apparent hiatus in deposition as older sediments suddenly transition to younger sediments. In an age-depth model generated by logarithmic interpolation, the proxy-rich YDB layer at 358 cmbs dates to ≈12.8 ka.

Archaeological Importance of Site. No Clovis artifacts or megafaunal bones were observed at this site.

SI FIG. 9. LINGEN SITE (lat/long: 52.508751°N, 7.313882°E) is on the banks of the Ems River, about 1km downstream from the bridge into Lingen, Germany. ***A)*** Lithostratigraphic sequence of eolian sands contains a thin dark, charcoal-rich layer that separates tan sands above from bleached gray sands below. ***B)*** The 5-cm-thick YDB layer is at 43.5 cmbs (yellow dotted line) at the top of a formation known as the Usselo sand, associated with abundant charcoal visible in the photo. ***C)*** A single ^{14}C date was acquired approximately 9 cm below the YDB layer (**Table S1**). Error bars are smaller than the dot size. The vertical gray bar represents 12.8 ± 0.15 ka, and the purple diamonds represent sample depths. Top of Usselo sand is

denoted by black dashed line. The green bar shows the depth of a peak in spherules in a 5-cm layer centered at 43.5 cmbs (Fig 7). Based on the known regional age of the Usselo sand, the age of the YDB layer is ≈12.8 ka.

Lingen Site. Stratigraphy and the YDB layer. Because Lingen is stratigraphically similar to Lommel and Ommen, discussed below, the general stratigraphy and setting for all three sites is discussed here. From about 14 to 13 kyrs ago, dune-like eolian sediments blanketed extensive areas of Northern Europe, extending from the UK to northern Russia and from Denmark to northern France, including these three sites. Called the Late-Pleistocene European Sand Belt, this area contains sediments known as cover-sands, comprised mostly of unconsolidated quartz sand that was deposited during the Allerød. When the YD cooling episode began at ≈12.8 ka, abundant charcoal was deposited and became intermixed with what is known as the Usselo Sand, forming a thin, few-cm-thick dark layer. In this thin, highly visible layer, Firestone et al. (2007) reported YDB spherules and Tian et al. (2010) reported nanodiamonds.

The charcoal-rich Usselo layer has been radiocarbon dated by others to about 10.95 ± 0.05 ^{14}C ka (calibrated to 12.9 ± 0.03 cal ka) (Van Geel et al., 1989) and has long been taken to represent the onset of the YD cooling episode in NW Europe. Recently, Van Hoesel et al. (2012) cited Hoek (1997) and adopted 10.95 ± 0.05 ^{14}C ka (calibrated to 12.9 ± 0.03 cal ka) as the onset of the YD cooling event, which was coeval with deposition of the charcoal in the Usselo layer. At their site, they processed several Usselo layer samples, including one that was 1.5 cm thick sample (AH-14) and found it to contain charcoal, carbon spherules, glasslike carbon, and nanodiamonds. From charcoal in that sample, they acquired three radiocarbon dates (10.84 ± 0.08 ^{14}C ka = 12.71 ± 0.09 cal ka; 10.87 ± 0.06 ^{14}C ka = 12.73 ± 0.09 cal ka; 11.02 ± 0.08 ^{14}C ka = 12.92 ± 0.15 cal ka), for an average of approximately 12.79 cal ka. Only one of those calibrated dates fall within their adopted range for the Younger Dryas onset of 12.9 ± 0.03 cal ka, which is similar to the date of 12.9 ± 0.10 cal ka for the YDB event, as presented by Firestone et al. (2007). Their other two dates are approximately two hundred years younger than the claimed YD onset. However, Van Hoesel et al. (2012) utilized the latest radiocarbon calibration curve, IntCal09 (Reimer et al., 2009), which returns very different calibrated dates than the previous curve, IntCal04. Using the earlier curve, as Firestone et al. did, we find that their dates yield calibrated ages of 12.8 ± 0.07, 12.81 ± 0.06, and 12.92 ± 0.10 cal ka, respectively, falling exactly within the predicted range of 12.9 ± 0.10 cal ka. Van Hoesel et al. (2012) neglected to address these calibration issues and concluded that the diamond-rich layer they identified was ≈200 years younger than the YD onset. Therefore, we maintain that their conclusions are invalid and that they actually found the diamond-rich YDB layer, as previously reported by Tian et al. (2010) and Kennett et al. (2009a, 2009b).

At all three sites, this dark Usselo layer contains abundance peaks in a variable assemblage of magnetic spherules, charcoal, glass-like carbon, and nanodiamonds (Firestone et al. 2007; Tian et al., 2010; Van Hoesel et al., 2012) as in the YDB layer in North America. The abundance of charcoal reflects widespread biomass burning at these sites and at many other locations across Europe, including the Netherlands (Hoek, 1997), Great Britain, France, Germany, Denmark, and Poland (Kloosterman, 1999, 2007), all of which date to the YD onset at ≈12.8 ka. Lingen, Lommel, and Ommen are up to 200 km apart, and the charcoal-rich sites in Poland are 800 km away from those in Belgium, indicating extensive, apparently synchronous fires across a large part of Northern Europe, coeval with the proposed impact event at ≈12.8 ka.

There was an energetic European explosion of the Lacher See volcano that has been variously dated to sometime between ≈13.2 and 12.8 ka (Baales M, et al., 2002, Bogaard and Schmincke, 1985, de Klerk et al., 2008, Litt et al., 2003, Schmitt et al., 2010). The eruption produced ash deposits as much as 18 m thick that thinned towards Finland and Italy. According to published maps of the fallout zone, the three sites of Lingen, Lommel, and Ommen were outside that zone, but volcanic ash and tephra deposits are detectable in sedimentary sequences in the region. To investigate the possibility that the region's magnetic spherules, charcoal, glass-like carbon, and nanodiamonds might be related to the eruption, we examined Laacher See tephra from Bettenroder Berg near Gottingen, Germany (51.458°N, 10.009°E), located about 220 km SE of the Lingen site, the closest YDB site. We detected no magnetic spherules, charcoal, or glass-like carbon in that sample, and at the three YDB sites, we found no detectible material that resembled the Laacher See tephra fragments. Thus, we found no connection between YDB material and the volcanic material from Laacher See eruption, as reported by Israde et al. (2012).

At Lingen, ten discontinuous samples of bulk sediment 3 to 5 cm thick were collected from a 70-cm-thick interval of sediment between 7.5 and 77.5 cmbs. Seven samples were examined for spherules revealing a peak of 30 spherules/kg at a depth of 43.5 to 47.5 cmbs in a 3-cm-thick

dark, charcoal-rich layer (**SI Tables 2 & 3**) at the top of the Usselo sand. This YDB layer correlates with the onset of the YD dated at ≈12.8 ka.

Chronology and the YDB layer. From charcoal extracted approximately 9 cm below the YDB layer at 52.5 cmbs, one ^{14}C date was acquired of 11.31 ± 0.06 ^{14}C ka BP (13.20 ± 0.08 cal ka BP). Based on this date and the position of the YDB layer at the top of the Usselo layer, the YDB age is consistent with an age of ≈12.8 ka.

Archaeological Importance of Site. No pre-YD artifacts or megafaunal bones were observed at this site, although they are numerous throughout the region (Vanmontfort et al., 2010). Artifacts at nearby sites provide temporally diagnostic support for the onset of the YD. The Magdalenian and related North European cultures experienced a significant population and cultural decline at the onset of the YD (Pereira, et al. 2005; Anderson et al. 2011), and the region was essentially abandoned during the YD. About a site near Lommel, Vanmontfort et al. (2010) wrote: *"The occupation was possibly interrupted during the major part of the Younger Dryas, for which no occupation in the region has been attested thus far."*

SI FIG. 10. LOMMEL SITE (lat/long: 51.236231°N, 5.254686°E) is 3 km west of the town center of Lommel, Belgium. ***A)*** Lithostratigraphic sequence of eolian sands contains a thin dark, charcoal-rich layer separating tan sands above from bleached gray Usselo sands below. ***B)*** Photo of sequence shows 1-cm-thick dark, charcoal-rich layer at 48.5 cmbs (yellow dotted line) at the top of the Usselo sand. This is the YDB layer and marks the onset of the YD cooling episode. ***C)*** Two ^{14}C dates were acquired with error bars smaller than the dot size (**Table S1**). The vertical gray bar represents 12.8 ± 0.15 ka, and the purple diamonds represent sample depths. Top of Usselo sand and the ground surface are denoted by black dashed lines. The green bar shows the depth of peak in spherules in a 1-cm layer centered at 48.5 cmbs. Based on ^{14}C dates and the position of the Usselo sand, the age of the YDB layer is ≈12.8 ka.

Lommel Site. Stratigraphy and the YDB layer. See Lingen above for general stratigraphic details. Nine 2- to 5-cm-thick discontinuous samples of bulk sediment were collected from a 60-cm-thick sequence between 17.5 and 77.5 cmbs. Eight samples were examined for spherules, revealing a peak of 10 spherules/kg in a 5-cm-thick layer at a depth of 48.5 to 52.5 cmbs at the top of the Usselo sand (**SI Tables 2 & 3**). Firestone et al. (2007) reported similar concentrations of 16 spherules/kg from this same level, the YDB layer (**Table S2)**. In addition, Tian et al. (2011) reported the presence of cubic nanodiamonds in the Lommel YDB layer, but not above or below.

Chronology and the YDB layer. One AMS ^{14}C date was acquired on charcoal extracted from the YDB layer at 48.5 cmbs, providing a date of 11.48 ± 0.10 ^{14}C ka BP (13.39 ± 0.12 cal ka BP). Van Geel et al. (1989) acquired an AMS ^{14}C date of 10.95 ± 0.05 ^{14}C ka BP (12.86 ± 0.07 cal ka BP) from nearby at the same site. These dates and the position of the YDB layer at the top of the Usselo sand are consistent with an age of ≈12.8 ka.

Archaeological Importance of Site. See Lingen site for archaeological context.

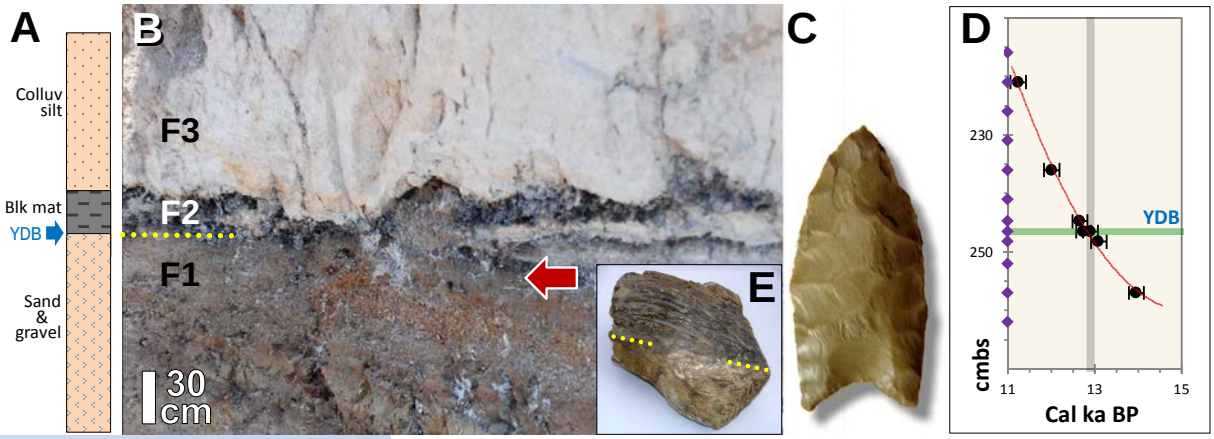

SI FIG. 11. MURRAY SPRINGS SITE (lat/long: 31.570912°N, 110.177996°W) is located 10 km east of Sierra Vista, Arizona. ***A)*** Lithostratigraphic section is shown, along with ***B)*** a site image showing 1-cm-thick YDB layer (yellow dotted line) found directly beneath the black mat at a depth of about 2.46 m. Abundant spherules and nanodiamonds occur in the YDB layer just below the black mat layer with none or low amounts above or below the YDB. ***C)*** Clovis point (4 cm) found nearby in the 12.8-ka YDB layer (Haynes, 2008) at equivalent depth indicated by red arrow. ***D)*** Interpolation by second-order polynomial regression used to develop an age-depth model (red line) based on seven AMS and conventional ^{14}C dates (**Table S1**). The vertical gray bar represents 12.8 ± 0.15 ka, and the purple diamonds are sample depths. The green bar shows the depth of peak in spherules in 1-cm layer centered at 246.5 cm. The YDB layer has an age of ≈12.8 ka. ***E)*** Mammoth tooth was found at equivalent depth indicated by red arrow and was stained black by contact with black mat (above yellow dotted line), indicating that the animal lived close to the time of the YDB impact.

Murray Springs Site. Stratigraphy and the YDB layer. This site displays deposits typically consisting of alluvium/colluvium, marl, and/or lacustrine mudstone. Marl deposits (stratum E) are locally incised and filled with sandy and gravelly stream-channel deposits (stratum F1), and these are frequently capped by a distinctive carbon-rich "black mat" (stratum F2) that is mostly of algal origin, according to Haynes, 2008, but also contains charcoal. The black mat, in turn, is overlain by silty sediment (stratum F3), resulting from colluvial and alluvial deposition, including slopewash. Based on radiocarbon dating and the presence of Clovis artifacts associated with mammoth bones, Haynes and Huckell (2007) concluded that stratum F1 is of Clovis age and that the black mat (Unit F2) was deposited atop stratum F1 beginning at the onset of YD cooling at ≈12.8 ka.

For this study, Vance Haynes, principal investigator at Murray Springs, accompanied several of the co-authors to the site twice and observed the collection of samples. Ten 1- to 5-cm-thick discontinuous samples of bulk sediment were collected from a 46-cm-thick interval of sediment between 216 and 262 cmbs, and V. Haynes identified these samples as belonging to strata E, F1, and F2. The 1-cm-thick YDB layer was found at a depth of about 2.46 m at the contact between strata F1 and F2, which Haynes and Huckell (2007) demonstrated is widespread but discontinuous across the approximately 300×400 m excavation area. All samples were examined for spherules, and the 1-cm-thick YDB F1/F2 contact layer at a depth of 246 to 247 cmbs displayed a peak of 55 spherules/kg, a decrease of 0.5× (**SI Tables 2 & 3**), compared to the results of Firestone et al. (2007), who reported finding 109 spherules/kg. Kennett et al. (2009b) reported finding abundant nanodiamonds in this same layer. Later, Haynes et al. (2010a) confirmed finding numerous spherules in the YDB layer.

Some have proposed that a hiatus in deposition accounted for the concentration of spherules in the YDB between strata F1 and F2 (Surovell et al., 2010). However, Haynes and Huckell (2007) noted that mammoth bones and footprints in stratum F1 had been draped by the black mat layer of stratum F2 within a very brief time estimated as just a few weeks. Also, YDB proxies were deposited at the F1/F2 contact on top of bones and artifacts but beneath the black mat within a brief temporal window of a few weeks (Firestone et al, 2007). These observations and interpretations are inconsistent with speculations by Surovell et al. (2009), Pinter et al. (2011), and Pigati et al. (2012) that YDB spherules are cosmic in origin and simply accreted gradually during a long hiatus in deposition. These results also refute the speculation of Pigati et al. (2012) that the black mat acts to concentrate the spherules since all of our observed spherules occurred below the black mat and none were found in it. Furthermore, our SEM-EDS analyses

of these spherules clearly indicate that they are not of cosmic origin but instead contain quench crystals formed from the high-temperature melting of terrestrial sediments.

Chronology and the YDB layer. For this site, we adopted the geochronology of Haynes and Huckell (2007), who conducted excavations over several decades, developing detailed stratigraphic profiles, along with 69 radiocarbon dates on humates, carbonates, and charcoal. They found that the ages of strata E, F1, and F2 are generally consistent across the site; stratum F1 dates to before 12.8 ka and stratum F1 dates afterward, beginning at the YD onset. Haynes and Huckell (2007) did not directly date the strata at our sampling location, and so, we integrated several locations to produce a generalized composite age-depth model that is consistent with the geochronology of Haynes and Huckell (2007) for strata F2 through strata E. For the 46-cm interval, we utilized the seven dates available on sub-strata that match the stratigraphic designations provided by Haynes and Huckell (2007). These conventional and AMS ^{14}C dates ranged from 9.81 ± 0.15 ^{14}C ka BP (11.24 ± 0.3 cal ka BP) at 221 cmbs to 11.88 ± 0.25 ^{14}C ka BP (13.96 ± 0.39 cal ka BP) at 1237.86 masl (**Table S1**). Interpolation by second-order polynomial regression dates the proxy-rich YDB layer at the F1/F2 contact to ≈12.8 ka, consistent with the age of the YDB at other sites.

Archaeological Importance of Site. At Murray Springs, dozens of bones of extinct megafauna were discovered with the black mat draped conformably over them and staining their upper surface, including the mammoth tooth shown in the inset. The evidence indicates that YDB spherules were deposited across those bones before the black mat was deposited (Haynes and Huckell, 2007; Firestone et al., 2007). Based on the articulation and preservation of a nearly-complete mammoth skeleton that was found draped with the black mat, Haynes (2008) concluded that the mammoth had been butchered by Clovis hunters perhaps a few weeks before deposition of the black mat began. By implication, this was also the time of deposition of the YDB layer. There is no evidence for any *in situ* bones of extinct mammoths, American horses, American camels, dire wolves, saber-toothed tigers, and other extinct megafaunal taxa above the base of the black mat at this or other sites in North America, consistent with these animals becoming extinct at or near the YD boundary (Haynes, 2008). Clovis points, including the 4-cm point in the inset (SI Fig 15), were found below and in contact with the 12.8-kyr-old layer and none were found above it (Haynes, 2008).

SI FIG. 12. OMMEN SITE (lat/long: 52.526950°N, 6.363517°E) is 3 km west of Ommen in the province of Overijssel, Netherlands. ***A)*** Lithostratigraphic sequence of eolian sands contains a thin dark, charcoal-rich layer separating YD-age sands above from Usselo sands below. ***B)*** Photo of sequence shows 5-cm-thick layer at 117.5 cmbs (yellow dotted line) associated with the charcoal-rich layer at the top of the Usselo sand. This is the YDB layer and marks the onset of the YD cooling episode. ***C)*** A single ^{14}C date of 13.33 ± 0.06 cal ka was acquired from a depth of 117.5 cmbs in the YDB layer (**Table S1**). It is somewhat older than typical charcoal in the YDB, perhaps because of bioturbation, redeposition, or the "old wood" effect. Error bars are smaller than the dot size. The vertical gray bar represents 12.8 ± 0.15 ka, and the purple diamonds represent sample depths. Top of Usselo sand is denoted by black dashed line. The green bar shows the depth of the peaks in spherules in the 5-cm YDB layer centered at 117.5 cmbs.

Ommen Site. Stratigraphy and the YDB layer. For stratigraphic details, see Lingen discussion above. Seven 5-cm-thick continuous samples of bulk sediment were collected from a 50-cm-thick sequence between 92.5 and 142.5 cmbs. Six samples were analyzed for spherules revealing a peak of five spherules/kg in a 5-cm-thick layer, centered at 117.5 cmbs in the YDB layer from 115 to 120 cmbs (**SI Tables 2 & 3**).

Chronology and the YDB layer. With the limited goal of establishing the approximate age of the dark Usselo layer, charcoal was extracted from a depth of 117.5 cmbs, and the sample returned an AMS ^{14}C date of 11.44 ± 0.04 ^{14}C ka BP (13.33 ± 0.05 cal ka BP). Although this date is older than that of the YDB, possibly due to the dating of old wood, the stratigraphic position of the YDB in this site at the top of the Usselo sand is consistent with an age of ≈12.8 ka, the onset of the YD in many sites in NW Europe, including Lommel and Lingen (above).

Archaeological Importance of Site. See Lingen site for archaeological context.

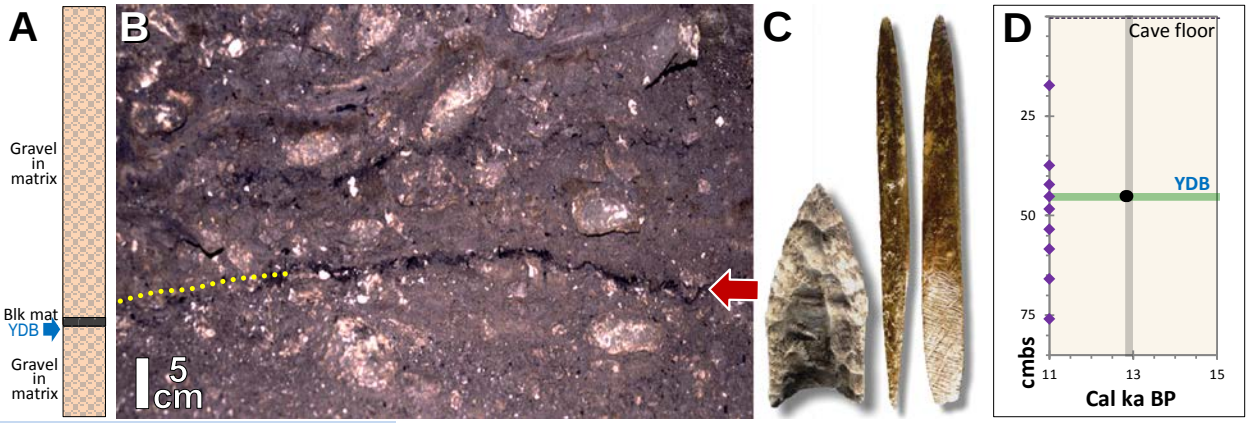

SI FIG. 13. SHERIDEN CAVE SITE (lat/long: 40.965055°N, 83.426038°W) is 4 km northwest of Carey, Ohio. ***A)*** Lithostratigraphic column shows that matrix-supported gravel dominates the cave sediment sequence. ***B)*** The YDB layer is a 1.5-cm-thick, charcoal-rich layer at 45.3 cm below cave floor (yellow dotted line). ***C)*** Illustrated Clovis projectile points made of chert (4 cm) and bone (14-cm) were found in the charcoal-rich YDB layer. ***D)*** Three ^{14}C dates, ranging from 12.80 ± 0.07 to 12.87 ± 0.08 cal ka were acquired on charcoal from the YDB layer (**Table S1**). Error bars are smaller than the dot size. The vertical gray bar represents 12.8 ± 0.15 ka, and the purple diamonds represent sample depths. Top of the cave floor is denoted by black dashed line. The green bar shows depth of peak in spherules in the 1.5-cm layer centered at 45.3 cmbs. The age of the YDB layer is ≈12.8 ka.

Sheriden Cave. Stratigraphy and the YDB layer. Samples were acquired from within a deeply stratified karst-collapse cavern situated in the once-glaciated Silurian plain of northwestern Ohio (Tankersley, 1997, 1999; Tankersley and Redmond, 1999a, 1999b; Redmond and Tankersley, 2011, Tankersley and Landefeld, 1998). The latest-Pleistocene deposits shown are dominated by matrix-supported gravel with angular limestone clasts related to freeze-thaw cycles and solifluction (slow downhill movement of material over frozen ground).

Nine continuous samples of bulk sediment 1.5 to 35 cm thick were collected from the 81-cm-thick sequence between 0 and 81 cmbs inside the cave. All samples were examined for spherules, revealing a peak of 110 spherules/kg centered at a depth 45.3 cmbs (44.5 to 46.0 cmbs) in a 1.5-cm-thick layer (**SI Tables 2 & 3**). This stratum is the YDB layer, composed of abundant wood-charcoal in a weakly stratified, dark-gray-and-white matrix with pebble gravel. It contains above-background levels of magnetic spherules, carbon spherules, charcoal, and nanodiamonds, including lonsdaleite, a hexagonal nanodiamond polymorph found at other YDB impact sites across North America (Redmond and Tankersley, 2011).

Chronology and the YDB layer. We adopted the chronology of Redmond and Tankersley (2005) and Waters et al. (2009b), based on 29 AMS radiocarbon dates on charcoal and burned bone. From various cave locations, those authors selected discontinuous samples, three of which were taken from the YDB layer. Those sample returned dates of 10.84 ± 0.08 ^{14}C ka BP (12.80 ± 0.07 cal ka BP), 10.92 ± 0.03 ^{14}C ka BP (12.83 ± 0.05 cal ka BP), and 10.96 ± 0.06 ^{14}C ka BP (12.87 ± 0.08 cal ka BP) (**Table S1**). All three dates indicate that the impact proxy-rich YDB layer at 45.3 cm dates to ≈12.8 ka, consistent with the age of the YDB at other sites.

Archaeological/Paleontological Importance.

Following retreat of the Laurentide Ice Sheet from this site during the Late Pleistocene, a sinkhole entrance formed prior to the YD onset, allowing plants, animals, and Clovis people to enter the cave (Tankersley, 1999). Later, during the YD episode, the cave rapidly filled with sediments, burying the entrance prior to ≈10 ka, thereby preserving a valuable archaeological/paleontological record. Abundant charcoal in the YDB layer at ≈12.8 ka provides evidence of intense biomass burning that charred many bones, including the youngest known specimens of two extinct megafauna, the giant beaver (*Castoroides ohioensis*) and the flat-headed peccary (*Platygonus compressus*) (Redmond and Tankersley, 2005). No *in situ* extinct megafaunal bones have been found above the 12.8-kyr-old charcoal-rich layer. Of the 63 taxa recovered in direct stratigraphic association from the Clovis layer, only two megafaunal species became extinct at the YDB, whereas 52 species of amphibians, arboreal plants, fish, mammals, and reptiles were not visibly affected by the impact event and remain extant in the vicinity of the cave.

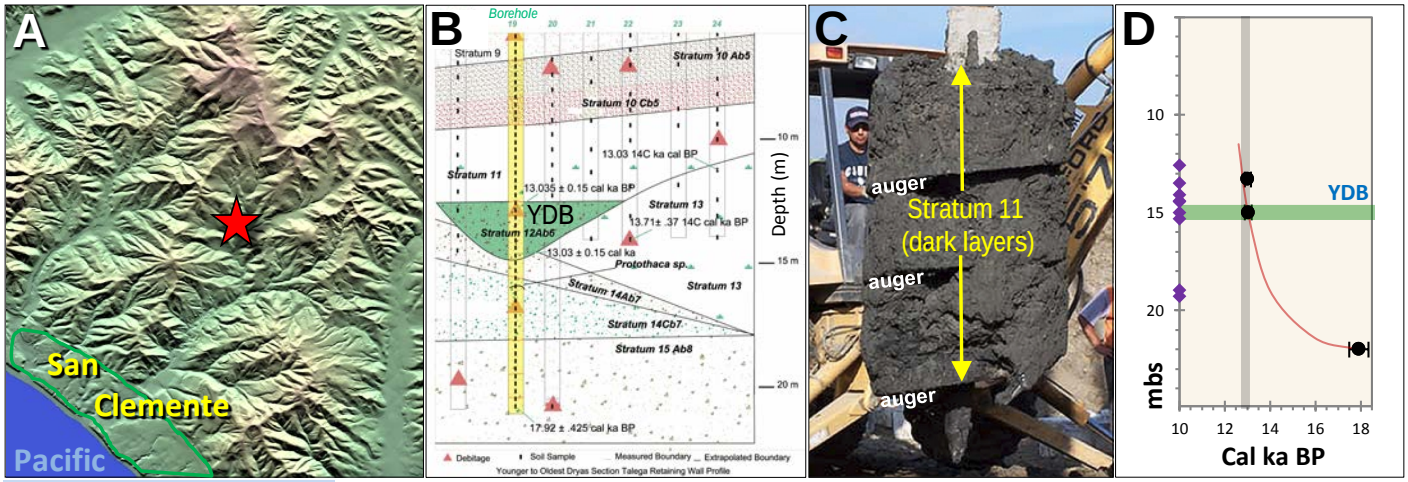

SI FIG. 14. TALEGA SITE (lat/long: 33.470292°N, 117.600471°W) is located 5 km north of San Clemente, California. ***A)*** Digital elevation model shows the site's location in the Santa Ana Mountains of Southern California. ***B)*** Generalized stratigraphic profile shows various strata. Borehole is in yellow with stratum containing YDB layer in green. ***C)*** Excavations with a backhoe-mounted auger exposed a thick peat-rich dark layer (Stratum 11, shown in photo). Below that layer extending to a depth of 15 m is a 2.4-m-thick interval (Stratum 12) containing abundant spherules in a 30-cm-thick sample (Bergin et al., 2011). ***D)*** Interpolation by second-order polynomial regression was used to develop an age-depth model (red line) based on three ^{14}C dates (**Table S1**). Some error bars are smaller than the dot size. The vertical gray bar represents 12.8 ± 0.15 ka, and the purple diamonds show sample depths. The green bar shows the depth of the spherule peak in the 30-cm layer centered at 15 mbs. Based on interpolation in the age-depth model, the age of the YDB layer is ≈12.8 ka.

Talega Site. Stratigraphy and the YDB layer. As part of an archaeological study mandated by the US Army Corps of Engineers and the State of California for a subdivision, trench and core samples were taken below Holocene-age layers to a depth of 21.5 mbs (Bergin et al., 2011). Nine 30-cm-thick discontinuous samples of bulk sediment, collected from a 6.7-m-thick interval of sediment between 12.6 and 19.3 mbs (strata 10-15) were examined for spherules.

Stratum 10, between 7.2 to 9.7 mbs, contained a YD-age soil, consisting of an A/C soil profile dating to between 11.22 ± 0.05 ^{14}C ka BP to 12.55 ± 0.4 ^{14}C ka BP. Stratum 11, located from approximately 9.7 to 12.8 m, is a YD-age layer of alluvial sand with bands of dark peat. The sequence indicates fluctuating water flow and possibly marshy conditions connected with intermittent ponding following the onset of YD climate change. Stratum 12, extending from approximately 12.8 to 15.2 m, was comprised of alluvial sand and silt intercalated with black silt loam laid down in a narrow channel fill structure. Two samples 1.7-m apart in this 2.4-m-thick section yielded an identical age of 13.02 ± 0.15 cal ka, suggesting that the channel was cut and refilled rapidly, possibly due to debris-flows. The dates also indicate that all or most of Stratum 12 is the YDB layer. Between approximately 14.9 to 15.2 mbs at the base of Stratum 12, a 30-cm-thick layer was sampled and found to contain a major abundance peak of 1930 impact spherules/kg, the fourth largest value and at the greatest depth (~15 mbs) of all 18 sites examined (SI Tables 2 & 3). Stratum 12 crosscuts stratum 13 which dates to

13.03 ± .37 and 13.71± .37 14C ka BP and which contained a small amount of impact debris, probably introduced from above by the drilling process. Stratum 14, the next below the YDB layer, extends from 15.2 to 18.4 m and consists of colluvium derived from the Monterey Formation that was redeposited on the canyon floodplain. Below 14, stream-laid stratum 15, dating to the Oldest Dryas (17.92 ± .425 cal ka BP), did not contain impact debris.

Chronology and the YDB layer. We adopted the dating for this site from Bergin et al. (2011), who collected bulk sediment samples across the YD interval and acquired three AMS radiocarbon dates, 11.06 ± 0.06 ^{14}C ka BP (13.02 ± 0.15 cal ka BP); 11.07 ± 0.05 ^{14}C ka BP (13.03 ± 0.15 cal ka BP); and 14.98 ± 0.43 ^{14}C ka BP (17.92 ± 0.425 cal ka BP) (**Table S1**). In an age-depth model generated by second-order polynomial regression, the spherule-rich, 30-cm-thick YDB layer at ≈15 mbs dates to ≈12.8 ka, consistent with the age of the YDB at other sites.

Archaeological Importance of Site. Chipped stone debitage (waste flakes) was uncovered in Younger Dryas age Stratum 10 above Stratum 12 and in strata 13, 14, and 15 below. No diagnostic projectile points or other lithic tools were recovered from any of those layers. The debitage found in the lower portion of the Talega site could be contamination introduce by the drilling process. However, if it is in place, the presence of artifacts in stratigraphic layers dating to nearly 18 ka indicates occupation of the California coast during the Oldest Dryas climatic interval. Moreover, accumulation of sediment in the coastal drainage at the Talega site appeared to keep pace with post Wisconsin sea level rise. Early archaeological sites located on the submerged portion of the coastal plain have been inundated, but also those sites located in drainages above modern sea level may have been buried by related sedimentation caused by encroaching shorelines.

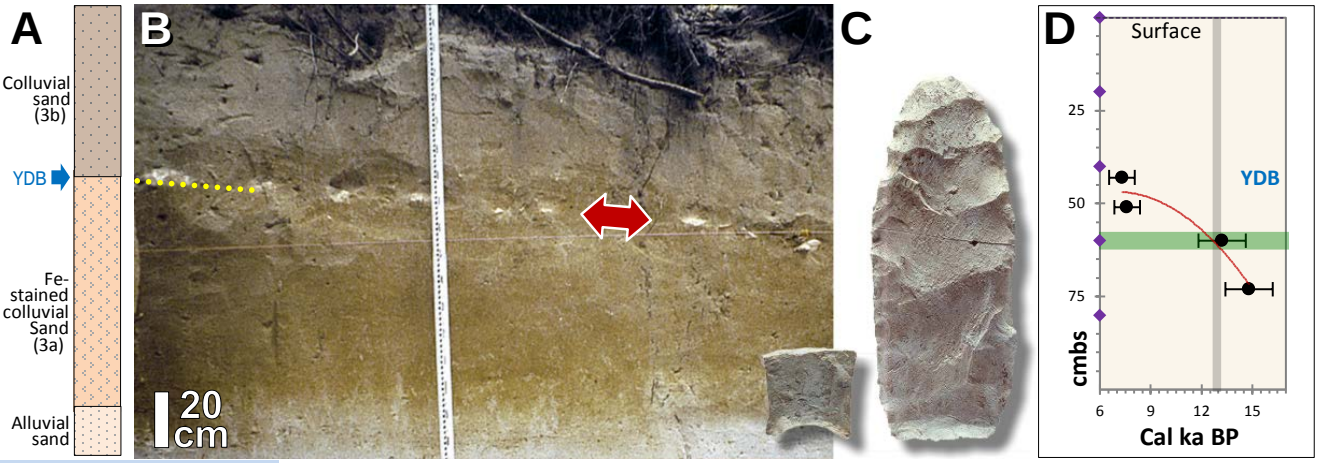

SI FIG. 15. TOPPER SITE (lat/long: 33.005763°N, 81.489266°W) is 17 km west of Allendale, South Carolina. ***A)*** Lithostratigraphic sequence shows dominance of colluvial and alluvial sand. ***B)*** Photo shows position of YDB layer within a 5-cm-thick interval at 60 cmbs (yellow dotted line) in contact with a distinctive, sharply delineated layer of Clovis debitage, or waste flakes, discarded during the chipping of tools (red double arrow). ***C)*** A 13-cm-long Clovis preform (unfinished projectile point) and lower portion of a broken Clovis fluted point were collected from the top of the Clovis interval immediately beneath the YDB layer. ***D)*** Second-order polynomial regression was used to develop an age-depth model (red line) based on three OSL dates (**Table S1**). The vertical gray bar represents 12.8 ± 0.15 ka, and the purple diamonds represent sample depths. Ground surface is denoted by black dashed line. The green bar shows the depth of a peak in spherules in a 5-cm layer centered at 60 cmbs. Based on interpolation, the YDB layer has an age of ≈12.8 ka.

Topper Site. Stratigraphy and the YDB layer. This site is located on an alluvial terrace adjacent to the Savannah River that cuts into relatively unconsolidated clastic sediments of Tertiary age (Waters, et al. 2009a). Sediments are largely represented by colluvial quartz-rich sands displaying several weakly defined stratigraphic units marked by variable amounts of iron staining. In the area sampled, abundant Clovis-age debitage occurs at the contact between lower stratigraphic Unit 3a and overlying Unit 3b. Seven 5-cm-thick discontinuous samples of bulk sediment were collected from a 180-cm-thick sequence between 0 and 180 cmbs. Six samples were analyzed for spherules revealing a peak of 110 spherules/kg in a 5-cm-thick YDB layer in Unit 3b centered at a depth of 60 cmbs (57.5 to 62.5 cmbs) (**SI Tables 2 & 3**). These results are consistent with YDB abundances reported by Firestone et al. (2007) of 97

spherules/kg and LeCompte et al. (2012) of 260 spherules/kg and contradict those of Surovell et al. (2009) who found no spherules (0 spherules/kg).

Chronology and the YDB layer. We adopted the chronology of Waters et al. (2009a), based on 18 OSL dates on quartz grains. Those authors examined discontinuous samples from various locations at Topper, none of which were at the same location sampled for this investigation. The closest sample location from Waters et al. (2009a) was in area D on transect A-G, approximately 60 m to the west of our sample site. From that area, we utilized the four OSL dates of Waters et al. that span the YDB interval: 7.3 ± 0.80 ka, 7.6 ± 0.90 ka, 13.2 ± 1.3 ka, and 14.8 ± 1.5 ka (**Table S1**); one charcoal sample dated to 12.8 ± 0.1 ka. Using these, we produced a generalized age-depth model using second-order polynomial regression that dates the proxy-rich YDB layer at 60 cmbs to ≈12.80 ka consistent with the age of the YDB at other sites.

Archaeological Importance of Site. During Clovis times, the Topper site was a chert quarry that has yielded tens of thousands of Paleoindian artifacts and debitage (Goodyear, 1999, 2005, 2006, 2010; Goodyear and Steffy, 2003; Goodyear et al., 2007). In a test conducted to determine the timing for emplacement of the spherules, LeCompte et al. (2012) found that sediments immediately overlying debitage exhibit a significant peak in spherules, whereas sediments immediately below the debitage contained negligible amounts. This was interpreted to reflect a shadow affect by the debitage preventing downward reworking of spherules. The stratigraphic distribution of artifacts at Topper shows that usage of the quarry by Paleoindians was abruptly interrupted at the onset of the YD at the time of the YDB impact (Anderson et al., 2011). Usage resumed by post-Clovis peoples in the latter half of the YD cooling episode up to 600 years later.

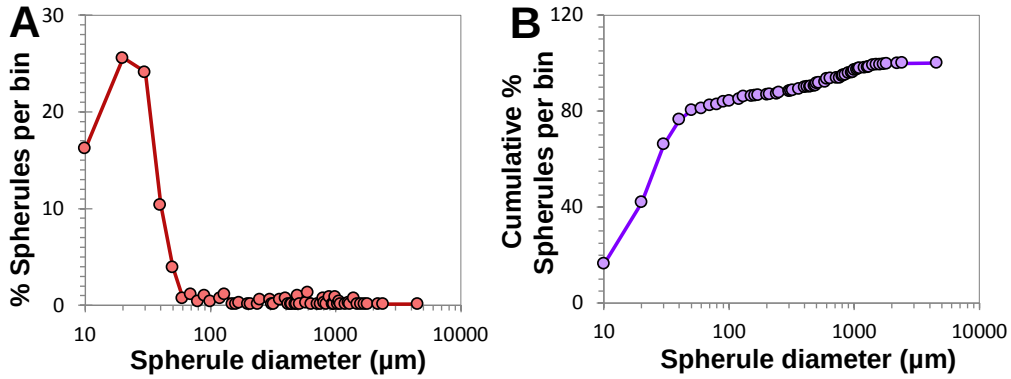

SI FIG. 16. DISTRIBUTION OF SPHERULE DIAMETERS. ***A)*** Plot of percentages of all YDB spherules by diameter in 10-µm bins. Average diameter is 135 µm, mean is 30 µm. ***B)*** Plot of cumulative percentages of all YDB spherules: 16% are ≤15 µm in diameter; 42% are ≤25 µm; 66% are ≤35 µm; 76% are ≤45 µm; and 80% are ≤55 µm.

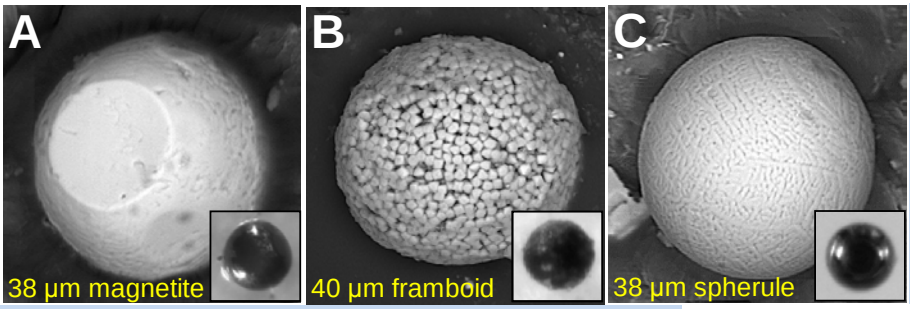

SI FIG. 17. SEM IMAGES OF COMMON YDB SPHERULITIC OBJECTS. Lake Cuitzeo, MEX: insets at lower right are light photomicrographs. Note all are rounded and reflective. ***A)*** Non-impact-related, rounded, monocrystalline magnetite grain. Note two instances of planar faceting. ***B)*** Non-impact-related, polycrystalline framboid. Note distinctive blocky, cube-like crystals. ***C)*** YDB impact spherule; note dendritic texture from growth of Fe crystals after high-temperature melting.

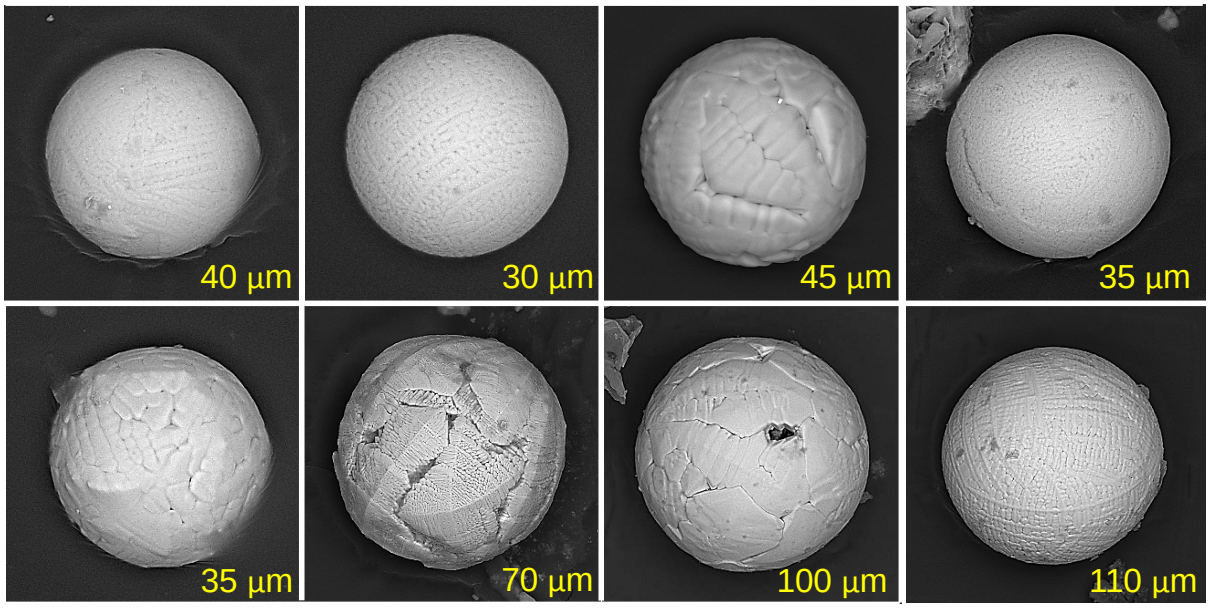

SI FIG. 18. SPHERULES FROM BLACKWATER DRAW, NEW MEXICO. SEM images display quench-melted textures indicative of rapid heating and cooling, consistent with an impact origin. Firestone et al. (2007), LeCompte et al. (2012), and this study all report finding numerous such spherules in the YDB at Blackwater Draw, whereas, Surovell et al. (2009) were unable to find any of these in the YDB layer. Spherule diameters shown in yellow.

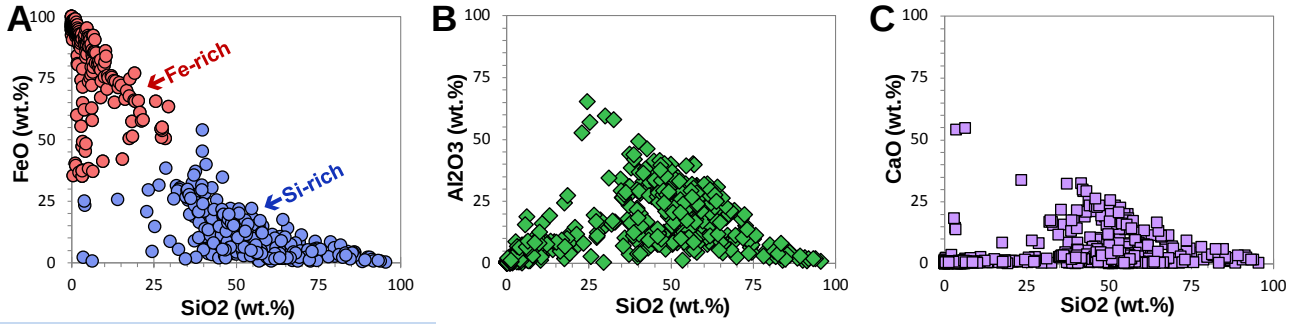

SI FIG. 19. TRANSITION DIAGRAMS. YDB spherule plots of oxide wt% for Fe, Al, Ca, and Si. ***A)*** The plot of FeO v. SiO_2 reveals two general groups of spherules, Fe-rich (upper left) and Si-rich (lower right) with some overlap. ***B)*** Al_2O_3 relative to SiO_2, showing that they vary inversely. ***C)*** CaO relative to SiO_2, showing that they typically vary inversely.

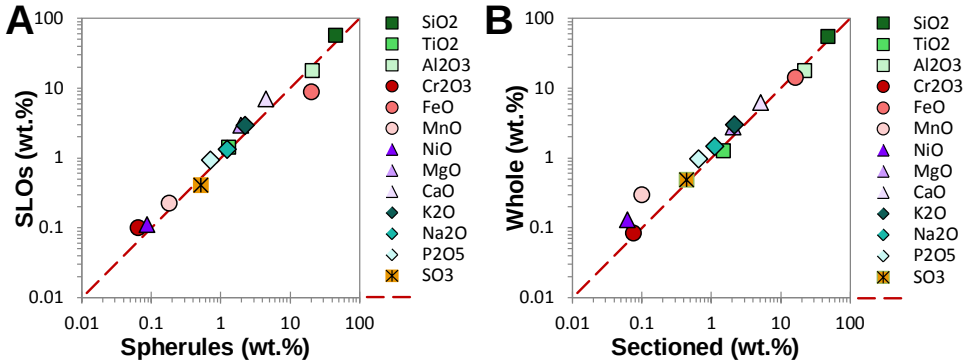

SI FIG. 20. COMPOSITIONAL PLOTS. ***A)*** Compares EDS analyses of all YDB spherules (n= 176 EDS) vs. SLOs (n= 153), all ≥200 µm, showing little difference. ***B)*** Compares EDS analyses of whole YDB objects (n= 173 EDS) with sectioned ones (n= 156), all ≥200 µm, also showing insignificant differences. Red dashed line represents equivalent values. Data shown are in **SI Tables S6-S7**.

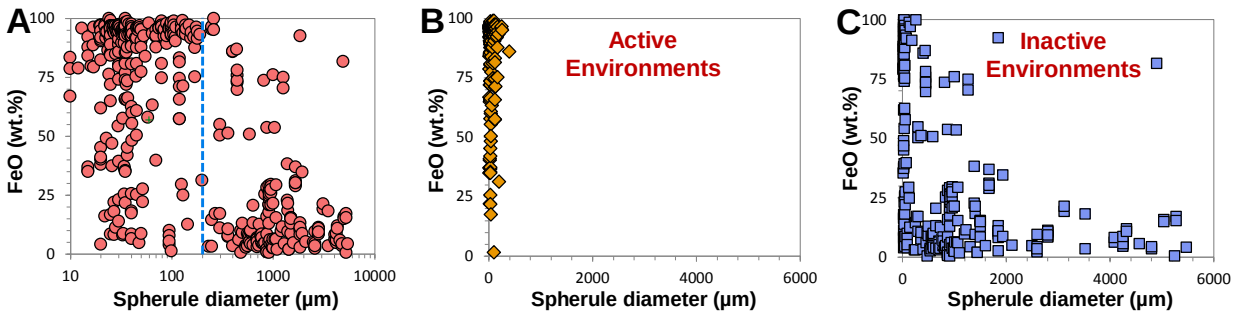

SI FIG. 21. SPHERULE DIAMETERS v. FeO WT%. ***A)*** Blue dashed line=200 µm. Most spherules <200 µm are biased toward high FeO wt%; those ≥200 µm have mostly lower FeO. ***B)*** Physically active paleoenvironments have smaller spherules with higher FeO wt%. ***C)*** Physically inactive paleoenvironments have larger ranges of sizes and FeO wt%.

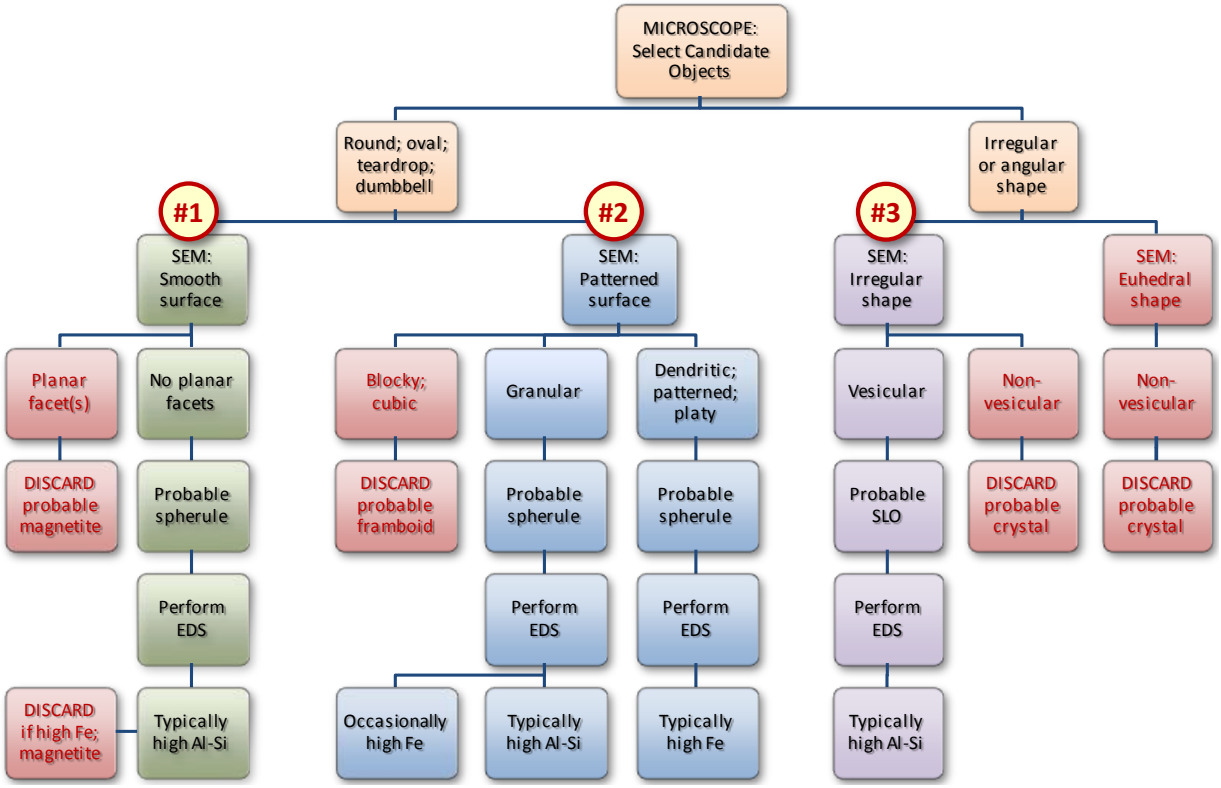

SI FIG. 22. FLOW CHART. Steps in identifying three main types of YDB objects: (**#1**; green) aerodynamically-shaped smooth spherules; (**#2**; blue) aerodynamically-shaped patterned spherules; and (**#3**; purple) angular SLOs.

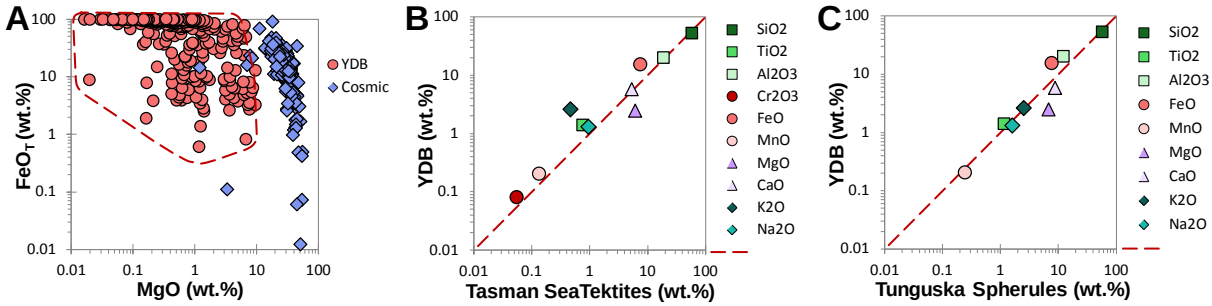

SI FIG. 23. POTENTIAL ORIGINS. ***A)*** Plot of MgO v. FeO shows that YDB spherules (red) have lower MgO wt% than nearly all Si-rich cosmic spherules from stony meteorites (blue), demonstrating that few YDB spherules are cosmic in origin. ***B)*** YDB spherules ≥200 µm closely resemble 5-Myr-old Tasman Sea tektites. ***C)*** YDB spherules ≥200 µm are similar in composition to spherules from the Tunguska airburst in 1908. Data shown in **SI Tables S6-S7**.

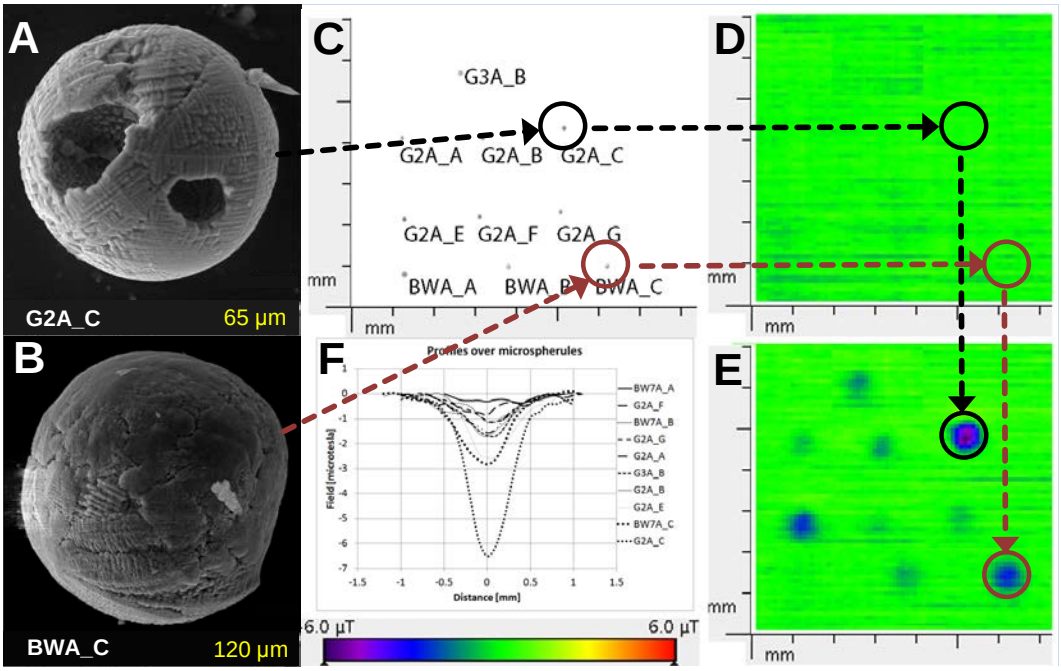

SI Fig. 24. MAGNETIC ANALYSES FOR LIGHTNING EXPERIMENTS. SEM images of microspherules. Diameters in yellow: ***A)*** Gainey, MI spherule (black arrows and circles) and ***B)*** Blackwater Draw, NM spherules (red arrows and circles). ***C)*** Distribution of optical images of selected spherules on the scanned substrate (circles around black dots). ***D)*** Image shows magnetic scan of the substrate in its natural state. Note that spherules are not visible above green background, indicating they are non-magnetized. ***E)*** Image shows magnetic scan of the substrate after magnetizing it with a 1-Tesla pulse field directed into the plane. Note that spherules are now visible above background, indicating they are magnetizable. ***F)*** Image shows magnetic profile of each spherule in horizontal direction.

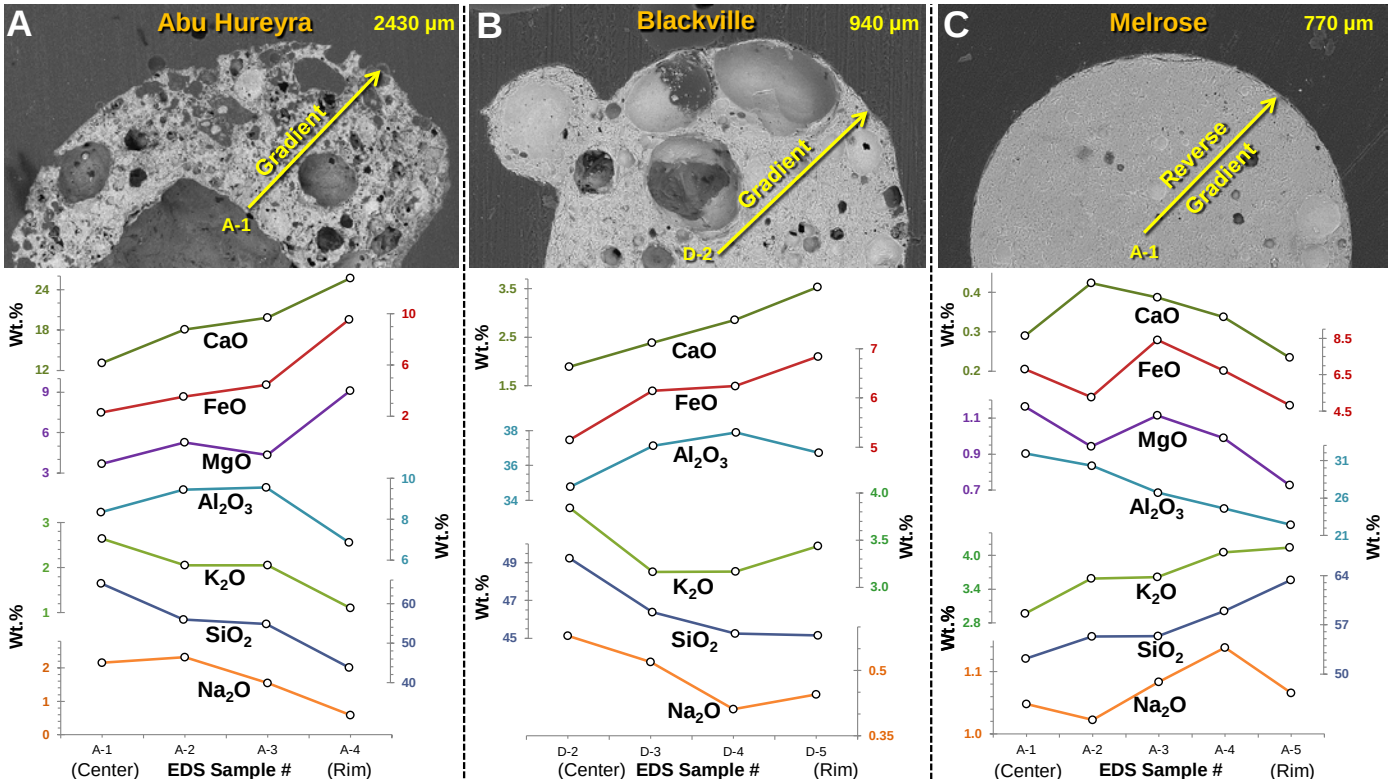

SI FIG. 25. SPHERULE GRADIENTS FROM CENTER TO RIM. ***A)*** Highly vesicular, oblong spherule from Abu Hureyra, Syria with refractory oxides increasing in percentage toward the rim, consistent with vaporization by boiling. ***B)*** Spherule from Blackville, SC, also indicating boiling. Note the smaller, hollow, accretionary spherule fused onto the larger one at upper left. ***C)*** Melrose, PA spherule shows a reverse gradient, with refractory oxides decreasing toward the rim. This spherule is fewer vesicles than most other YDB spherules. These observations are consistent with growth by condensation, although other processes may have been involved. Most of the gradients for each oxide trend predictably, although the trend in some is irregular, perhaps due to inclusions or heterogeneous mixing. Data shown in **SI Tables S5-S6**.

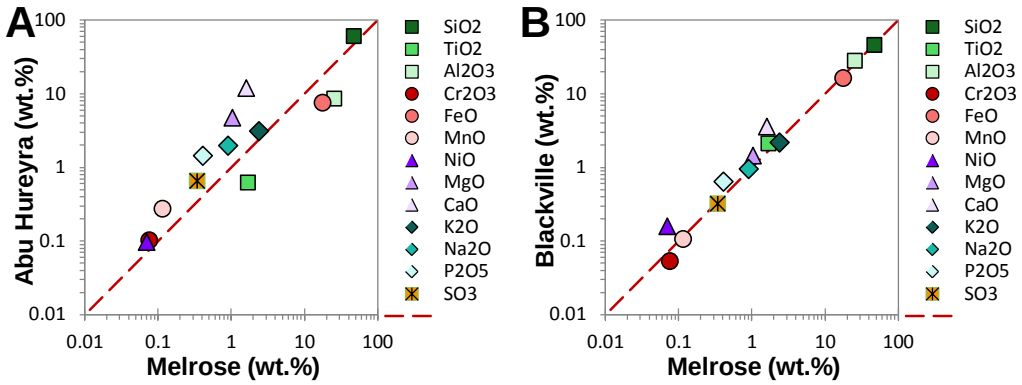

SI FIG. 26. COMPOSITIONAL COMPARISON OF KEY SITES. ***A)*** Melrose spherules ≥200 μm are compositionally dissimilar to those from Abu Hureyra, which contain less FeO and Al_2O_3 and more CaO, consistent with local presence of substantial limestone outcrops near the Euphrates River in Northern Syria. The similarity to local sediments suggests Abu Hureyra spherules are melted area rocks, which are comparatively enriched in Ca and Mg; Melrose spherules are comparatively enriched in Al, Fe, and Ti. ***B)*** Plot demonstrates that Melrose and Blackville spherules ≥200 μm are compositionally similar to each other. Red dashed line represents equivalent values. Data shown in **SI Tables S6-S7**. These results support the occurrence of at least two airbursts/impacts, one in Eastern North America and the other in Syria.

SUPPORTING MATERIAL: TABLES

TABLE S1. SITE LOCATIONS and CHRONOLOGIES. Age of YDB layer is highlighted in yellow. For most sites, the YDB layer was dated directly, but for some sites, it was dated through interpolation using the age-depth model, as noted.

Site	Latitude	Longitude	Elev. (m)	Lab	Depth	RCYBP	±	Cal BP*	±	Type	Material	Reference
Abu Hureyra	35.86670°N	38.40000°E	310	OxA-170	285.33 masl	10600	200	12430	270	AMS	Carbonized grain	Moore, et al. 2000
	--	--		OxA-407	285.13	10050	180	11680	320	AMS	Charred bone	Moore, et al. 2000
	--	--	--	OxA-386	285.12	10800	160	12780	140	AMS	Charred grain	Moore, et al. 2000
	--	--	--	OxA-473	284.95	10000	170	11610	290	AMS	Charred bone	Moore, et al. 2000
	--	--	--	OxA-397	284.91	10420	140	12310	240	AMS	Charred grain	Moore, et al. 2000
	--	--	--	OxA-434	284.91	10490	150	12370	230	AMS	Charred bone	Moore, et al. 2000
	--	--	--	OxA-171	284.72	10600	200	12430	270	AMS	Charred grain	Moore, et al. 2000
	--	--	--	UCIAMS-105429	284.70	11070	40	12932	176	AMS	Charcoal	Bunch et al. 2012
	--	--	--	BM-1718R	284.67	11140	140	13040	150	AMS	Charcoal	Moore, et al. 2000
	--	--	--	OxA-430	284.56	11020	150	12940	130	AMS	Charred bone	Moore, et al. 2000
	--	--	--	OxA-172	284.29	10900	200	12870	160	AMS	Charred seed	Moore, et al. 2000
	--	--	--	OxA-468	284.29	11090	150	13000	160	AMS	Charred bone	Moore, et al. 2000
	--	--	--	OxA-883	284.29	11450	300	13370	300	AMS	Charred grain	Moore, et al. 2000
Arlington Cyn	33.988587°N	120.158047°W	78	UCIAMS-47239	394 cmbs	11105	30	13020	50	AMS	Charcoal	Kennett, et al. 2009a
	--	--	--	UCIAMS-42816	404.5	11095	25	13010	50	AMS	Wood	Kennett, et al. 2009a
	--	--	--	UCIAMS-36308	461.5	11095	25	13010	50	AMS	Wood	Kennett, et al. 2009a
	--	--	--	UCIAMS-36307	471.0	11070	25	13000	50	AMS	Wood	Kennett, et al. 2009a
	--	--	--	UCIAMS-36959	487.0	11075	30	13000	50	AMS	Charcoal	Kennett, et al. 2009a
	--	--	--	UCIAMS-36960	487.0	11185	30	13090	60	AMS	Glassy Carbon	Kennett, et al. 2009a
	--	--	--	UCIAMS-36961	487.0	11440	90	13310	80	AMS	Carbon Sphere	Kennett, et al. 2009a
	--	--	--	UCIAMS-36962	487.0	11110	35	13020	60	AMS	Carbon Elongate	Kennett, et al. 2009a
	--	--	--	UCIAMS-36306	495.0	11375	25	13250	40	AMS	Wood	Kennett, et al. 2009a
	--	--	--	UCIAMS-36305	495.5	11235	25	13150	40	AMS	Wood	Kennett, et al. 2009a
	--	--	--	UCIAMS-36304	500.5	11020	25	12960	50	AMS	Wood	Kennett, et al. 2009a
Barber Creek	35.600592°N	77.303636°W	6	UW 1907	80.0 cmbs	--	--	9200	700	OSL	Quartz grains	Moore, et al. 2009
	--	--	--	UW 1908	100.0	--	--	12100	700	OSL	Quartz grains	Moore, et al. 2009
	--	--	--	UW 1909	140.0	--	--	14500	1000	OSL	Quartz grains	Moore, et al. 2009
Big Eddy	37.736470°N	93.786128°W	232	AA-27488	--	10470	80	12400	180	AMS	Charcoal	Lopinot, et al. 1998
	--	--	--	AA-26654	--	10710	85	12700	50	AMS	Charcoal	Lopinot, et al. 1998
	--	--	--	AA-75720	--	10896	54	12830	60	AMS	Charcoal	Lopinot, et al. 1998
	--	--	--	Beta-230984	--	10940	60	12860	70	AMS	Charcoal	Lopinot, et al. 1998
	--	--		AA-72612	--	10959	54	12870	70	AMS	Charcoal	Lopinot, et al. 1999
	--	--	--	AA-27485	--	11280	75	13180	80	AMS	Charcoal	Lopinot, et al. 1998
	--	--	--	AA-34589	--	11375	80	13260	100	AMS	Charcoal	Lopinot, et al. 1998
Blackville	33.361545°N	81.304348°W	98	LB862	107 cmbs	--	--	11500	1030	OSL	Quartz grains	Bunch et al. 2012
	--	--	--	LB861	152.0	--	--	18540	1680	OSL	Quartz grains	Bunch et al. 2012
	--	--	--	LB859	183.0	--	--	12960	1190	OSL	Quartz grains	Bunch et al. 2012
Blackwater	34.275687°N	103.326101°W	1243	A-4703	1237.97 masl	10000	910	11480	1160	^{14}C	Humates	Haynes, et al. 1995
	--	--		A-4705	1237.86	9260	320	10500	470	^{14}C	Humates	Haynes, et al. 1995
	--	--		AA-2261	1237.76	9950	100	11480	180	AMS	Humates	Haynes, et al. 1995
	--	--		SMU-1880	~1237.56	10780	110	12770	80	AMS	Humates	Johnson, et al. 1997
	--	--	--	AA-2262	1237.48	11810	90	13650	110	AMS	Humates	Haynes, et al. 1995
Chobot	52.956004°N	114.734872°W	882	--	20 cmbs	--	--	13025	225	--	Archaeology	Waters, et al. 2007
Cuitzeo	19.936516°N	101.155676°W	1833	A9353	1.35 mbs	6165	70	7070	90	AMS	Bulk carbon	Israde, et al. 2012
	--	--	--	A9354	1.95	8830	215	9910	260	AMS	Bulk carbon	Israde, et al. 2012
	--	--	--	--	2.80	--	--	12800	150	--	Age-depth	Israde, et al. 2012
	--	--	--	T11-M47	3.35	15500	130	18670	80	AMS	Bulk carbon	Israde, et al. 2012
Gainey	42.885973°N	83.614324°W	302	MI-2	--	--	--	12360	1230	OSL	Quartz grains	Simons, et al. 1984
Kimbel Bay	34.981811°N	78.776820°W	34	UCIAMS 52613	147 cmbs	1195	15	1130	40	AMS	Charcoal	This paper*
				--	--	--	--	12800	150	--	Age-depth	This paper
	--	--	--	LB863	375.0	--	--	25500	2720	OSL	Quartz grains	This paper†
	--	--	--	LB864	406.0	--	--	26080	2940	OSL	Quartz grains	This paper†
	--	--		AW-SKB-6	436.0	--	--	21640	2630	OSL	Quartz grains	This paper†
	--	--	--	UCIAMS 52622	445.0	27250	130	31900	120	AMS	Charcoal	This paper*
	--	--	--	UCIAMS 52622	450.0	39690	710	43460	610	AMS	Charcoal	This paper*
Lingen	52.508751°N	7.313882°E	25	--	--	--	--	12800	150		Age-depth	This paper
				UCIAMS 46302	52.5 cmbs	11310	60	13200	80	AMS	Charcoal	This paper*
Lommel	51.236231°N	5.254686°E	44	--	--	10950	50	12860	70	AMS	Charcoal	Van Geel, et al. 1989
	--	--	--	UCIAMS 46303	48.5 cmbs	11480	100	13390	120	AMS	Charcoal	This paper*
Melrose	41.925410°N	75.510436°W	419	--	--	--	--	12800	150		Age-depth	Bunch et al. 2012
				LB860a	30.0	--	--	16400	1600	OSL	Quartz grains	Bunch et al. 2012
Murray Spgs	31.570912°N	110.177996°W	1274	TX-1238	F2	9810	150	11240	300	AMS	Carbonate	CARD, et al. 2011
	--	--	--	A-977	F2b	10250	170	12010	370	AMS	Carbonate	Haynes, et al. 2007
	--	--	--	AA-26212	F2a1	10628	60	12660	50	OSL	Residue	Haynes, et al. 2007
	--	--	--	A-1045	F2/D	10760	100	12740	70	OSL	Charcoal	Haynes, et al. 2007
	--	--	--	TX-1462	F1	10930	170	12900	140	OSL	Charcoal	Haynes, et al. 2007
	--	--	--	SMU-18	F1 (E2)	11190	180	13090	180	AMS	Charcoal	Haynes, et al. 2007
	--	--	--	SMU-33	E	11880	250	13960	390	AMS	Carbonate	Haynes, et al. 2007
Ommen	52.526950°N	6.363517°E	6	UCIAMS 46307	117.5 cmbs	11440	35	13300	50	AMS	Charcoal	This paper*
Sheriden	40.965055°N	83.426038°W	274	Beta-127909	Charc. layer	10840	80	12800	70	AMS	Charcoal	Redmond, et al. 2005
	--	--		UCIAMS-38249	Charc. layer	10915	30	12830	50	AMS	Charcoal	Redmond, et al. 2005
	--	--	--	Beta-127910	Charc. layer	10960	60	12870	80	AMS	Charcoal	Redmond, et al. 2005
Talega	33.470292°N	117.600471°W	104	Beta-196150	13 mbs	11060	60	13020	145	AMS	Bulk carbon	Bergin, et al. 2007
	--	--	--	Beta-196151	15.0	11070	50	13030	145	AMS	Bulk carbon	Bergin, et al. 2007
	--	--	--	Beta-196153	21.0	14980	425	17920	425	AMS	Bulk carbon	Bergin, et al. 2007
Topper	33.005763°N	81.489266°W	36	UIC-782	--	--	--	7300	800	OSL	Quartz grains	Waters, et al. 2009a
	--	--	--	UIC-835	--	--	--	7600	900		Quartz grains	Waters, et al. 2009a
	--	--	--	AA100294 2012-3	Clovis layer	--	--	12835	114	AMS	Charcoal	Goodyear, 2013
	--	--	--	UIC-763	Clovis layer	--	--	13200	1300	OSL	Quartz grains	Waters, et al. 2009a
	--	--	--	UIC-764	--	--	--	14800	1500	OSL	Quartz grains	Waters, et al. 2009a

*^{14}C Dating by: University of California, Irvine with prep by University of Oregon or Penn State University

†OSL Dating by: IIRMES laboratory, California State University Long Beach.

TABLE S2. DISTRIBUTION OF SPHERULES BY SITE AND REGION. Columns list site location information. The abundances in number of spherules per kg are roughly equivalent to the number per 150 cm^2. The numbers of spherules per kg in this study is compared to that of Firestone, et al. (2007) and LeCompte et al. (2012). Regional data compare average diameters and concentrations of spherules. The three sites with largest values (Abu, Blackville, and Melrose) vary from 1,000 to 12,000 km apart, suggesting multiple impact sites.

SITE		Region	YDB depth (m)	Thick (cm)	Bulk sed (g)	Mag grns (g)	SLOs g kg^{-1}	# MSp found	# SEM/ EDS	Avg (μm)	Msp/ cm^2	Msp/ 150 cm^2	# kg^{-1}	# kg^{-1} [Firestone (2007)]	Vari-ance	# kg^{-1} [LeCompte (2012)]	Vari-ance
Abu Hureyra	SYR	Asia	4.10	3.0	25	73.6	15.76	59	131	712	3.0	446	595	--	--	--	--
Arlington Cyn	CA	SW	5.03	5.0	217	3.0	--	13	7	45	0.4	54	60	--	--	--	--
Barber Creek	NC	SE	1.00	2.5	23	1.8	--	24	20	41	8.0	1194	1035	--	--	--	--
Big Eddy	MO	SE	3.31	8.0	260	0.5	--	26	11	19	0.5	77	100	--	--	--	--
Blackville	SC	SE	1.83	15.0	53	1.3	0.06	36	151	104	4.9	735	525	205	160%	--	--
Blackwater Draw	NM	SW	2.50	1.0	107	1.4	--	103	103	25	5.7	855	960	768	30%	624	19%
Chobot	ALB	NW	0.13	1.0	24	2.0	--	6	2	30	0.6	90	250	578	60%	--	--
Cuitzeo	MEX	C.Am	2.80	5.0	12	5.8	--	25	12	41	10.3	1541	2055	--	--	--	--
Gainey	MI	NE	0.33	5.0	34	2.9	--	46	33	40	9.9	1485	1350	2144	40%	--	--
Kimbel Bay	NC	SE	3.58	15.0	10	13.2	--	47	28	25	44.6	6690	4900	--	--	--	--
Lingen	GER	Eur	0.44	5.0	400	4.5	--	12	9	23	0.3	45	30	--	--	--	--
Lommel	BEL	Eur	0.49	3.0	400	2.7	--	4	4	73	0.1	15	10	16	40%	--	--
Melrose	PA	NE	0.19	8.0	45	2.7	0.80	140	98	236	14.3	2145	3110	--	--	--	--
Murray Spgs	AZ	SW	2.46	1.0	309	2.6	--	17	6	28	0.2	30	55	109	50%	--	--
Ommen	NED	Eur	1.18	5.0	1600	3.2	--	8	3	54	0.1	15	5	--	--	--	--
Sheriden	OH	NE	0.45	1.5	245	7.2	--	27	7	48	0.5	81	110	--	--	--	--
Talega	CA	SW	15.00	30.0	30	0.4	--	57	12	25	9.7	1455	1930	--	--	--	--
Topper	SC	SE	0.60	5.0	309	0.5	--	34	22	21	0.9	128	110	97	10%	260	168%
		AVG/SITE	**2.52**	**6.6**	**228**	**7.2**	**5.54**	**35**	**37**	**135**	**6.3**	**949**	**955**	**560**	**56%**	**442**	**94%**
		MEDIAN	**1.50**	**5.0**	**80**	**2.7**	**0.80**	**27**	**--**	**30**	**1.9**	**287**	**388**	**205**	**--**	**--**	**--**
		TOTAL	**--**	**--**	**4100**			**684**	**659**	**--**	**--**	**17080**	**17190**	**3917**	**--**	**884**	**--**

REGION	Avg. Diam	Msp/ cm^2
N.Am, NE	43	8.2
N.Am, SE	26	11.8
N.Am, NW	30	0.6
N.Am, SW	26	4.0
EUR	41	0.2
C.Am	41	10.3
SLO SITES		
Abu Hureyra	712	3.0
Blackville	104	4.9
Melrose	236	14.3

TABLE S3. STRATIGRAPHIC DISTRIBUTION OF YDB SPHERULES AND SLOs. For this table, "cm" =depth relative to YDB, "Thick" =thickness in cm, "MGr" = magnetic grain in g/kg, "MSp" = spherules in #/kg, and "SLO" =scoria-like objects in g/kg. The zero layer is the YDB and corresponds to the YDB date in yellow in Table S1.

Abu Hureyra, SYR					Arlington Cyn, CA				Barber Crk, NC				Big Eddy, MO				Blackwater, NM				Chobot, AB, CAN			
cm	Thick	MGr	MSp	SLO	cm	Thick	MGr	MSp	cm	Thick	MGr	MSp	cm	Thick	MGr	MSp	cm	Thick	MGr	MSp	cm	Thick	MGr	MSp
290	5	94.7	0	0.00	39	5	4.5	0	2.5	2.5	2.2	60	16	8	0.3	0	50,55	6	0.3	0	5.5	1	0.4	0
210	5	124.2	--	0.00	34	5	2.3	--	0	2.5	1.8	1035	8	8	0.3	15	43	8	0.2	--	4	1	0.4	0
180	5	77.8	0	0.02	28	6	3.7	--	-2.5	2.5	2.7	55	0	8	0.5	100	28	10	0.0	0	3	1	0.4	0
175	5	113.4	--	0.04	23	5	4.8	0					-8	8	0.4	0	14,17	6	0.3	2	2	1	0.4	0
78	5	129.0	0	0.23	18	5	3.3	--					-16	8	0.4	0	8	6	0.7	110	1	1	0.6	80
0	3	73.6	595	15.76	13	6	3.4	--									0	1	1.4	960	0	1	2.0	250
-12	5	181.6	20	0.66	9	2	2.0	0									-10,-7	10	0.5	80	-1	1	0.8	100
					5	5	6.0	25									-27,-32	6	0.5	0	-2	1	0.8	0
					0	5	3.0	60									-42	10	0.8	2	-3	1	0.5	0
																	-52,-57	10	1.1	175	-5	1	0.5	0
																					-7	1	0.4	0

Blackville, SC					Cuitzeo, ,MEX				Gainey, MI				Kimbel Bay, NC				Lingen, GER				Lommel, BEL			
cm	Thick	MGr	MSp	SLO	cm	Thick	MGr	MSp	cm	Thick	MGr	MSp	cm	Thick	MGr	MSp	cm	Thick	MGr	MSp	cm	Thick	MGr	MSp
76	15	1.2	190	0.00	45	10	3.0	120	25	5	0.2	40	75	15	8.8	55	36.0	5	3.8	0	31	5	3.2	0
61	15	1.1	115	0.01	25	10	0.1	125	20	5	0.3	60	45	15	7.3	15	26.0	5	1.3	--	21	5	1.7	0
46	15	1.1	90	0.00	15	5	1.0	80	15	5	1.9	--	30	15	7.1	985	16.0	5	2.7	0	11	5	1.9	0
30	15	0.1	70	0.04	10	5	1.2	310	10	5	0.3	185	15	15	8.2	135	3.5	4	6.2	5	2.5	3	4.4	0
15	15	1.3	205	0.03	5	5	0.8	215	5	5	0.3	400	0	15	13.2	4900	0.0	3	4.5	30	0	3	2.7	10
0	15	1.3	525	0.06	0	5	5.8	2055	0	5	2.9	1350	-16	15	9.7	0	-4.0	5	5.9	0	-4	5	1.4	3
-15	15	1.7	0	0.00	-10	10	15.3	220	-5	5	3.2	110					-9.0	5	7.7	--	-9	5	1.8	0
-30	15	4.0	0	0.00	-20	10	5.6	0	-10	5	2.5	0					-14.0	5	4.1	0	-19	5	2.5	--
-46	15	4.4	2	0.00	-30	10	8.9	0	-15	5	2.4	0					-24.0	5	4.6	--	-29	5	3.3	0
-61	15	1.4	0	0.00	-40	10	6.1	0	-20	5	1.5	--					-34.0	5	2.3	0				
-76	15	1.4	5	0.00																				

Melrose, PA					Murray Sprgs, AZ				Ommen, NED				Sheriden Cave, OH				Talega, CA				Topper, SC (upper)			
cm	Thick	MGr	MSp	SLO	cm	Thick	MGr	MSp	cm	Thick	MGr	MSp	cm	Thick	MGr	MSp	cm	Thick	MGr	MSp	cm	Thick	MGr	MSp
9	10	7.0	310	0.76	20.5	5	0.0	0	25	5	3.9	0	27.75	35	1.8	0	244	30	3.4	120	60	5	0.1	0
0	8	2.7	3110	0.80	15.5	5	0.0	0	15	5	4.5	0	7.75	5	1.2	0	152	30	0.5	20	40	5	0.2	0
-6	5	4.2	1190	0.05	10.5	5	0.0	0	5	5	4.1	0	3	4.5	2.1	40	91	30	1.6	30	20	5	0.3	20
-14	10	11.1	70	0	5.5	5	0.1	0	0	5	3.2	5	0	1.5	7.2	110	61	30	0.0	0	0	5	0.5	110
-24	10	0.7	210	0	1.8	2.5	0.4	8	-5	5	2.4	0	-3.25	5	2.5	0	57	30	0.5	25	-20	5	0.3	0
					0.0	1	2.6	55	-15	5	3.6	--	-8.25	5	1.7	0	0	30	0.4	1930	-40	5	0.3	--
					-1.8	2.5	0.7	9	-25	5	2.0	0	-13.25	5	1.5	0	-30	30	0.3	10	-60	5	0.3	0
					-5.5	5	1.3	0					-20.75	10	1.0	0	-396	30	0.3	230				
					-10.5	5	0.4	0					-30.75	10	1.0	0	-427	30	0.1	38				
					-16.5	5	0.0	0																

TABLE S4. AVERAGE OXIDE PERCENTAGES of YDB spherules and SLOs, with magnetic grains for some sites. Spherule wt% acquired by EDS; magnetic grain wt% by NAA and PGAA. Uncertainties for major oxides are approximately ±5% and for minor oxides, ±20%. Average crustal values shown for comparison (Rudnick and Gao, 2005).

SITE	Al_2O_3	CaO	Cr_2O_3	FeO	K_2O	MgO	MnO	Na_2O	NiO	P_2O_5	SiO_2	SO_3	TiO_2
Abu Hureyra: spherules	9.4	10.4	0.0	11.6	3.2	4.9	0.3	1.9	0.1	1.0	55.1	0.7	1.3
SLOs	7.5	11.7	0.1	7.0	3.0	4.3	0.3	1.8	0.1	1.6	61.2	0.6	0.7
Arlington Cyn: spherules	3.7	3.1	0.1	68.6	0.3	1.2	0.5	0.7	0.2	2.5	5.1	0.6	13.4
Barber Creek: spherules	4.6	0.4	0.1	84.3	0.4	0.3	0.3	1.0	0.2	0.3	7.5	0.4	0.2
Big Eddy: spherules	6.2	1.0	0.1	61.6	0.4	2.5	1.3	0.9	0.1	1.9	10.7	0.9	12.5
Blackville: spherules	26.3	4.4	0.1	18.1	1.8	1.7	0.1	1.1	0.1	0.8	43.1	0.4	2.0
SLOs	30.0	1.6	0.1	11.6	2.9	0.9	0.1	0.6	0.2	0.2	49.4	0.1	2.3
Magnetic grains	15.7	1.0	0.1	31.6	1.0	0.2	0.2	0.3	0.0	0.1	41.8	0.2	7.7
Blackwater: spherules	1.5	0.4	0.1	87.8	0.1	0.8	0.4	0.5	0.1	0.3	3.0	0.7	4.2
Magnetic grains	6.4	1.3	0.1	23.2	0.9	0.8	0.9	0.6	0.0	0.0	54.9	0.0	10.9
Chobot: spherules	4.0	0.7	0.0	82.5	0.2	1.2	2.5	1.5	0.0	2.1	4.5	0.5	0.2
Magnetic grains	12.8	1.4	0.0	13.6	2.7	0.0	0.6	1.6	0.0	0.0	66.2	0.0	1.0
Cuitzeo: spherules	0.2	0.4	0.1	96.4	0.1	0.2	0.3	0.3	0.2	0.4	0.7	0.7	0.2
Gainey: spherules	3.8	0.9	0.1	81.3	0.2	0.2	0.2	0.2	0.1	0.2	7.3	0.3	5.3
Magnetic grains	11.1	2.3	0.0	13.3	2.1	3.0	0.4	3.1	0.0	0.0	62.9	0.0	1.6
Kimbel Bay: spherules	0.9	0.3	0.2	94.3	0.1	0.2	0.5	0.5	0.2	0.5	1.6	0.5	0.2
Lingen : spherules	1.7	0.6	0.3	86.4	0.2	0.2	0.5	4.4	0.2	0.7	3.8	0.8	0.2
Lommel: spherules	13.7	5.3	0.2	32.8	0.8	1.1	3.6	3.2	0.0	0.3	22.9	0.8	15.3
Magnetic grains	5.9	1.7	0.8	24.6	0.2	0.7	1.5	1.5	0.0	0.0	39.2	0.1	23.7
Melrose: spherules	23.8	1.5	0.1	26.1	1.9	0.7	0.1	1.0	0.1	0.6	42.5	0.4	1.3
SLOs	27.7	1.7	0.1	10.2	2.9	1.6	0.2	0.9	0.1	0.2	52.1	0.3	2.1
Magnetic grains	15.0	0.3	0.1	13.4	2.6	0.5	0.7	0.8	0.0	0.0	55.0	4.9	1.0
Murray Spgs: spherules	3.9	0.6	0.1	80.1	0.4	0.4	0.4	0.3	0.2	0.3	12.6	0.5	0.2
Magnetic grains	6.9	4.4	0.0	21.5	1.5	1.5	2.6	0.7	0.0	0.1	39.0	0.0	21.6
Ommen: spherules	4.2	0.8	0.0	85.1	0.2	0.3	0.0	0.7	0.1	0.5	7.8	0.0	0.4
Sheriden: spherules	2.8	0.5	0.1	86.1	0.2	0.3	0.2	0.3	0.1	0.0	9.3	0.0	0.1
Talega: spherules	8.3	8.6	0.1	50.9	0.8	2.4	0.4	1.1	0.2	0.6	24.1	0.8	1.6
Magnetic grains	10.6	6.8	0.3	23.0	1.2	1.0	1.3	1.7	0.0	0.0	39.0	0.4	13.6
Topper: spherules	8.9	0.4	0.1	67.9	0.2	0.8	0.6	0.3	0.1	1.1	11.1	0.2	8.3
Magnetic grains	1.4	0.2	0.1	37.3	0.4	0.2	1.8	0.1	0.0	0.0	17.2	0.1	41.1
Spherule AVG:	**7.1**	**2.2**	**0.1**	**66.8**	**0.6**	**1.1**	**0.7**	**1.1**	**0.1**	**0.8**	**15.1**	**0.5**	**3.7**
SLOs AVG:	**21.7**	**5.0**	**0.1**	**9.6**	**2.9**	**2.3**	**0.2**	**1.1**	**0.1**	**0.7**	**54.2**	**0.3**	**1.7**
Magnetic grains AVG:	**9.5**	**2.2**	**0.2**	**22.4**	**1.4**	**0.9**	**1.1**	**1.2**	**0.0**	**0.0**	**46.1**	**0.6**	**13.6**
Crustal Values AVG:	**15.4**	**4.0**	**0.0**	**5.3**	**3.1**	**2.8**	**0.1**	**3.3**	**0.0**	**0.2**	**65.2**	**0.0**	**0.6**

TABLE S5. COMPOSITIONAL PERCENTAGES for 36 spherules, including the 18 in Fig. 3A-3R, by letter. Shows location, active/inactive paleoenvironments, object types, diameters, catalog numbers, and weight percentages.

Fig. 3	SITE	State, Country	Continent	Active/ Inactive	Type	Diam (μm)	Catalog #	Al2O3	CaO	Cr2O3	FeO_T	K2O	MgO	MnO	Na2O	NiO	P2O5	SiO2	SO3	TiO2
A	Abu Hureyra	SYR	Asia	I	sph	830	E301-3, Grain 8	6.8	21.6	0.0	25.3	1.6	4.8	0.0	2.3	0.2	0.2	35.5	0.0	1.6
	Abu Hureyra	SYR	Asia	I	SLO	910	ABU 910 glass	10.2	11.9	0.1	14.2	2.5	5.6	0.2	1.7	0.4	2.0	50.0	0.5	0.6
B	Arlington Cyn	CA	N Am, SW	A	sph	25	340_11	4.7	0.6	0.3	64.8	0.3	3.2	0.4	0.5	0.1	1.1	3.5	0.7	19.7
	Arlington Cyn	CA	N Am, SW	A	sph	25	340_02	7.2	0.4	0.1	84.6	0.1	0.6	0.1	0.4	0.2	0.8	4.7	0.7	0.2
C	Barber Creek	SC	N Am, SE	A	sph	35	Spherule 1barb 2	7.8	0.4	0.1	65.8	1.1	0.9	0.0	3.0	0.4	0.0	19.0	0.7	0.8
	Barber Creek	SC	N Am, SE	A	sph	60	Spherule 2barb 10	0.6	0.0	0.1	97.9	0.0	0.0	0.1	0.3	0.0	0.5	0.0	0.4	0.1
D	Big Eddy	MO	N Am, SE	A	sph	120	01-mid peanut	7.6	0.9	0.1	71.0	0.4	0.7	0.3	0.3	0.2	3.2	14.3	0.7	0.4
	Big Eddy	MO	N Am, SE	A	sph	10	18 #1	8.1	1.0	0.0	66.8	0.5	6.1	0.3	1.5	0.2	3.3	9.0	2.7	0.4
E	Blackville	SC	N Am, SE	I	sph	1070	3-grain 7, BV-D-3	37.1	2.4	0.2	6.1	3.2	1.4	0.1	0.5	0.0	0.5	46.4	0.3	1.9
	Blackville	SC	N Am, SE	I	SLO	1280	#7 bulk glass	31.2	0.5	0.0	1.2	5.2	1.0	0.0	0.4	0.1	0.0	57.8	0.0	2.5
F	Blackwater Draw	NM	N Am, SW	A	sph	25	DC_09	0.7	0.5	0.1	95.5	0.1	0.3	0.1	0.2	0.1	0.7	0.9	0.7	0.1
	Blackwater Draw	NM	N Am, SW	A	sph	37	D-22	6.8	0.6	0.0	41.9	0.2	5.0	2.0	0.9	0.0	0.0	15.5	0.2	27.0
G	Chobot	NM	N Am, SW	A	sph	42	2	3.5	0.2	0.0	87.7	0.0	0.9	3.2	1.2	0.0	0.3	2.6	0.3	0.0
	Chobot	NM	N Am, SW	A	sph	50	4	4.6	1.2	0.0	77.4	0.3	1.5	1.8	1.7	0.0	4.0	6.4	0.7	0.3
H	Cuitzeo	MEX	C.Am	A	sph	95	ACM 6 spher	0.6	0.7	0.0	96.0	0.0	0.0	0.3	0.7	0.5	0.0	0.0	1.2	0.0
	Cuitzeo	MEX	C.Am	A	sph	75	280 02	0.3	0.4	0.1	96.2	0.1	0.2	0.2	0.3	0.2	0.6	0.5	0.7	0.1
I	Gainey	MI	N Am, NE	I	sph	40	G1-c1	2.2	0.0	0.0	88.8	0.0	0.0	0.0	0.0	0.0	0.0	6.0	0.0	3.0
	Gainey	MI	N Am, NE	I	sph	40	Spherule 1B	24.8	0.0	0.0	18.2	0.0	0.0	0.0	0.0	0.0	0.0	55.0	0.0	2.0
J	Kimbel B	NC	N Am, SE	A	sph	138	156_6	0.7	0.3	0.1	95.7	0.1	0.2	0.5	0.1	0.2	0.2	1.2	0.4	0.1
	Kimbel B	NC	N Am, SE	A	sph	30	156_3	2.8	0.5	0.7	88.9	0.1	0.2	0.4	2.0	0.2	0.7	2.8	0.4	0.2
K	Lingen	GER	Europe	A	sph	30	229 01	3.3	0.5	0.7	85.9	0.2	0.4	0.7	1.7	0.2	0.9	4.4	1.0	0.3
	Lingen	GER	Europe	A	sph	37	229 06	4.6	0.7	0.1	66.3	0.4	0.1	0.1	9.9	0.2	0.4	16.3	0.5	0.3
L	Lommel	BEL	Europe	A	sph	35	5	1.6	0.3	0.1	35.3	0.1	0.3	4.1	0.8	0.0	0.3	0.5	0.2	56.1
	Lommel	BEL	Europe	A	sph	100	grain B surface	33.7	11.5	0.0	1.4	3.1	1.3	0.0	11.8	0.0	0.6	34.7	2.0	0.0
M	Melrose	PA	N Am, NE	I	sph	760	3-Y1B, 25 core	29.4	1.0	0.0	7.6	3.0	0.2	0.0	0.4	0.3	0.0	54.3	2.1	1.7
	Melrose	PA	N Am, NE	I	SLO	2500	Y10 grain 01	31.5	0.3	0.2	3.5	4.2	1.3	0.0	0.4	0.2	0.0	56.4	0.2	1.7
N	Murray Spgs	AZ	N Am, SW	A	sph	30	NG3_10	0.5	0.4	0.1	95.9	0.1	0.2	0.3	0.2	0.2	0.3	0.9	0.6	0.2
	Murray Spgs	AZ	N Am, SW	A	sph	27	NG3_04	17.1	1.2	0.0	21.8	2.1	0.7	0.1	0.5	0.1	0.5	54.8	0.5	0.5
O	Ommen	NED	Europe	A	sph	35	3	0.0	0.0	0.0	98.3	0.0	0.0	0.0	0.2	0.3	0.0	0.4	0.0	0.8
	Ommen	NED	Europe	A	sph	36	6	8.3	1.6	0.0	71.9	0.3	0.6	0.0	1.2	0.0	0.9	15.1	0.0	0.1
P	Sheriden	OH	N Am, NE	A	sph	55	2	2.3	0.4	0.4	83.8	0.3	0.5	0.1	0.4	0.9	0.0	10.6	0.0	0.3
	Sheriden	OH	N Am, NE	A	sph	120	4	6.6	0.6	0.0	74.4	0.2	0.0	0.0	0.3	0.0	0.0	17.8	0.0	0.0
Q	Talega	CA	N Am, SW	I	sph	125	10 glass	7.7	33.5	0.0	29.5	2.0	2.0	0.0	1.1	0.0	0.2	23.4	0.1	0.5
	Talega	CA	N Am, SW	I	sph	95	01-head	26.6	1.7	0.1	3.8	1.8	1.3	0.1	2.1	0.1	0.3	56.4	0.7	4.9
R	Topper	SC	N Am, SE	I	sph	30	U2_1	1.1	0.4	0.2	39.4	0.0	0.2	5.8	0.2	0.1	0.6	1.3	0.3	50.5
	Topper	SC	N Am, SE	I	sph	12	U2_9_mosaic	8.2	0.7	0.1	78.9	0.3	0.4	0.3	0.3	0.2	1.2	8.4	0.7	0.4
							AVERAGE	9.7	2.7	0.1	57.8	0.9	1.2	0.6	1.4	0.2	0.7	19.1	0.6	5.0

TABLE S6. AVERAGE OXIDE PERCENTAGES for the YDB spherules and SLOs (orange), along with other material types (blue) used in various figures in this paper, as noted in row labeled "Figure." References are in **SI Table S5**. Uncertainties for major oxides are approximately ±5 wt%; for minor oxides, uncertainties are approximately ±20 wt%.

	YDB: all spher+SLOs	YDB: range (%)	YDB: all >200 µm	YDB: all <67%	YDB: all <63%	YDB: spher >200 µm	YDB: SLOs >200 µm	YDB: all whole	YDB: all sectioned	YDB: all inactive	YDB: all active	YDB: all <50 µm	Abu Hureyra >200 µm	Blackville >200 µm	Melrose >200 µm	Si-rich cosmic spher	Fe-rich cosmic spher	Meteorites	Anthropogenic	Volcanic	Mantle	Metamorphic-US+CAN	Ivory Coast tektites	Argentine escoria	Oak + Pine	Oak only	Pine only	Tasman Sea tektites	Tunguska spherules
Figure	5A	--	m any	4A	4B	SI 20	SI 20	SI 20	SI 20	SI 21	SI 21	SI 21	SI 26	SI 26	SI 26	4A	4B	4C	5A	5B	5C	6A	6B	6C	8C	--	--	SI 23	SI 23
Al2O3	12.2	0-65%	19.8	18.7	2.3	21.2	17.6	17.6	22.3	2.4	17.2	4.3	8.4	27.5	25.9	3.2	0.2	3.0	23.0	15.2	4.5	14.2	16.3	15.5	13.9	15.2	11.5	19.2	12.4
CaO	3.5	0-55%	5.7	5.4	0.6	4.6	6.9	6.2	5.2	0.6	5.0	0.9	11.7	3.5	1.6	2.6	0.1	2.2	10.5	11.3	3.6	6.1	2.5	7.6	11.5	7.5	19.0	5.4	8.9
Cr2O3	0.1	0-2%	0.1	0.1	0.1	0.1	0.1	0.1	0.1	0.1	0.1	0.1	0.1	0.1	0.1	0.3	0.2	0.7	0.0	0.0	0.4	0.0	0.0	0.0	0.1	0.1	0.1	0.1	0.0
FeO	44.9	0-100%	15.2	15.1	90.9	20.3	8.8	14.0	16.4	85.5	24.5	77.0	7.5	16.1	17.7	19.4	97.6	30.4	9.2	10.2	8.4	8.7	6.0	4.8	17.7	20.8	11.7	7.5	7.6
K2O	1.5	0-16%	2.6	2.4	0.1	2.2	2.9	3.0	2.2	0.2	2.2	0.3	3.1	2.1	2.4	0.3	0.1	0.1	1.7	0.2	0.0	2.0	1.9	3.2	2.1	2.1	2.1	0.5	2.6
MgO	1.7	0-41%	2.4	2.5	0.5	2.0	2.9	2.8	2.1	0.7	2.1	0.9	4.6	1.4	1.1	29.2	0.3	22.6	2.5	7.2	37.3	4.8	2.9	3.3	3.4	2.6	4.8	6.2	6.9
MnO	0.3	0-9%	0.2	0.3	0.3	0.2	0.2	0.3	0.1	0.5	0.2	0.5	0.3	0.1	0.1	0.3	0.0	0.3	0.1	0.2	0.1	0.2	0.0	0.2	0.2	0.2	0.2	0.1	0.2
Na2O	1.0	0-12%	1.3	1.3	0.6	1.2	1.3	1.5	1.1	0.8	1.1	0.8	1.9	0.9	0.9	0.5	0.4	0.6	1.1	2.7	0.3	2.5	2.5	5.3	1.3	1.5	1.0	1.0	1.6
NiO	0.1	0-1%	0.1	0.1	0.1	0.1	0.1	0.1	0.1	0.1	0.1	0.1	0.1	0.2	0.1	0.3	0.8	0.9	0.0	0.0	0.2	0.0	0.0	0.0	0.0	0.0	0.0	0.0	0.0
P2O5	0.7	0-37%	0.8	0.8	0.5	0.7	0.9	1.0	0.7	0.5	0.8	0.6	1.4	0.6	0.4	0.3	0.0	0.3	0.7	0.2	0.0	0.2	0.0	0.5	1.4	1.3	1.6	0.0	0.0
SiO2	30.9	0-95%	51.4	48.8	3.7	45.6	56.4	53.5	49.1	4.5	44.2	9.2	59.5	45.1	47.7	44.0	0.9	38.8	48.8	50.9	44.9	60.6	67.3	58.9	47.3	47.4	47.1	59.2	58.6
SO3	0.5	0-12%	0.5	0.5	0.5	0.5	0.4	0.5	0.4	0.6	0.4	0.5	0.7	0.3	0.3	0.5	0.0	0.0	1.3	0.0	0.0	0.0	0.0	0.0	0.3	0.3	0.3	0.0	0.0
TiO2	2.6	0-70%	1.4	4.0	0.4	1.3	1.4	1.3	1.5	3.4	2.1	5.0	0.6	2.1	1.7	0.2	0.1	0.1	1.1	1.6	0.2	0.8	0.6	0.8	0.9	1.1	0.7	0.8	1.2

TABLE S7. DATA SOURCES FOR TERNARY DIAGRAMS of various materials, shown by type, sampling location, number of analyses per site, and references. "Micromet." = micrometeorites.

TYPE	LOCATION or TYPE	ANAL.	REFERENCE
COSMIC			
Spherules	Antarctica	20	Engrand, 1999
	Antarctica	71	Genge, 1997
	Antarctica	20	Genge, 1998
	Antarctica	14	Rochette, 2008
	Antarctica	279	Taylor, 2000,2002
	Antarctica	207	Rochette, 2008
	Atlantic Ocean	45	Dekov, 2007
	Greenland	8	Maurette, 1986
Micromet.	Antarctica	21	Engrand, 1999
	Antarctica	86	Genge, 1997
	Antarctica	78	Kurat, 1994
	Meteorites, misc.	77	Genge, 1999
	TOTAL COSMIC:	**926**	
IMPACTS			
Spherules	Lonar Crater, IND	40	Misra, 2009
	Nuussuaq, Greenland	79	Jones, 2005
	Tunguska, Russia	13	Dolgov, 1973
	Tunguska, Russia	4	Glass, 1969
Tektites	Bahia Blanca, Argentina	2	Schultz, 2004
	Lake Botsumtwi crater	1	Glass, 1990
	Lake Botsumtwi crater	5	Koeberl, 2006
	Lake Botsumtwi crater	194	Koeberl, 2007
	Lake Botsumtwi crater	30	Luetke, 2008
	Tasman Sea	4	Kelly, 2004
	TOTAL IMPACT:	**372**	

TYPE	LOCATION or TYPE	ANAL.	REFERENCE
ANTHROPOGENIC			
Spherules	USA	42	This paper
Fly ash	BUL	3	Shoumkova, 2006
	CAN, USA, UK, FRA	5	Gikunoo, 2004
	CZE	1	Sulc, 2009
	EST	1	Marini, 2009
	USA, GER	10	Oymael, 2007
	NLD	1	Nugteren, 2009
	POL	12	Jablonska, 2003
	POL	10	Uscinowicz, 2009
	SPN	13	Acosta, 1997
	SPN, NLD, GRE, ITA	23	Towler, 2002
	UK	5	Snelson, 2007
	USA	7	Bhatty, 2001
	USA	2	Giere, 2003
	USA	19	Jewell, 2009
	USA	5	McKeen, 1998
	USA	13	White, 2005
	USA, POL, ITA, SPN,	13	Rawlings, 2006
	TOTAL ANTHROPO:	**185**	
VOLCANIC			
Glass	Atlantic, Pacific, Indian, Carib.	10026	Melson, 2002
Spherules	Pacific	57	Melson, 1988
	Pacific	119	Vallier, 1977
	TOTAL VOLCANIC:	**10202**	

TABLE S8. GRADIENT OXIDE PERCENTAGES ACROSS THIN-SECTIONED SPHERULES. EDS wt% compositional values for four spherules displayed in Figs. 7 and SI 25, as noted.

	Abu				Blackville				Melrose (1)					Melrose (2)				
Figure	SI 25	SI 25	SI 25	SI 25	SI 25	SI 25	SI 25	SI 25	7	7	7	7	7	SI 25	SI 25	SI 25	SI 25	SI 25
Sample	A-1	A-2	A-3	A-4	D-2	D-3	D-4	D-5	C-1	C-2	C-3	C-4	C-5	A-1	A-2	A-3	A-4	A-5
Al2O3	8.3	9.4	9.6	6.9	34.8	37.1	37.9	36.7	19.4	25.7	28.9	30.5	30.3	31.9	30.3	26.7	24.6	22.4
CaO	13.1	18.0	19.8	25.7	1.9	2.4	2.9	3.5	0.4	0.5	0.5	0.5	0.5	0.3	0.4	0.4	0.3	0.2
Cr2O3	0.1	0.1	0.1	0.0	0.0	0.2	0.0	0.1	0.1	0.0	0.1	0.0	0.0	0.1	0.0	0.0	0.1	0.0
FeO	2.3	3.5	4.4	9.5	5.2	6.1	6.2	6.8	0.9	1.5	1.8	1.9	2.1	6.8	5.3	8.4	6.7	4.8
K2O	2.6	2.1	2.1	1.1	3.8	3.2	3.2	3.4	3.4	3.2	2.9	2.8	3.0	3.0	3.6	3.6	4.1	4.1
MgO	3.7	5.3	4.3	9.1	1.5	1.4	1.5	1.2	0.4	0.6	0.7	0.7	0.7	1.2	0.9	1.1	1.0	0.7
MnO	0.2	0.1	0.1	0.1	0.0	0.1	0.1	0.0	0.0	0.0	0.0	0.0	0.0	0.0	0.0	0.0	0.1	0.0
Na2O	2.2	2.3	1.6	0.6	0.6	0.5	0.4	0.4	0.8	0.9	0.9	0.8	0.8	1.0	1.0	1.1	1.1	1.1
NiO	0.1	0.0	0.1	0.1	0.0	0.0	0.1	0.0	0.0	0.1	0.0	0.1	0.1	0.1	0.0	0.1	0.0	0.0
P2O5	1.2	1.4	1.7	1.7	0.4	0.5	0.4	0.3	0.8	0.9	0.8	0.8	0.8	1.1	1.0	1.0	1.0	1.1
SiO2	65.2	55.9	54.8	43.8	49.2	46.4	45.2	45.1	72.4	64.7	61.4	59.6	59.5	52.2	55.3	55.4	59.0	63.4
SO3	0.6	0.8	0.7	0.4	0.3	0.3	0.2	0.3	0.5	0.5	0.5	0.5	0.4	0.7	0.6	0.7	0.6	0.6
TiO2	0.5	1.0	0.6	0.9	2.2	1.9	1.9	1.9	0.9	1.3	1.5	1.7	1.8	1.5	1.5	1.6	1.3	1.5

TABLE S9. STREWNFIELD TONNAGE OF YDB SPHERULES. List of variables used to calculate the estimated metric tonnage, as presented in **Fig. 1** and **Table 1**. For the tonnage calculations, we used average spherule diameter, following the convention of Glass et al. (1979; 1985). Densities were assumed similar to tektites. The value for average spherules per cm^2 is from Table S2.

YDB TONNAGE--VARIABLES	VALUE
Diameter of average YDB spherule	135 µm
Volume of average spherule	1.3×10^{-6} cm^3
Density of spherule (similar to tektites)	2.5 g cm^{-3}
Weight of average spherule	3.25×10^{-6} g
Average number of spherules per cm^2	6.3 cm^{-2}
Average weight of spherules per cm^2	20.5×10^{-6} g cm^{-2}
Area of YDB strewnfield	5×10^7 km^2
Metric tonnes in YDB strewnfield	**10.25×10^6**

REFERENCES

Acosta A, Aineto M, Iglesias I, Romero I, and Rincon JM. (2001) Physico-chemical characterization of slag waste coming from IGCC thermal power plant. *Mater Lett*, 50: 246-250.

Agenbroad LD, Johnson JR, Morris D, Stafford TW, Jr. (2005) Mammoths and humans as late Pleistocene contemporaries on Santa Rosa Island, in *Proceedings of the Sixth California Islands Symposium*, eds Garcelon DK, Schwemm CA (Institute for Wildlife Studies, Arcata, CA), pp 3–7.

Anderson DG, Goodyear AC, Kennett J, West A. (2011) Multiple lines of evidence for possible Human population decline/settlement reorganization during the early Younger Dryas. *Quaternary International* 242 (2011) 570-583.

Baales M, Joris O, Street M. (2002) Impact of the late glacial eruption of the Laacher See volcano, Central Rhineland, Germany. *Quaternary Research*, 58(3), 273-288.

Baker DW, Miranda PJ, Gibbs KE. (2008) Montana Evidence for Extra-Terrestrial Impact Event that caused Ice-Age Mammal Die-Off. Eos Trans. AGU, 89(23), Jt. Assem. Suppl., no. P41A-05.

Berg TM, et al. (1980) Geologic map of Pennsylvania: Pennsylvania Geological Survey, 4th ser., Map 1, 2nd ed., 3 sheets, scale 1:250,000.

Bergin KA, et al. (2011) The Archaeology of the Talega Site (CA-ORA-907), Orange County, California: Perspective on the Prehistory of Southern California. Viejo California Associates, Mission Viejo. Prepared for the District of the US Army Corps of Engineers, Los Angeles.

Bhatty JI, Gadja J, Miller FM. (2001) Commercialization of High-Carbon Fly Ash in Cement Manufacture; Report No. 00-1/3 1A-1; *Illinois Clean Coal Institute*: Canterville, IL.

Bogaard P, Schmincke HU. (1985) Laacher See Tephra - a Widespread Isochronous Late Quaternary Tephra Layer in Central And Northern Europe. *Geological Society of America Bulletin*, 96(12), 1554-1571.

Bunch TE, et al. (2012) Very High-Temperature Impact Melt Products as Evidence for Cosmic Airbursts and Impacts 12,900 years ago. *Proc Natl Acad Sci USA, 109: 11066-11067.*

CARD (Canadian Archaeological Radiocarbon Database). 2009. Canadian Museum of Civilization, (http://www.canadianarchaeology.ca/)

Casson MA and Feathers JK. (2001) The Application of Luminescence Dating to Cultural Resource Management. Society for American Archaeology, New Orleans, LA.

Choate BC. (2011) Stratigraphic Investigations at Barber Creek (31PT259): *Reconstructing the Culture-History of a Multicomponent Site in the North Carolina Coastal Plain.* Unpublished M.A. thesis, East Carolina University, Greenville.

Colgan PM, Mickelson DM, and Cutler PM. (2003) Ice-Marginal Terrestrial Landsystems: Southern Laurentide Ice Sheet, in Evans, D.A. and Rea, B.R., (eds.), *Glacial Landsystems*, Edwin Arnold, London, 111-142.

Corona Nuñez JC. (1988). Historia de los antiguos habitantes de Michoacan: Desde su origen hasta la conquista espanola (History of the ancient inhabitants of Michoacan: Since its origin to the Spanish conquest). Balsal Editores, 86 pages.

Daniel IR Jr, Seramur KC, Potts TL, Jorgenson MW. (2008) Searching a Sand Dune: Shovel Testing the Barber Creek Site. *North Carolina Archaeology* 57:50-77.

Daniel IR Jr. (2002) Stratified Early-Middle Holocene Remains in the North Carolina Coastal Plain. *Southeastern Archaeological Conference Special Publication 7*:6-11.

Daniel, IR Jr and Moore CR. (2011) Current Research into the Paleoindain and Archaic Periods in the North Carolina Coastal Plain. In Charles R. Ewen, Thomas Whyte, R. P. Stephen Davis, Jr. (Ed.) *The Archaeology of North*

Carolina: Three Archaeological Symposia, (pp. 93-117). North Carolina Archaeological Council Publication Number 30.

Daulton T, Pinter N, Scott AC. (2010) No evidence of nanodiamonds in Younger-Dryas sediments to support an impact event. *Proc Natl. Acad. Sci. USA*, 107 (37): 16043–16047.

de Klerk P, Janke WF, Kuehn P, Theuerkauf M. (2008) Environmental impact of the Laacher See eruption at a large distance from the volcano: Integrated palaeoecological studies from Vorpommern (NE Germany). *Palaeogeography Palaeoclimatology Palaeoecology*, 270(1-2), 196-214.

Dekov VM, et al. (2007) Cosmic spherules from metalliferous sediments:A long journey to the seafloor. *N. Jb. Miner. Abh.*, Vol.183/3, p. 269–282.

Dolgov YA, Vassil'ev AN, Shugurova NA, Lavrent'ev YG, L'vov YA. (1973) The composition of the microscopic spherules from the fallsite of the Tunguska meteorite. *Meteoritika*, 2, 147-149.

Dorale JA, et al. (2010) Isotopic evidence for Younger Dryas aridity in the North American midcontinent. *Geology*, vol. 38; no. 6; p. 519–522.

Engrand C, Deloule E, Robert F, Maurette M, Kurat G. (1999) Extraterrestrial water in micrometeorites and cosmic spherules from Antarctica: An ion microprobe study. *Meteoritics & Planetary Science* 34, 773-786.

Erlandson JM, Rick TC, Jones TL, Porcasi J. (2007) One if by land, two if by sea: who were the First Californians? In: Jones TL, Klar K, eds., California Prehistory: Colonization, Culture, and Complexity. Altamira Press, Walnut Creek, CA, pp. 53–62.

Fayek M, Anovitz LM, Allard LF, Hull S. (2012) Framboidal iron oxide: chondrite-like material from the black mat, Murray Springs, Arizona. *Earth and Planetary Science Letters* 319-320: 251-258.

Feathers JK. (2003) Use of luminescence dating in archaeology. *Measurement Science and Technology* 14:1493-1509.

Firestone RB, et al. (2007) Evidence for an extraterrestrial impact 12,900 years ago that contributed to the megafaunal extinctions and the Younger Dryas cooling. *Proc Natl. Acad. Sci. USA*, 104:16016-16021.

Firestone RB, et al. (2010) Analysis of the Younger Dryas Impact Layer. Journal of Siberian Federal University. *Engineering & Technologies* 1 (2010 3) 30-62.

Florenskiy KP. (1963) Preliminary Results From The 1961 Combined Tunguska Meteorite Expedition. Tenth Conference on Meteorites in May 1962, *Meteoritica*, Vol. XXIII.

Fullerton DS, Bush CA, Pennell JN. (2003) Surficial deposits and materials in the eastern and central United States (east of 102 degrees west longitude) U.S. Geological Survey Geologic Investigations Series, I-2789, Edition: 1.0, U.S. Geological Survey, Denver, CO.

Genge M and Grady M. (1998) Melted micrometeorites from Antarctic ice with evidence for the separation of immiscible Fe-Ni-S liquids during entry heating. *Meteoritics &Planetary Science* 33, 425-434.

Genge M and Grady M. (1999) The fusion crusts of stony meteorites: Implications for the atmospheric reprocessing of extraterrestrial materials. *Meteoritics & Planetary Science* 34, 341-356.

Genge MJ, Grady M, and Hutchison R. (1997) The textures and compositions of fine-grained Antarctic micrometeorites: Implications for comparisons with meteorites. *Geochimica et Cosmochimica Acta*, Vol. 61, No. 23, pp. 5149-5162.

Giere R, Carleton LE, and Lumpkin GR. (2003) Micro- and nanochemistry of fly ash from a coal-fired power plant. *American Mineralogist*, Volume 88, pages 1853–1865.

Gikunoo E. (2004) Effect of Fly Ash Particles on the Mechanical Properties and Microstructure of Aluminium Casting Alloy A535. Thesis, Department of Mechanical Engineering, University of Saskatchewan, CAN.

Glass BP. (1969) Silicate Spherules from the Tunguska Impact Area: Electron Microprobe Analysis, *Science* 164, 547-549.

Glass BP. (1990) Tektites and microtektites: key facts and inferences. *Tectonophysics*, Vol. 171, No. 1-4, p. 393 - 404.

Goodyear AC. (1999) The Early Holocene Occupation of the Southeastern United States: A Geoarchaeological Summary. In *Ice Age Peoples of North America*, edited by R. Bonnichsen and K. Turnmire, 432-481. Center for the Study of the First Americans, Corvallis, Oregon.

Goodyear AC and Steffy K. (2003) Evidence of a Clovis Occupation at the Topper Site, 38AL23, Allendale County, South Carolina. *Current Research in the Pleistocene* 20:23-25.

Goodyear AC. (2005) Evidence of Pre-Clovis Sites in the Eastern United States. In *Paleoamerican Origins: Beyond Clovis*, 103–12. Center for the Study of the First Americans, Texas A&M University, College Station.

Goodyear AC. (2006) Recognizing the Redstone fluted point in the South Carolina Paleoindian point data base. *Current Research in the Pleistocene* 23:100-103.

Goodyear AC, Miller S, and Smallwood S. (2007) Introducing Clovis at the Topper Site,38AL23, Allendale County, South Carolina. Paper presented at the 72nd Annual Meeting of the Society for American Archaeology, Austin, Texas.

Goodyear AC. (2010) Instrument-Assisted Fluting as a technochronological Marker among North American Paleoindian Points. *Current Research in the Pleistocene* Vol 2, 86 - 88.

Goodyear AC. (2013) Update on the 2012-2013 activities of the Southeastern Paleoamerican Survey. Legacy, Vol. 17, No. 1, May. Newsletter of the South Carolina Institute of Archaeology and Anthropology, University of South Carolina, Columbia.

Grachev AF, Korchagin OA, Tselmovich VA, Kollmann HA. (2008) Cosmic dust and micrometeorites in the transitional clay layer at the Cretaceous-Paleogene boundary in the gams section (Eastern Alps): Morphology and chemical composition. Izvestiya, *Physics of the Solid Earth*, Vol. 44, No. 7, 555–569.

Haynes CV Jr. (1995) Geochronology of Paleoenvironmental Change, Clovis Type Site, Blackwater Draw, New Mexico. *Geoarchaeology*, Vol 10, No 5, 317-388.

Haynes CV Jr, et al. (1999) A Clovis Well at the Type Site 11,500 B.C.: The Oldest Prehistoric Well in America, *Geoarchaeology: An International Journal*, 14(5), 455-470.

Haynes, CV Jr. (2007) Appendix B: Nature and Origin of the Black Mat, Stratum F2, in *Murray Springs: A Clovis Site with Multiple Activity Areas in the San Pedro Valley, Arizona.* Haynes, CV Jr. and Huckell BB, editors. University of Arizona Press, Tucson, AZ, pp. 240-249.

Haynes CV Jr. (2008) Younger Dryas "black mats" and the Rancholabrean termination in North America. *Proc Natl. Acad. Sci. USA* 105:6520–6525.

Haynes CV Jr., et al. (2010). The Murray Springs Clovis site, Pleistocene extinction, and the question of extraterrestrial impact. *Proc Natl Acad Sci USA* 107: 4010-4015.

Hillman G, Hedges R, Moore A, Colledge S, and Pettitt P. (2001) New evidence of Lateglacial cereal cultivation at Abu Hureyra on the Euphrates. *The Holocene* 11, 4, 383-393.

Hoek WZ (1997) Late-Glacial and early Holocene climatic events and chronology of vegetation development in the Netherlands. *Veget Hist Archaeobot* 6:197-213.

Horton, JW, and Dicken CL. (2001) Preliminary Geologic Map of the Appalachian Piedmont and Blue Ridge, South Carolina Segment: U.S. Geological Survey, *Open-File Report* 01-298, CD.

Israde-Alcántara I, et al. (2010) Evolucion paleolimnologica del Lago Cuitzeo, Michoacan, durante el Pleistoceno-Holoceno (Paleolimnologic evolution of the Cuitzeo lake, Michoacan, during the Pleistocene-Holocene). Juan Pablo Bernal, Priyadarsi D. Roy (eds.) *Numero especial Paleoclimas del Cuaternario en ambientes tropicales y subtropicales*, Volumen 62, Numero 3.

Israde-Alcántara I, et al. (2012) Evidence from Central Mexico supporting the Younger Dryas Extraterrestrial Impact Hypothesis. *Proc Natl. Acad. Sci. USA*, 109, 13, E738-E747.

Jablonska M and Smola-Danielowska D. (2003) Aluminosilicate particles in fly ash and atmospheric dust. Mineralogical Society of Poland, special papers 22, 82-89.

Jewell RB and Rathbone RF. (2009) Optical Properties of Coal Combustion Byproducts for Particle-Size Analysis by Laser Diffraction. *Coal Combustion and Gasification Products*, Vol. 1, pp. 1-7.

Johnson E and Holliday VT. (1997) Analysis of Paleoindian Bonebeds at the Clovis Site: New Data from Old Excavations. *Plains Anthropologist*, Vol 42, 329-352.

Johnson JR, Stafford TW Jr, Ajie HO, Morris DP (2002) in *Proceedings of the Fifth California Islands Symposium*, eds Browne DR, Mitchell KL, Chaney HW (Santa Barbara Museum of Natural History, Santa Barbara, CA), pp 541–545.

Jones AP, et al. (2005) Are there signs of a large Paleocene impact, preserved around Disko Bay, West Greenland?: Nuussuaq spherule beds origin by impact instead of volcanic eruption?, in Kenkmann, T., Hörz, F., and Deutsch, A., eds., *Large meteorite impacts III*: Geological Society of America Special Paper 384.

Kelly DC and Elkins-Tanton LT. (2004) Bottle-green microtektites from the South Tasman Rise: Deep-sea evidence for an impact event near the Miocene/Pliocene boundary. *Meteoritics & Planetary Science* 39, Nr 12, 1921–1929.

Kennett DJ, et al. (2008) Wildfire and abrupt ecosystem disruption on California's Northern Channel Islands at the Ållerød–Younger Dryas boundary (13.0–12.9 ka). *Quaternary Science Reviews* 27, 2530-2545.

Kennett DJ, et al. (2009a) Shock-synthesized hexagonal diamonds in Younger Dryas boundary Sediments, *Proc Natl. Acad. Sci. USA*, 106 (31): 12623-12628.

Kennett DJ, et al. (2009b) Nanodiamonds in the Younger Dryas boundary sediment layer. *Science* 323:5910:94.

Kloosterman JB. (1999) The Usselo Horizon, a worldwide charcoal-rich layer of Allerod age. In *New Scenarios on the Evolution of the Solar System and Consequences on History of Earth and Man.* Eds. Spedicato E and Notarpietro A. Milan.

Kloosterman JB. (2007) Correlation of the Late Pleistocene Usselo Horizon (Europe) and the Clovis layer (North America). *Eos Trans*. AGU, 88(23), Jt. Assem. Suppl.

Koeberl C and Sigurdsson H. (1992) Geochemistry of impact glasses from the K/T boundary in Haiti: Relation to smectites, and a new type of glass. *Geochimica et Cosmochimica Acta* 56, 2113- 2129.

Koeberl C, et al. (2006) Uppermost Impact Fallout Layer in a Drillcore at the Bosumtwi Impact Crater (Ghana): A Preliminary Study. 37th Annual Lunar and Planetary Science Conference, March 13-17, 2006, League City, Texas, abstract no.1552.

Koeberl C. (2007) The geochemistry and cosmochemistry of impacts. In: *Treatise of Geochemistry*, Vol. 1 (ed. A. Davis), Elsevier, p. 1.28.1 - 1.28.52, doi:10.1016/B978-008043751-4/00228-5.

Kolesnikov EM, Kolesnikova NV. (2010) Traces of cometary material in the area of the Tunguska impact (1908). *Solar System Research* 44, 110-121.

Kulik LA. (1940) The meteorite expedition to Podkamennaya Tunguska in 1939. *Comptes Rendus De L Academie Des Sciences De L Urss* 28, 596-600.

Kurat G, Koeberl C, Presper T, Brandstätter F, Maurette M. (1994) Petrology and geochemistry of Antarctic micrometeorites. *Geochimica et Cosmochimica Acta*, vol. 58, Issue 18, pp.3879-3904.

LeCompte MA, et al. (2012) Independent evaluation of conflicting microspherule results from different investigations of the Younger Dryas impact hypothesis. *Proc Natl. Acad. Sci. USA* 106: doi: 10.1073/pnas.1208603109.

Litt T, Schmincke HU, Kromer B. (2003) Environmental response to climatic and volcanic events in central Europe during the Weichselian Lateglacial. *Quaternary Science Reviews*, 22(1), 7-32.

Lopinot NH, Ray JH, and Conner MD. (1998) *The 1997 Excavations at the Big Eddy Site (23CE426) in Southwest Missouri*. Special Publication No. 2. Center for Archaeological Research, Southwest Missouri State University, Springfield.

Lopinot NH, Ray JH, and Conner MD. (2000) *The 1999 Excavations at the Big Eddy Site (23CE426).* Special Publication No. 3. Center for Archaeological Research, Southwest Missouri State University, Springfield.

Lopinot NH, Ray JH, and Conner MD. (2005) *Regional Research and the Archaic Record at the Big Eddy Site (23CE426), Southwest Missouri*. Special Publication No. 4. Center for Archaeological Research, Southwest Missouri State University, Springfield.

Luetke S, Deutsch A, Berndt J, Langenhorst F. (2008) Trace Elements in Ivory Coast Tektites, Microtektites, and Fallback Particles of the Lake Bosumtwi Impact Crater, Ghana: A LA-ICP-MS Study. 39th Lunar and Planetary Science Conference, (Lunar and Planetary Science XXXIX), held March 10-14, 2008 in League City, Texas. LPI Contribution No. 1391., p.1613.

Marini F and Raukas A. (2009) Lechatelierite-bearing microspherules from semicoke hill (Kiviõli, Estonia): contribution to the contamination problem of natural microtektites. *Oil Shale* 26(3), 415-423.

Maurette M, Hammer C, Reeh N, Brownlee DE, Thomsen HH. (1986) Placers of cosmic dust in the blue ice lakes of Greenland. *Science*, vol. 233, Aug. 22, 1986, p. 869-872.

McFadden P. (2009) *Geoarchaeological Investigations of Dune Formation and Artifact Deposition at Barber Creek (31PT259)*, Unpublished M.A. thesis, East Carolina University, Greenville.

McKeen RG, Lenke LR, Pallachulla KK. (1998), Mitigation of Alkali Silica Reactivity in New Mexico. Materials Research Center, University of New Mexico, Albuquerque, NM.

Melson WG, O'Hearn T, and Jarosewich E. (2002) A data brief on the Smithsonian Abyssal Volcanic Glass Data File. *Geochemistry Geophysics Geosystems*, Vol. 3 No. 4, 10.

Melson WG, O'Hearn T, Fredriksson K. (1988) Composition and Origin of Basaltic Glass Spherules in Pelagic Clay from the Eastern Pacific. *Marine Geology*, 83 (1988) 253-271.

Misra S, et al. (2009) Geochemical identification of impactor for Lonar crater, India. *Meteoritics & Planetary Science*, vol. 44, Issue 7, p.1001-1018.

Moore AMT and Hillman GC. (1992) The Pleistocene to Holocene transition and human economy in Southwest Asia: the impact of the Younger Dryas. *American Antiquity* 57, 3, 482-494.

Moore AMT, Hillman GC, and Legge AJ. (2000) *Village on the Euphrates*. Oxford University Press: New York, 585 pages.

Moore CR and Daniel IR Jr. (2011) Geoarchaeological Investigations of Stratified Sand Ridges along the Tar River, North Carolina. In Charles R. Ewen, Thomas Whyte, R. P. Stephen Davis, Jr. (Ed.) North Carolina Archaeology: Three Archaeological Symposia, (pp. 1-42). North Carolina Archaeological Council Publication 30.

Moore CR. (2009) *Late Quaternary Geoarchaeology and Geochronology of Stratified Eolian Deposits, Tar River, North Carolina.* Unpublished Ph.D. Dissertation, Coastal Resources Management Program, East Carolina University, Greenville.

Murray AS and Wintle AG. (2000) Luminescence dating of quartz using an improved single-aliquot regenerative-dose protocol. *Radiation Measurements* 32 (1): 57-73.

Nugteren HW, Butselaar-Orthlieb VCL, Izquierdo M. (2009) High Strength Geopolymers Produced from Coal Combustion Fly Ash. *Global NEST Journal*, Vol 11, No 2, pp. 155-161.

Oymael S. (2007) Suitability of Oil Shale Ash as a Constituent of Cement. Oil Shale, Vol. 24, No. 1, pp. 45–58.

Pereira L, et al. (2005) High-resolution mtDNA evidence for the late-glacial resettlement of Europe from an Iberian refugium. Gen. Res, 15:19-24.

Pigati JS, et al. (2012) Accumulation of "impact markers" in desert wetlands and implications for the Younger Dryas impact hypothesis. *Proc. Natl. Acad. Sci. USA*, doi: 10.1073/pnas.1200296109.

Pinter N, et al. (2011) The Younger Dryas impact hypothesis: A requiem. *Earth Science Reviews*, Vol. 106, Issues 3-4, 247-264.

Rawlings RD, Wu JP, Boccaccini AR. (2006) Glass-ceramics: Their production from wastes-a review. *J Materials Science* 41 (3) 733-761.

Ray JH, Lopinot NH, Hajic ER, and Mandel RD. (1998) The Big Eddy Site: A Multicomponent Paleoindian Site on the Ozark Border, Southwest Missouri. *Plains Anthropologist*:43(163):73-81.

Redmond BG and Tankersley KB. (2011) Species Response to the Theorized Clovis Comet Impact at Sheriden Cave, Ohio. *Current Research in the Pleistocene*, vol. 28, 141-143.

Redmond BG and Tankersley KB (2005) Evidence of Early Paleoindian Bone Modification and Use at the Sheriden Cave Site (33WY252), Wyandot County, Ohio. *American Antiquity*Volume 70:3;503-526.

Reimer PJ, et al. (2009) IntCal09 and Marine09 Radiocarbon Age Calibration Curves, 0-50,000 Years cal BP. Carbon, Vol 51, No 4, p 1111–1150.

Renssen H, Isarin RFB, Vandenberghe J, and Workshop Participants. (2001) Rapid climatic warming at the end of the last glacial: new perspectives. *Global and Planetary Change* 30, 1-2, 155-165.

Robinson SA, Black S, Sellwood BW, and Valdes PJ. (2006) A review of palaeoclimates and palaeoenvironments in the Levant and Eastern Mediterranean from 25,000 to 5000 years BP: setting the environmental background for the evolution of human civilization. *Quaternary Science Reviews* 25, 13-14, 1517-1541.

Rochette P. (2008) Micrometeorites from the Transantarctic Mountains. *Proc Natl. Acad. Sci. USA* November 25, 2008 vol. 105 no. 47 18206-18211.

Rudnick RL and Gao S. (2005) "Composition of the Continental Crust," Ch. 3 of *The Crust*, ed. R.L. Rudnick, Elsevier.

Schmitt AK, Wetzel F, Cooper KM, Zou H, Worner G. (2010) Magmatic Longevity of Laacher See Volcano (Eifel, Germany) Indicated by U-Th Dating of Intrusive Carbonatites. *Journal of Petrology*, 51(5), 1053-1085.

Schultz P. (2004) The Quaternary impact record from the Pampas, Argentina. *Earth and Planetary Science Letters* 219 (2004) 221-238.

Scott AC, et al. (2010) Fungus, not comet or catastrophe, accounts for carbonaceous spherules in the Younger Dryas 'impact layer'. *Geophysical Research Letters*, Vol. 37, L14302, 5 pages.

Scruggs MA, Raab LM, Murowchick JS, Stone MW, Niemi TM. (2010) Investigation of Sediment Containing Evidence of the Younger Dryas Boundary (YDB) Impact Event, El Carrizal, Baja California Sur, Mexico. Geological Society of America Abstracts with Programs, Vol. 42, No. 2, p. 101.

Shoumkova AS. (2006) Physico-Chemical Characterization and Magnetic Separation of Coal Fly Ashes from "Varna," "Bobov Dol" And "Maritza-Istok I" Power Plants, Bulgaria: Physico-Chemical Characteristics. *Journal of the University of Chemical Technology and Metallurgy*, 41, 2, 175-180.

Simons DB, Shott MJ, Wright HT. (1984) The Gainey site: variability in Great Lakes Paleo-Indian assemblage. *Archaeology of Eastern North America* 12, 266–279.

Snelson DG, Kinuthia JM, Davies P, Chang S-R. (2007) Sustainable road construction in the United Kingdom: Combined use of waste tyres and PFA. The 9th International Conference, Modern Building Materials, Structures and Techniques, pp. 168-173.

Sulc R. (2009) Effect of Water Ratio in Fly-Ash Concrete on the Process of Alkali Activation. In Mlady vedec [CD-ROM]. Košice: Technická universita v Košiciach, Stavebná fakulta.

Surovell TA, et al. (2009) An Independent Evaluation of the Younger Dryas Extraterrestrial Impact Hypothesis. *Proc. Natl. Acad. Sci. USA*, 104: 18155–18158.

Tankersley KB and Landefeld CS. (1998) Geochronology of Sheriden Cave, Ohio: The 1997 Field Season. *Current Research in the Pleistocene* 15:136-138.

Tankersley KB and Redmond B. (1999a) Fluoride/Radiocarbon Dating of Late Pleistocene Bone from Sheriden Cave, Ohio. *Current Research in the Pleistocene* 16:107-108.

Tankersley KB and Redmond B. (1999b) Radiocarbon Dating of a Projectile Point from Sheriden Cave, Ohio. *Current Research in the Pleistocene* 16:76-77.

Tankersley KB. (1997) Sheriden: A Clovis Cave Site in Eastern North America. *Geoarchaeology: An International Journal* 12:713-724.

Tankersley KB. (1999) Sheriden: A Stratified Pleistocene-Holocene Cave Site in the Great Lakes Region of North America. *BAR International Series* 800:67-75.

Taylor S, Lever JH, Harvey RP. (2000) Numbers, types, and compositions of an unbiased collection of cosmic spherules. *Meteoritics & Planetary Science*, vol. 35, no. 4, 651-666.

Taylor S. (2002) Micrometeorites from the South Pole water well. Boulder, CO, USA: National Snow and Ice Data Center. Digital media.

Tian H, Schryvers D, Claeys P. (2011) Nanodiamonds do not provide unique evidence for a Younger Dryas impact. *Proc. Natl. Acad. Sci. USA*, vol. 108, issue 1, 40-44.

Towler MR, et al. (2002) Modelling of the glass phase in fly ashes using network connectivity theory. International Workshop on Novel Products from Combustion Residues, pp. 240-245.

Uścinowicz G. (2009) Micro-scale magnetic grains from shallow water sediments of the Gulf of Gdańsk. *Journal of Oceanography and Hydrobiology*. Vol. XXXVIII, No.4, pp. 21-30.

Vallier T, Bohrer D, Moreland G, McKee EE. (1977) Origin of basalt microlapilli in lower Miocene pelagic sediment, northeastern Pacific Ocean. *Geol. Soc. Am. Bull.*, 88: 787-796.

Van Geel B, Coope GR, Vander Hammen T. (1989) Palaeoecology and stratigraphy of the lateglacial type section at Usselo (The Netherlands). *Rev Paleont Palyn* 60:25-129.

Van Hoesel, et al. (2012) Nanodiamonds and wildfire evidence in the Usselo horizon postdate the Allerød-Younger Dryas boundary. *Proc Natl. Acad. Sci. USA*, (in press).

Vanmontfort B, et al. (2010) Human occupation of the Late and Early Post-Glacial environments in the Liereman Landscape (Campine, Belgium). Journal of Archaeology in the Low Countries, issue 2-2, pp.31 - 51, published by Amsterdam University Press.

Waters MR and Stafford TW Jr. (2007) Redefining the Age of Clovis: Implications for the Peopling of the Americas. *Science* 315:5815:1122-1126.

Waters MR, Forman S, Stafford TW, and Foss J. (2009a) Geoarchaeological investigations at the Topper and Big Pine Tree sites, Allendale County, South Carolina. *Journal of Archaeological Science* 36:1300-1311.

Waters MR, Stafford TW Jr, Redmond BG, Tankersley KB. (2009b) The Age of the Paleoindian Assemblage at Sheriden Cave, Ohio. *American Antiquity* 74:107-111.

White DJ, Harrington D, Thomas Z. (2005) Fly ash soil stabilization for non-uniform subgrade soils, Volume I: *Engineering properties and construction guidelines.* Iowa State University, Ames, IA: Center for Transportation Research and Education Iowa State University.

Wu Y. (2011) Origin and Provenance of Magnetic Spherules at the Younger Dryas Boundary. Thesis, Dartmouth College, NH.